# Lecture 7: InSAR

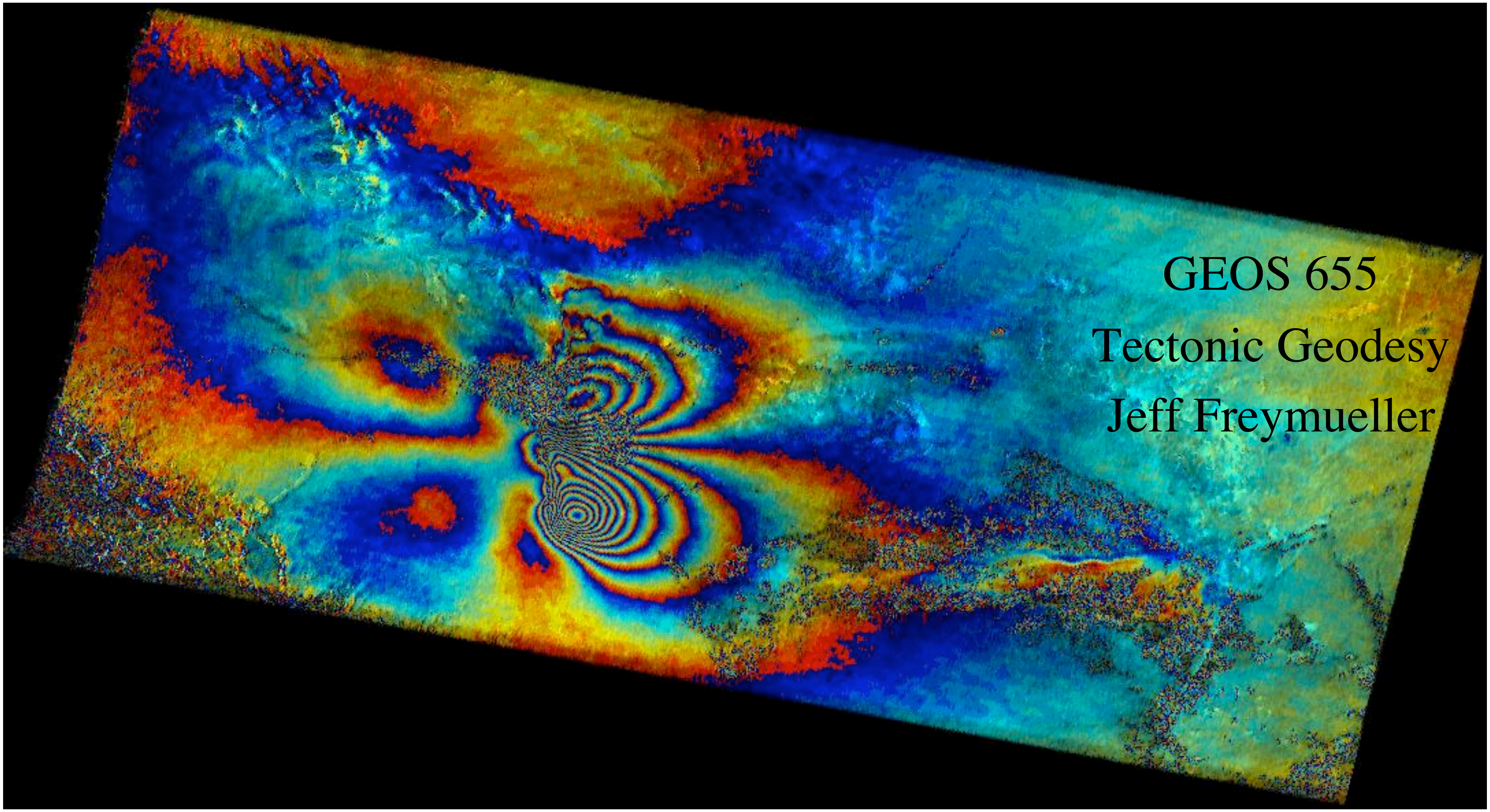

GEOS 655

Tectonic Geodesy

Jeff Freymueller

Thanks to Ramón Hanssen, Mark Simons, Dörte Mann, and Howard Zebker for slides and images

# The Picture That Started the Excitement

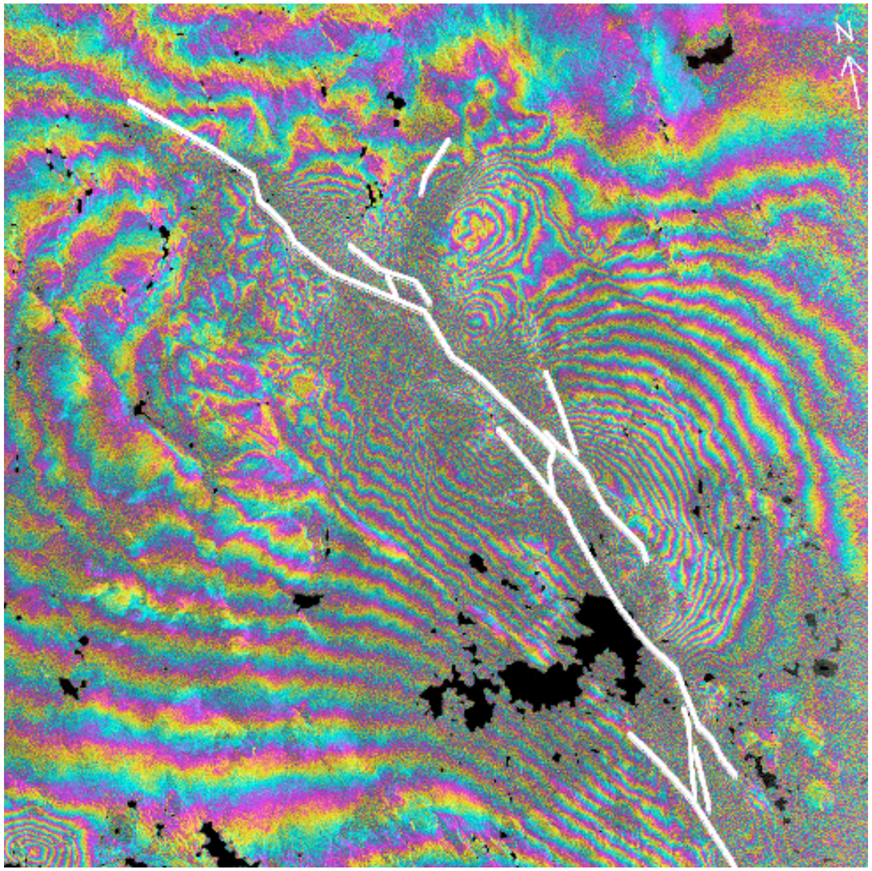


Landers earthquake, first shown by Massennet et al. (1993)

# Early ground based radar
# RAdio Detection and Ranging

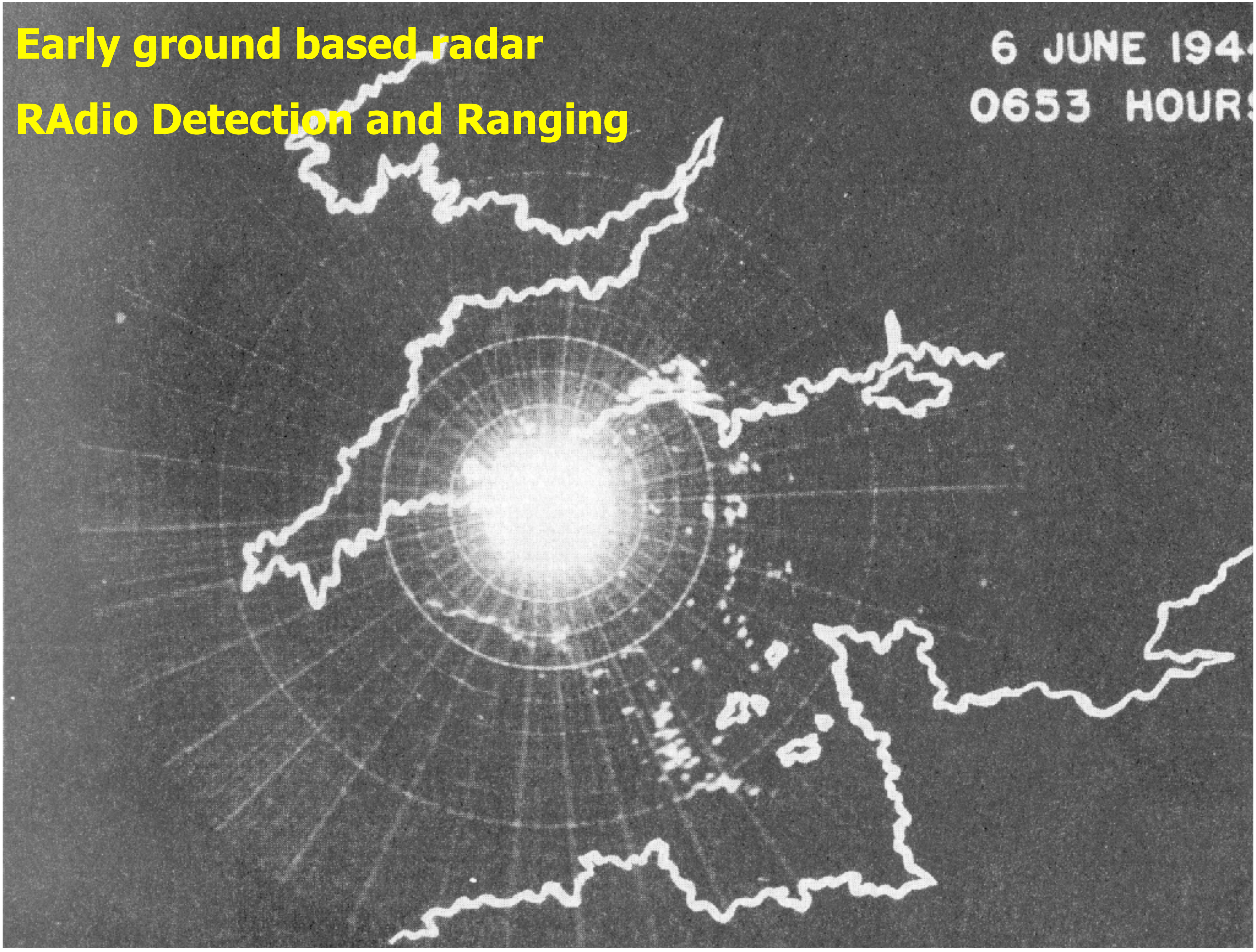

# InSAR Platforms

Aircraft: Shown here: AIRSAR
Measures topography, ocean currents


Satellites: Repeat pass
Fly over once, repeat days-years later
* Measures deformation and topography

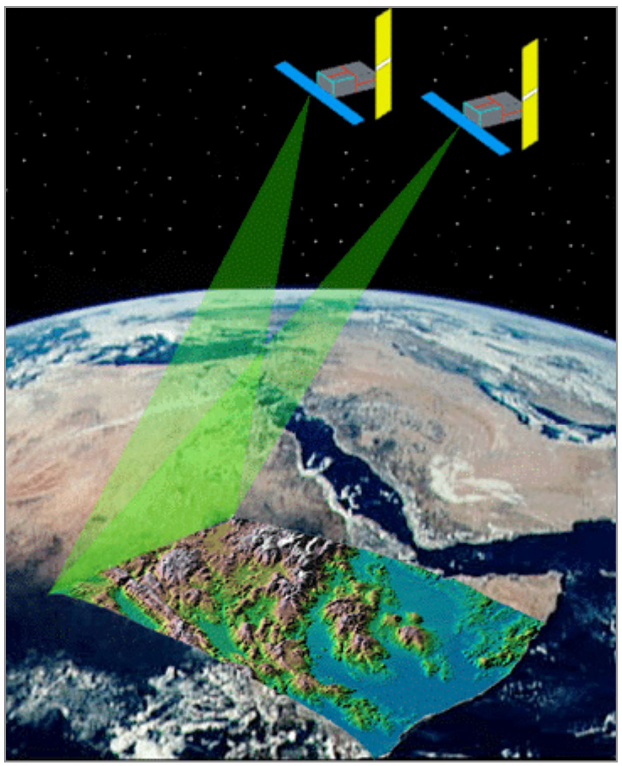

Space shuttle:
Shuttle Radar Topography Mission (SRTM)

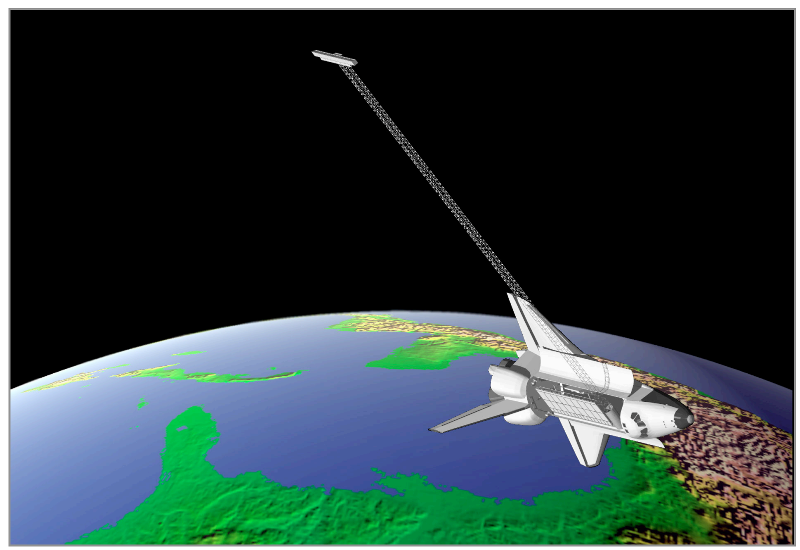

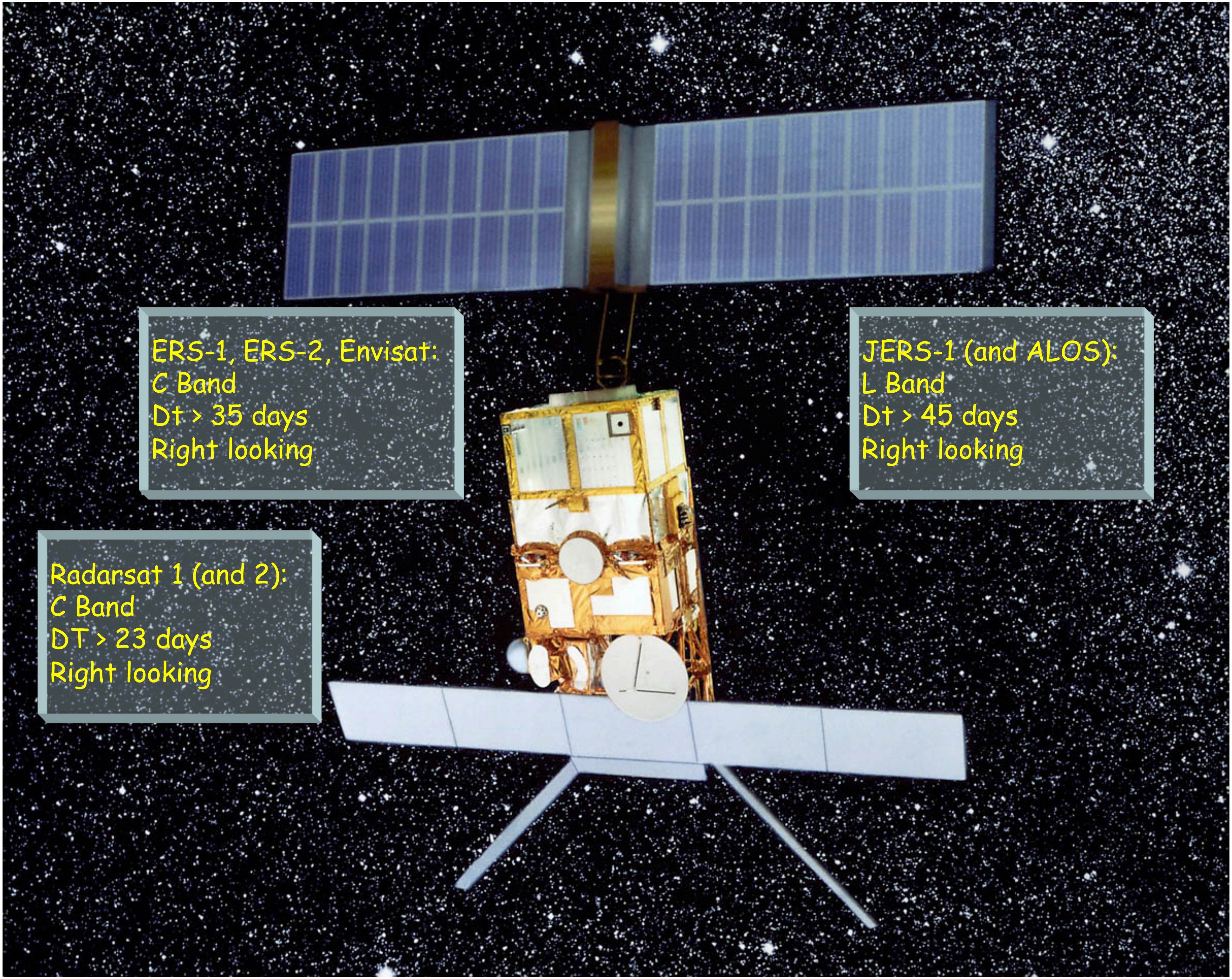
ERS-1, ERS-2, Envisat:
C Band
Dt > 35 days
Right looking
JERS-1 (and ALOS):
L Band
Dt > 45 days
Right looking
Radarsat 1 (and 2):
C Band
DT > 23 days
Right looking

# Radio waves, active sensor

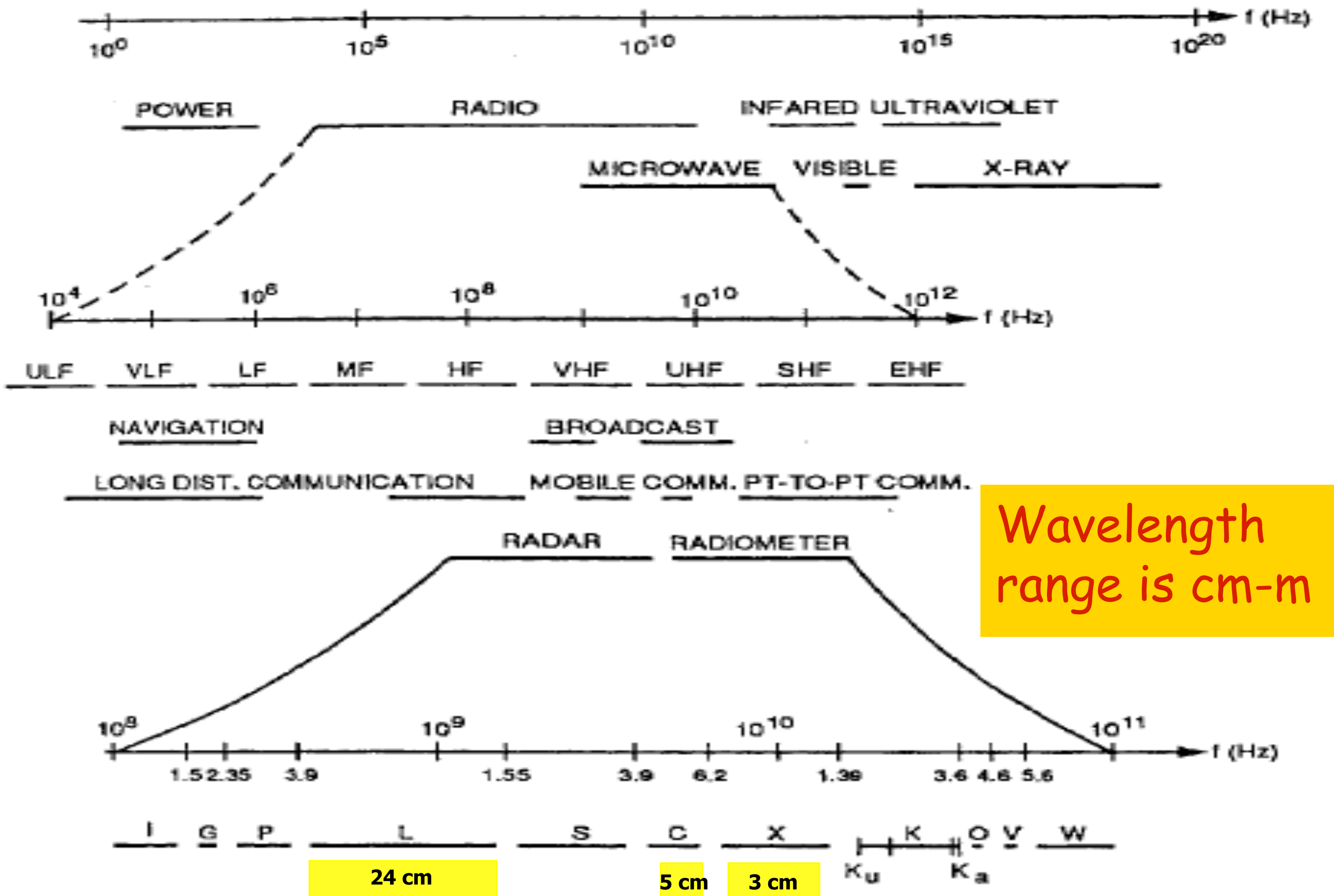

# Penetration (weather independent)

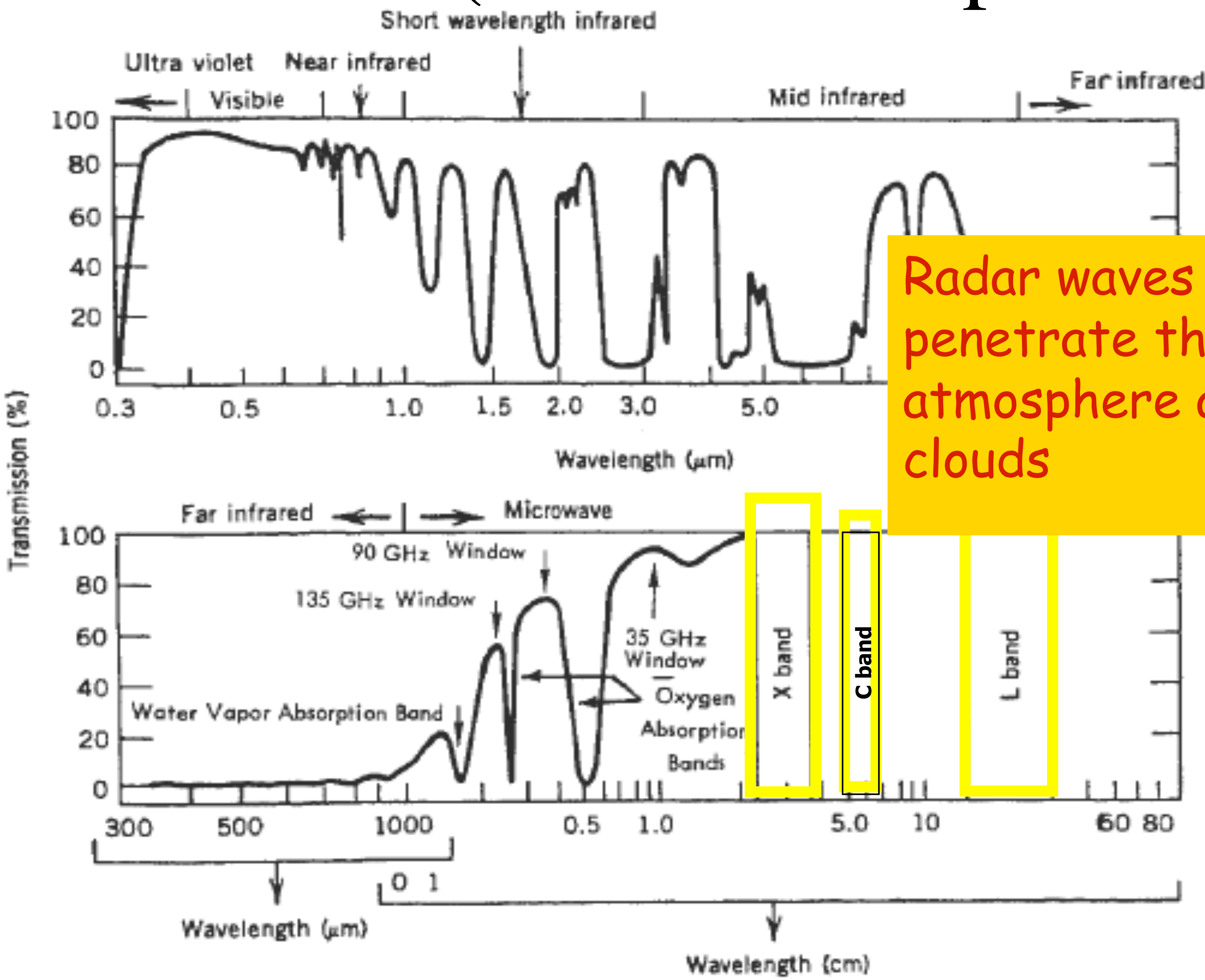


Radar waves penetrate the atmosphere and clouds


# Physics

Sahara, NW Sudan (SIR-A)

- Landsat optical
- Shuttle L-band radar
- What do we see?

Radar penetrates material with a low dielectric constant (dep. on wavelength)

*Here about 3 m.*

# Physics - Scattering

- Scattering is dominated by wavelength-scale structures
- Wavelength shorter: image brighter
- Specular and Bragg scattering
- Speckle

# Backscatter

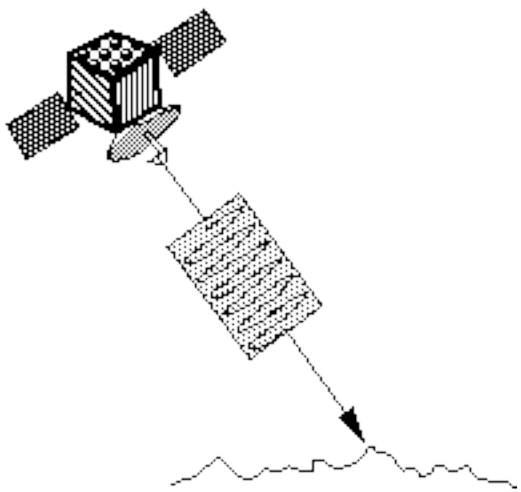

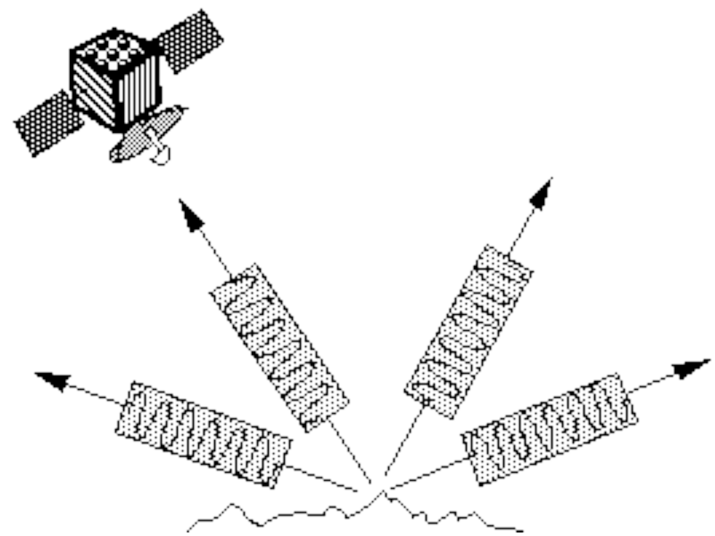

# Scattering

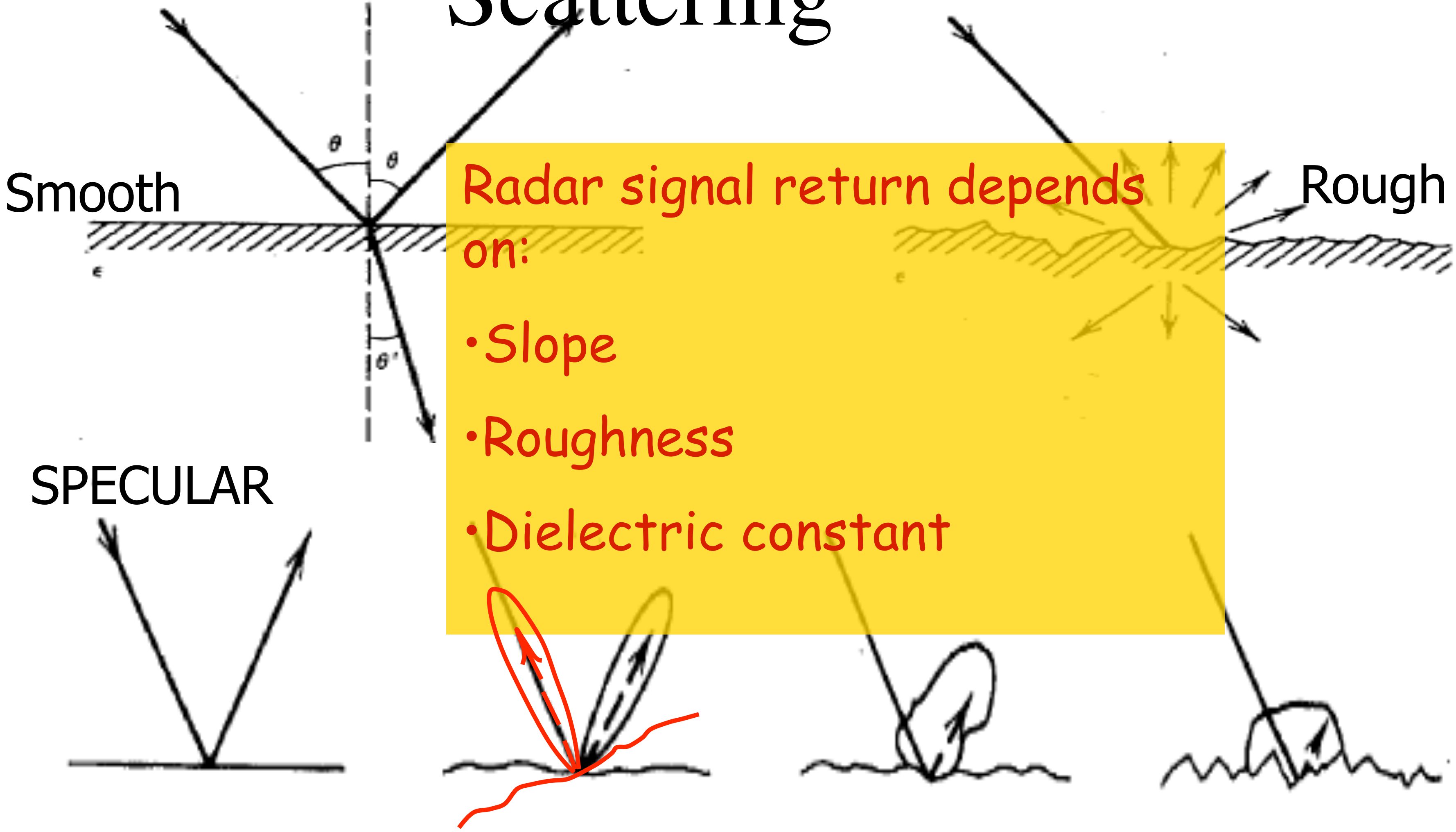


Radar signal return depends on:

- Slope
- Roughness
- Dielectric constant

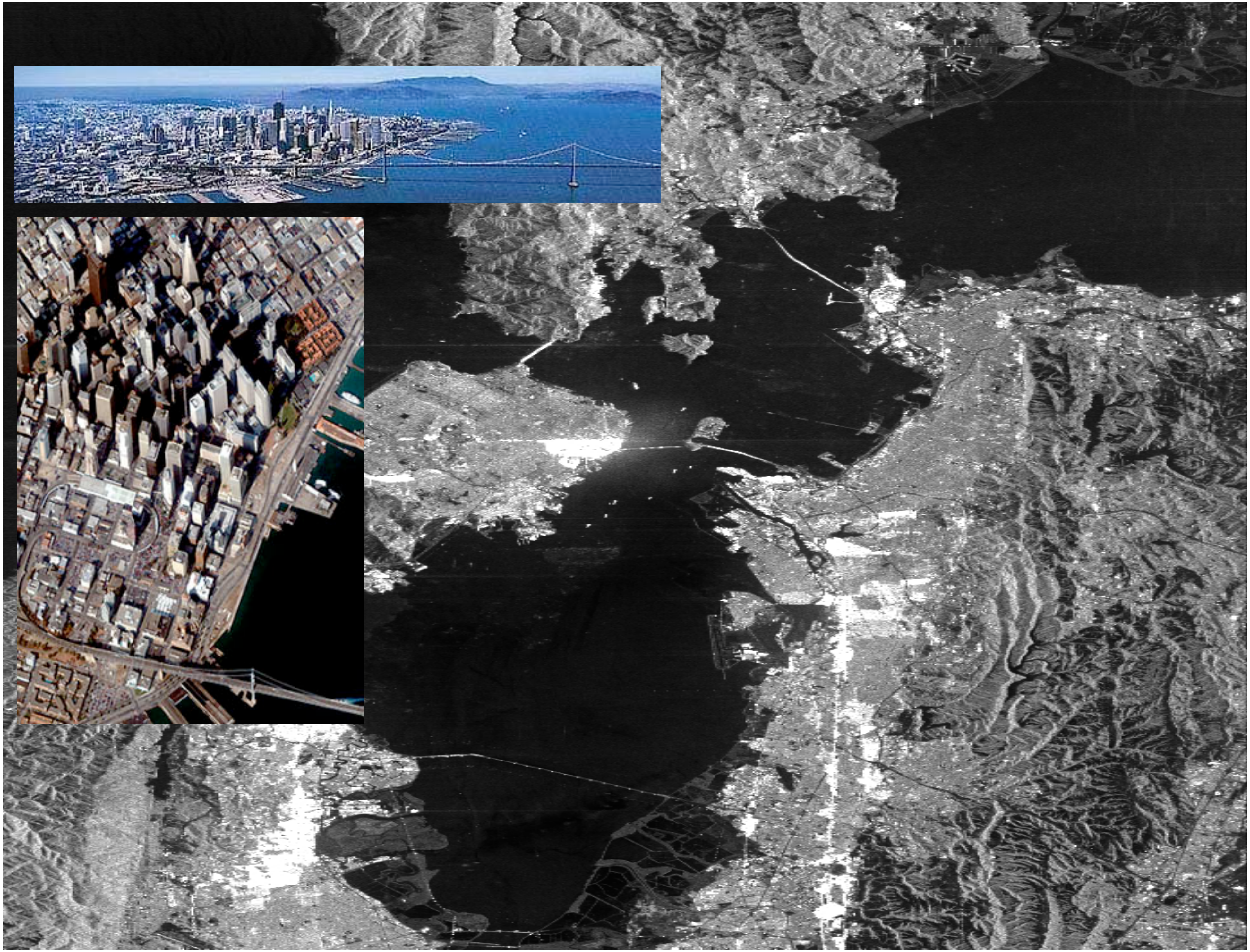

# Physics – scattering phase

Radar pixel phase is superposition of near-random scattering elements:

Unpredictable!

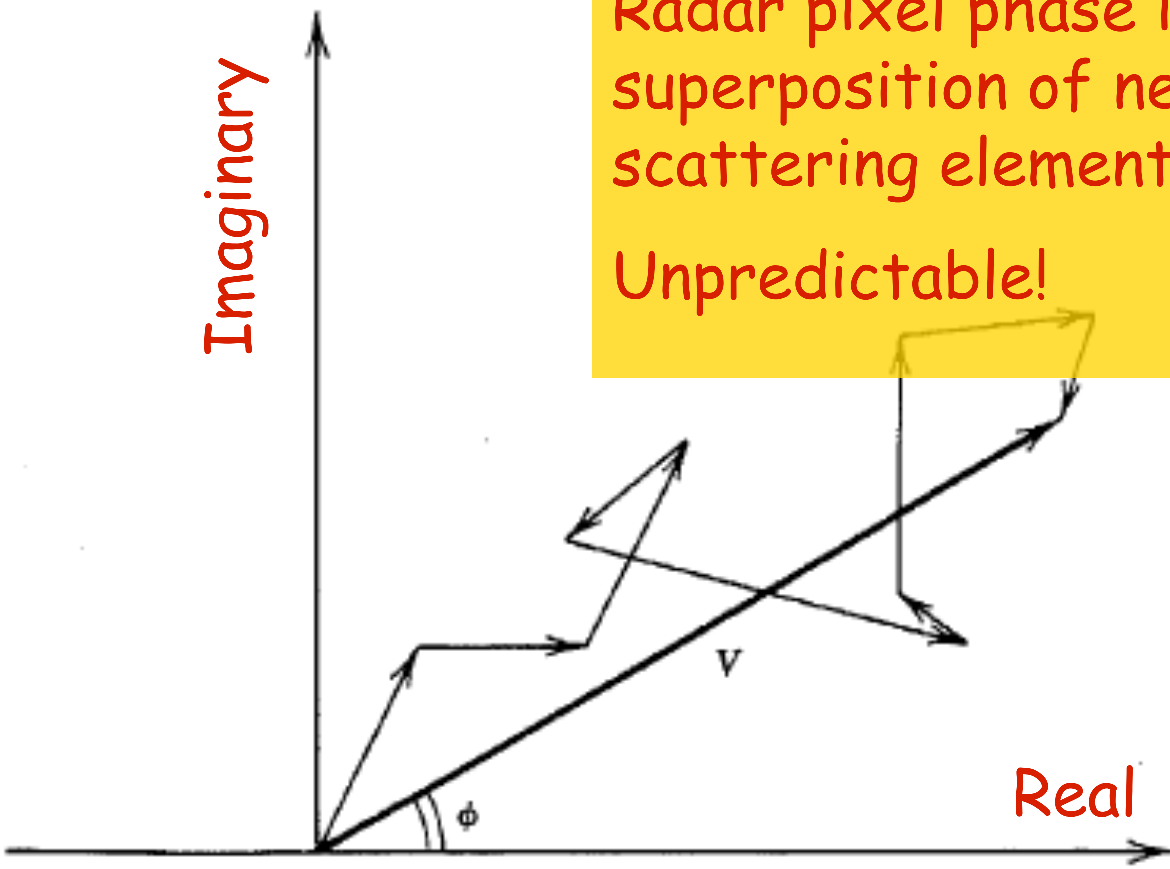


Composite return from an area with multiple scatters.

# Scattering Mechanisms

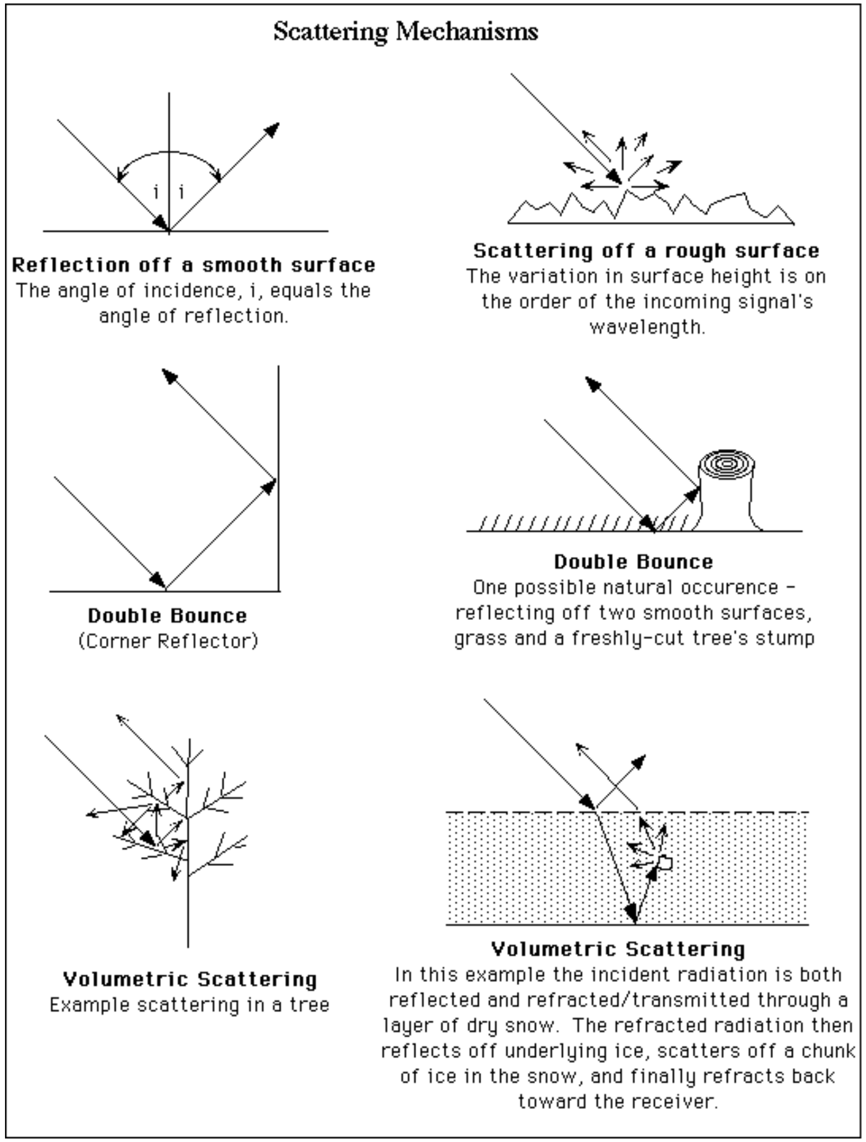

# Rule of Thumb in SAR images

•Backscattering Coefficient

•Smooth – Black
•Rough surface – white

•Calm water surface – black
•Water in windy day – white

•Hills and other large-scale surface variations tend to appear bright on one side and dim on the other.

•Human-made objects - bright spots (corner reflector)
•Strong corner reflector- Bright spotty cross (strong sidelobes)

# Geometry

Terminology

- Foreshortening, layover, shadow
- Why side-looking?
- Incidence angle,
- Coordinates range, azimuth

# Geometry

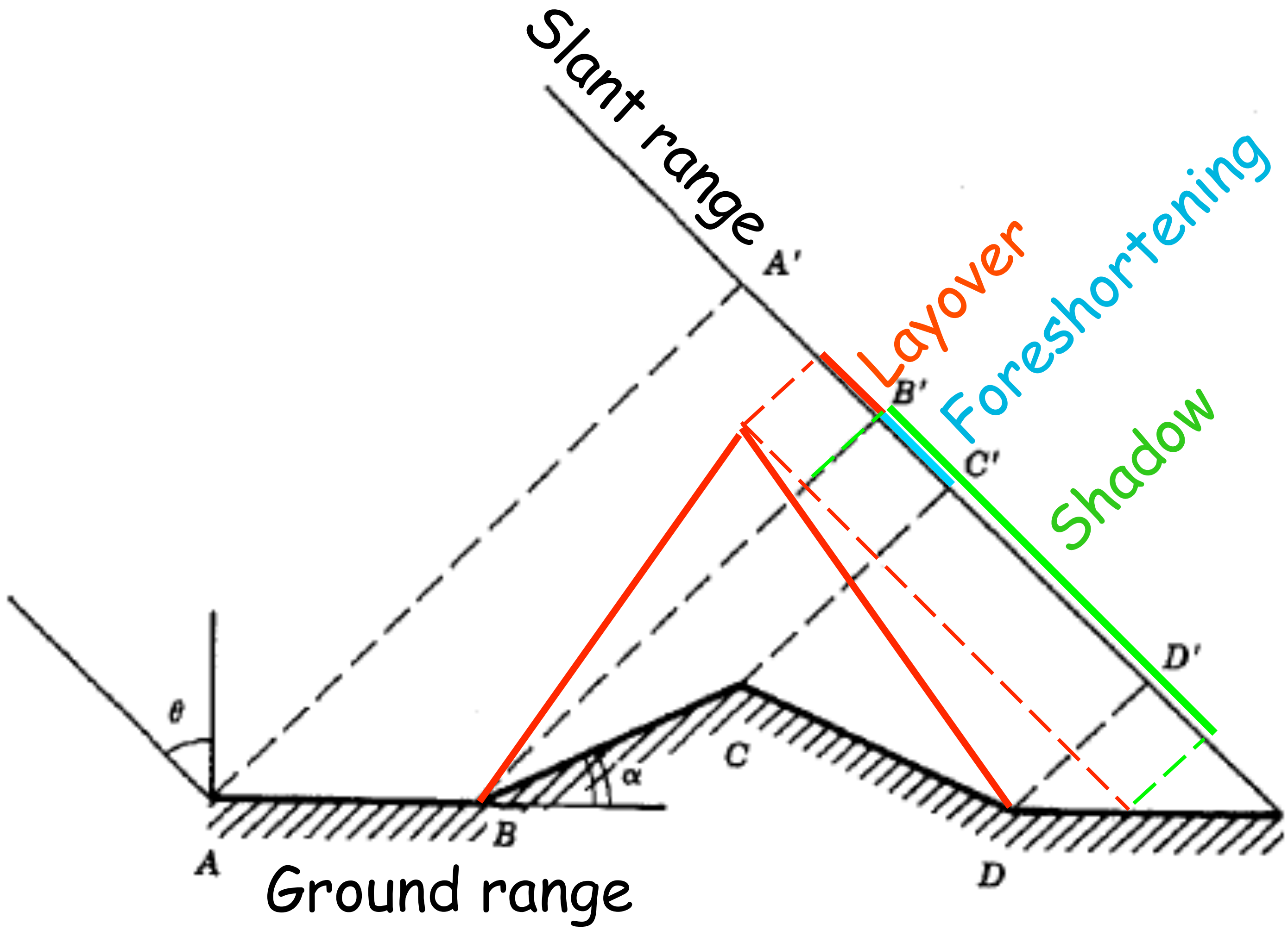
Slant range
A'
Layover
B'
Foreshortening
C'
Shadow
D'
θ
α
A
B
C
D
Ground range

# Geometry

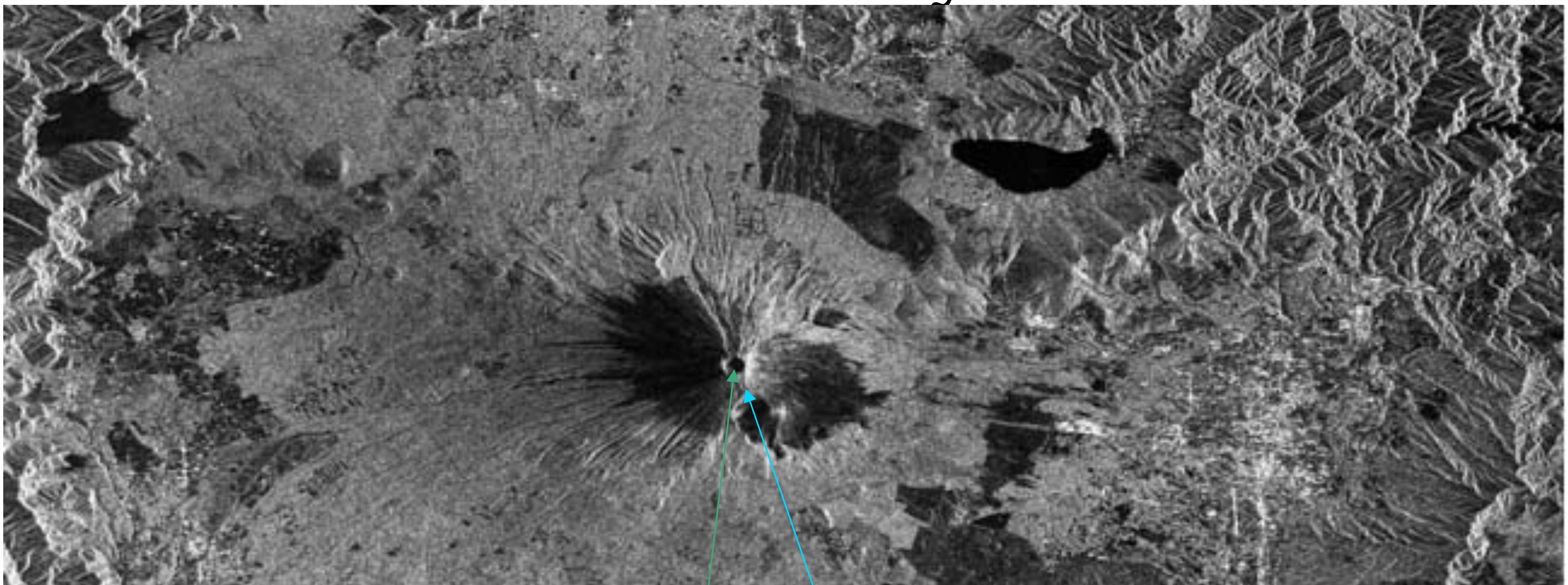


JERS-1 data (M.Shimada)

# Real Aperture vs. Synthetic Aperture

- Real Aperture :
  resolution ~ $R\lambda/L$

- Synthetic Aperture:
  resolution ~ $L/2$

  Irrespective of R
  Smaller, better?!
  - Carl Wiley (1951)

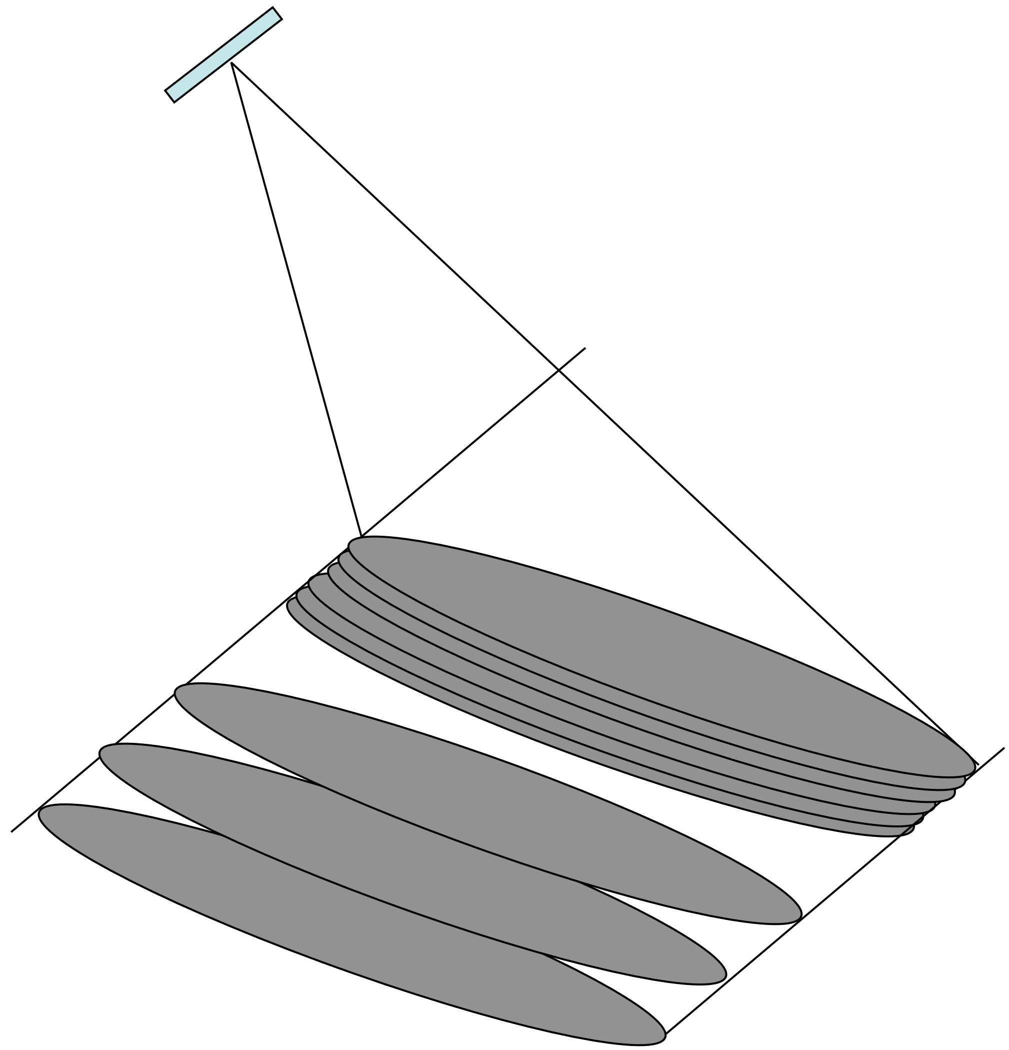

# Resolution I: RAR

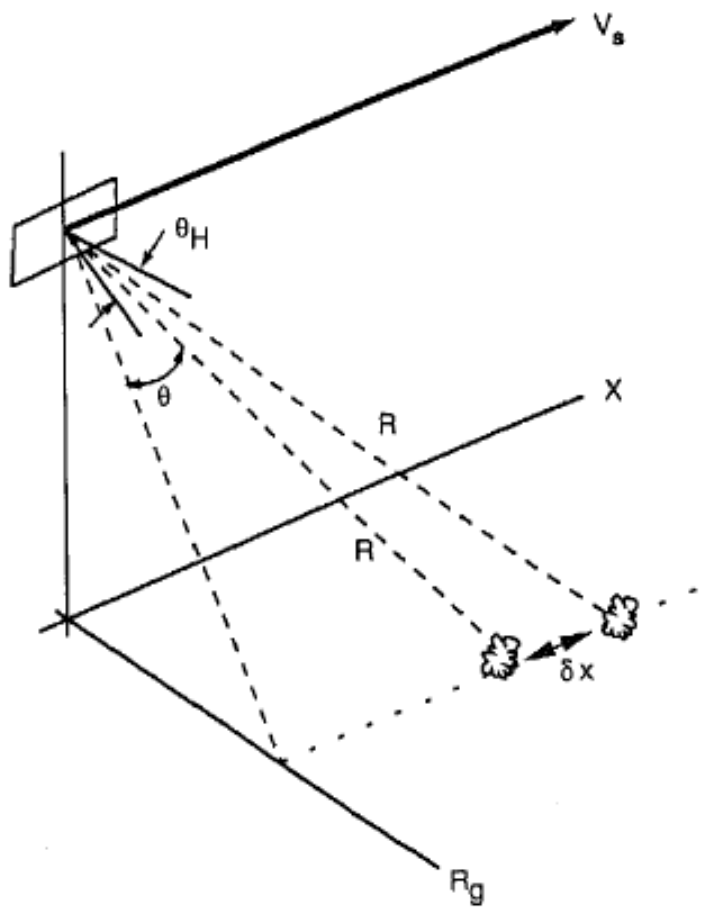


**Figure 1.8** Illustration of real-aperture radar capability to resolve two targets separated in azimuth.

- Real Aperture Radar
- Resolution dependent on antenna dimension/pulse length
- Beam width (half power width) is ratio of wavelength over antenna size:

$$\theta = \alpha \frac{\lambda}{D} \text{ with } 0.9 < \alpha < 1.4$$

# Antenna dimensions

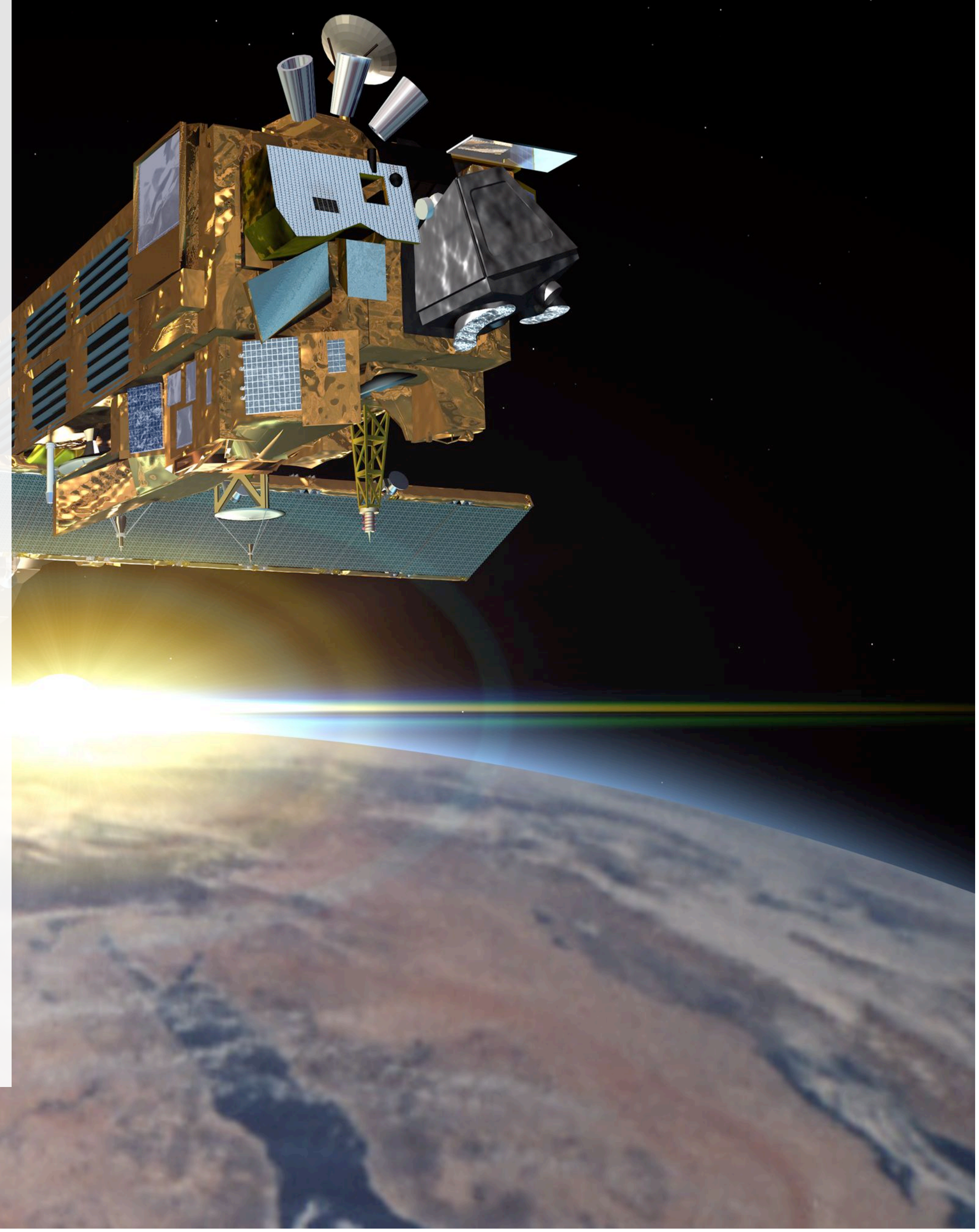

## Calculate Ground Resolution

C-band $\lambda$= ~0.05 m

D=10 m antenna

Beam angle = $5.10^{-2}/10$ = $5.10^{-3}$ rad

R=850 km

times $8.5.10^{5}$ = $42.10^{2}$[m] = 4.2 km

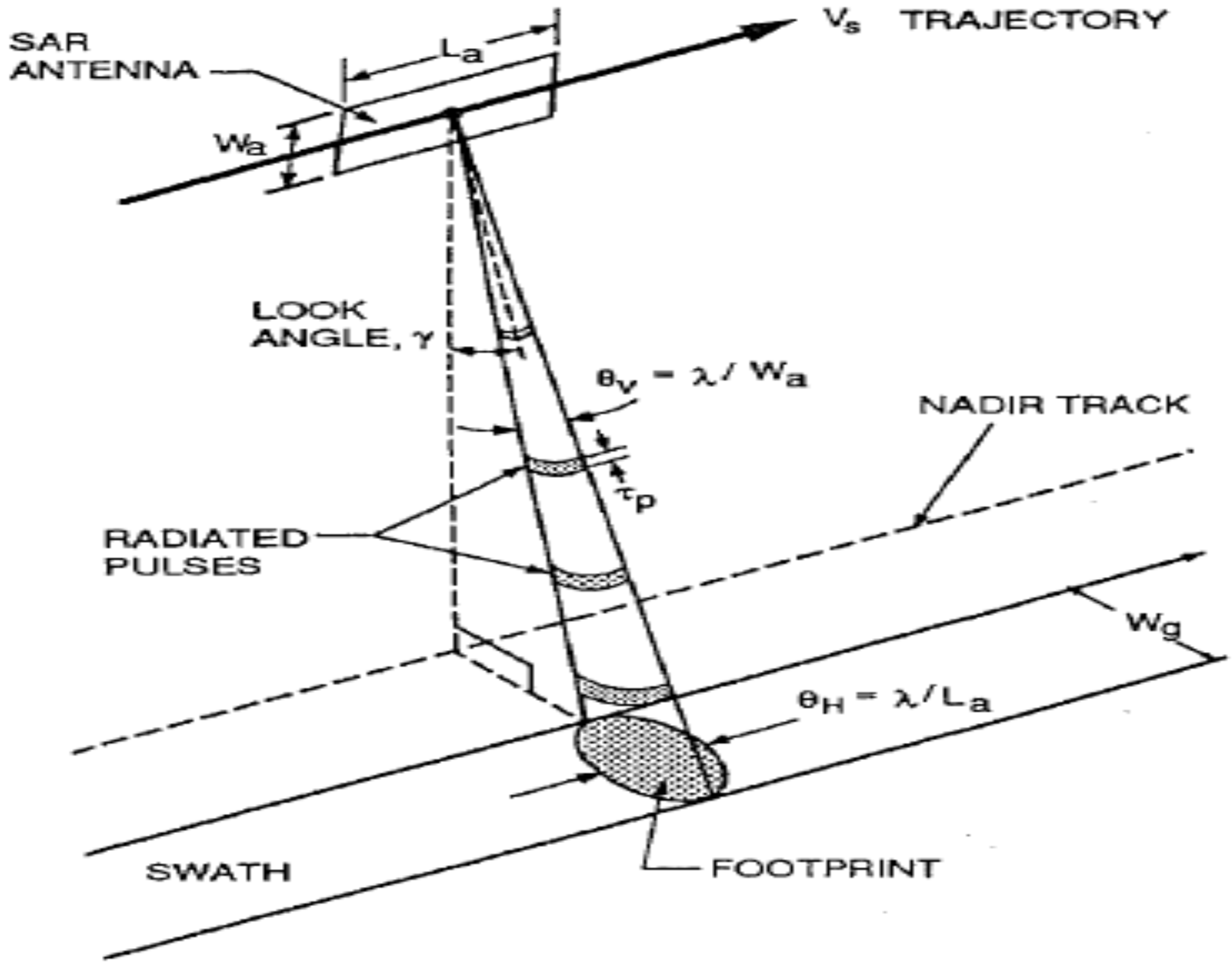

$V_s$ TRAJECTORY
SAR ANTENNA
$L_a$
$W_a$
LOOK ANGLE, $\gamma$
$\theta_V = \lambda / W_a$
NADIR TRACK
$\tau_p$
RADIATED PULSES
$W_g$
$\theta_H = \lambda / L_a$
SWATH
FOOTPRINT

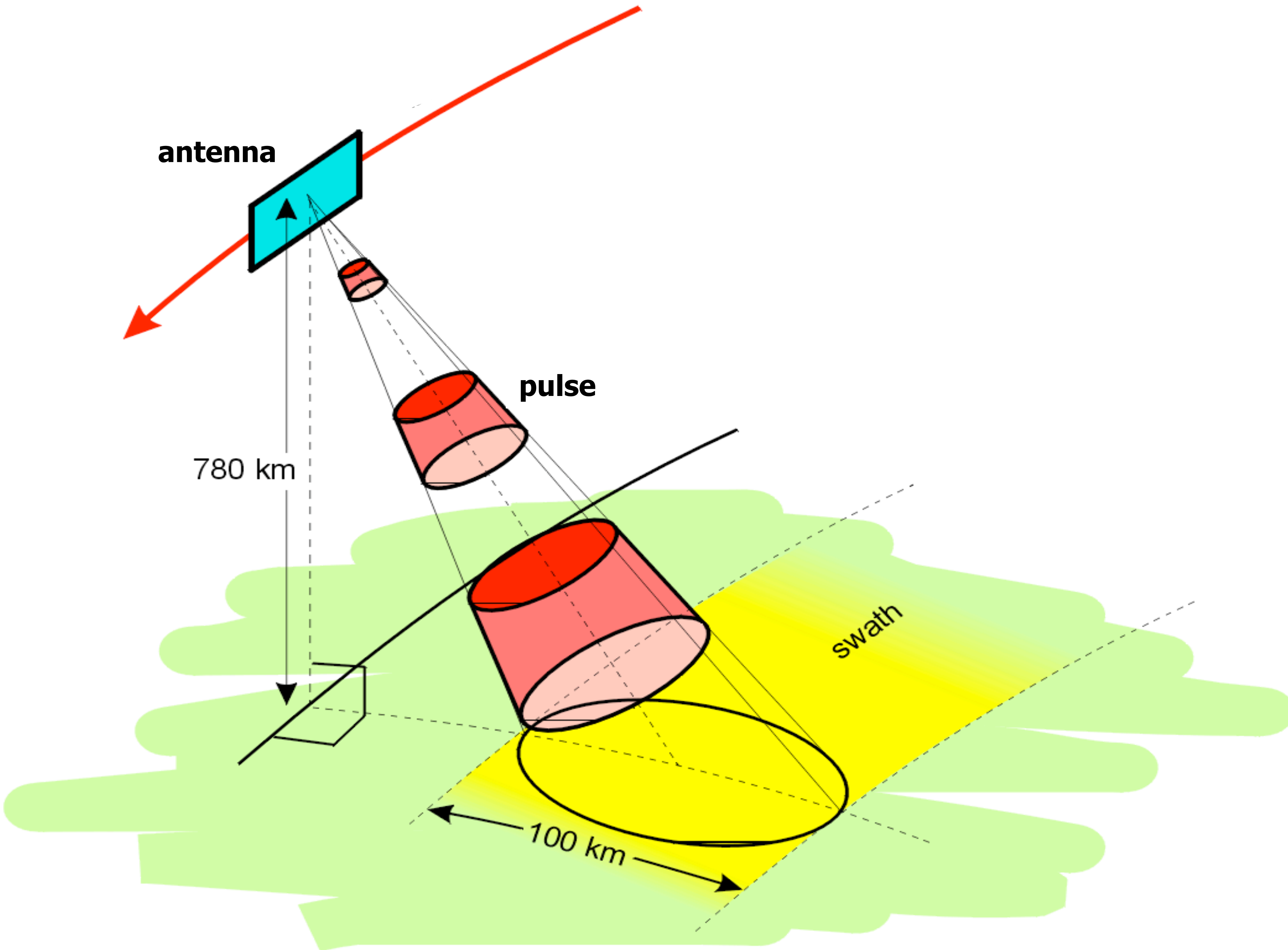

antenna
pulse
780 km
swath
100 km

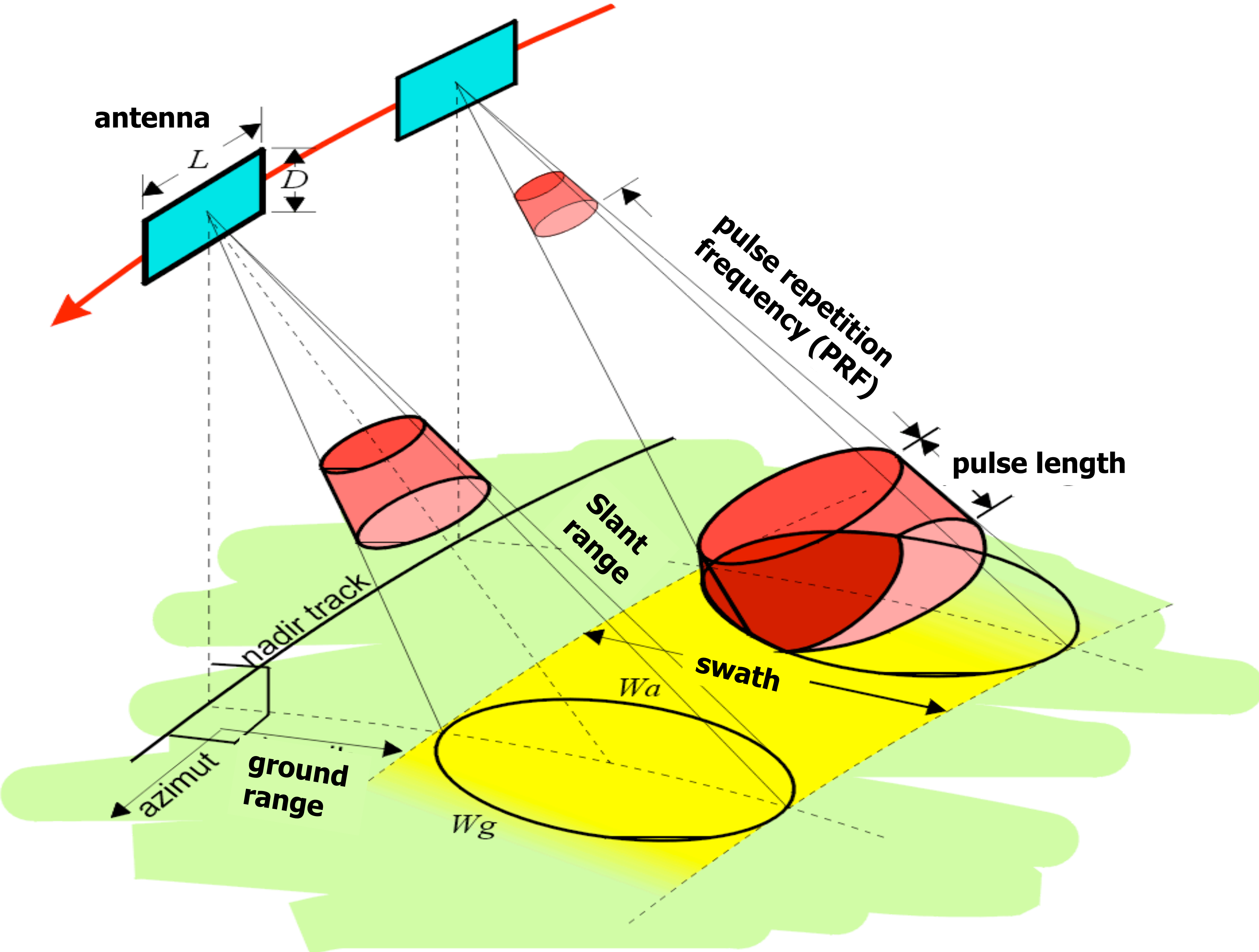

antenna
L
D
pulse repetition frequency (PRF)
pulse length
Slant range
nadir track
swath
Wa
Wg
azimut
ground range

# Improvement in Resolution
## (Crimea, Ukraine)

Real Aperture Radar

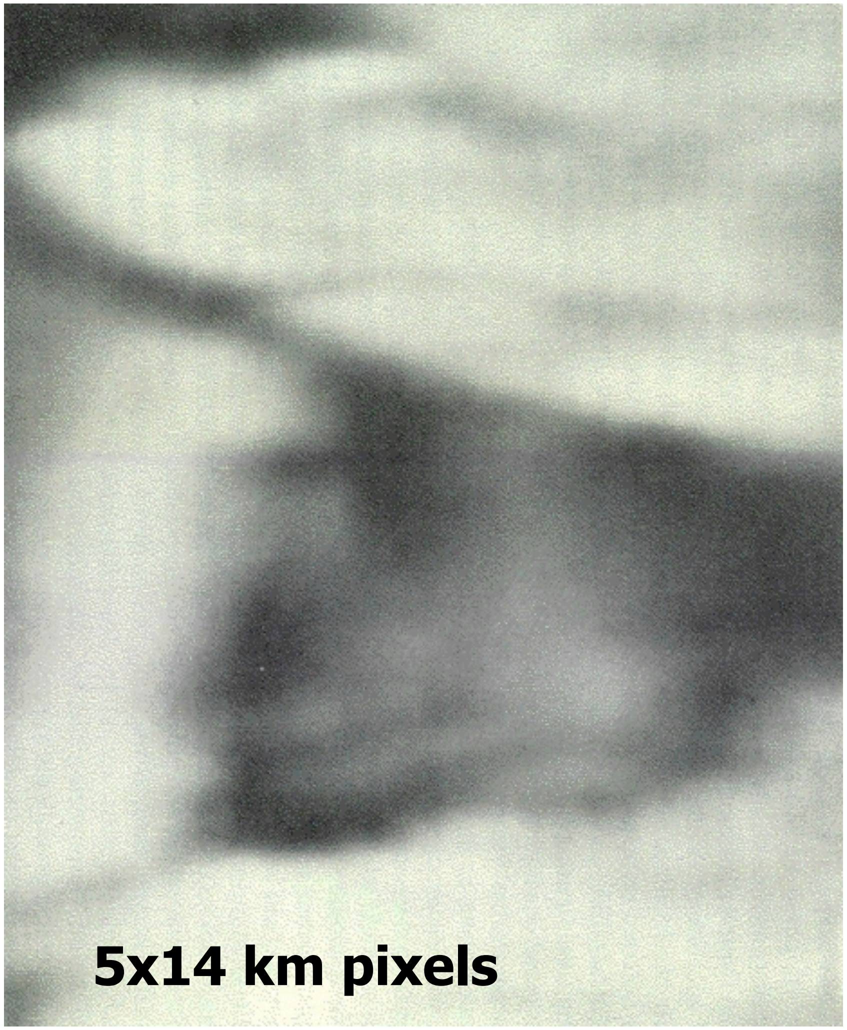


Massonnet and Feigl, 1998

# Improvement of along-track resolution

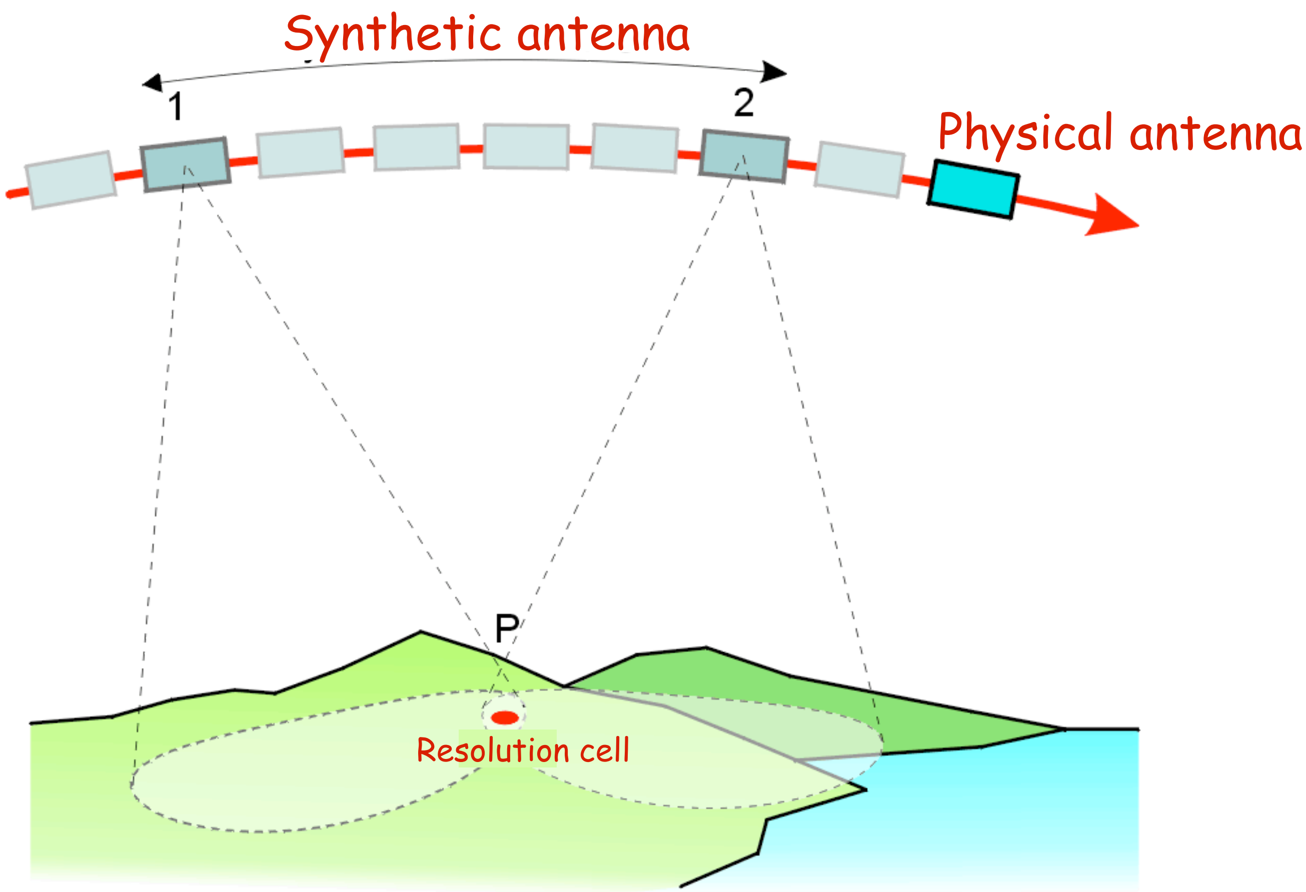

# Improvement in Resolution

## (Crimea, Ukraine)

Real Aperture Radar

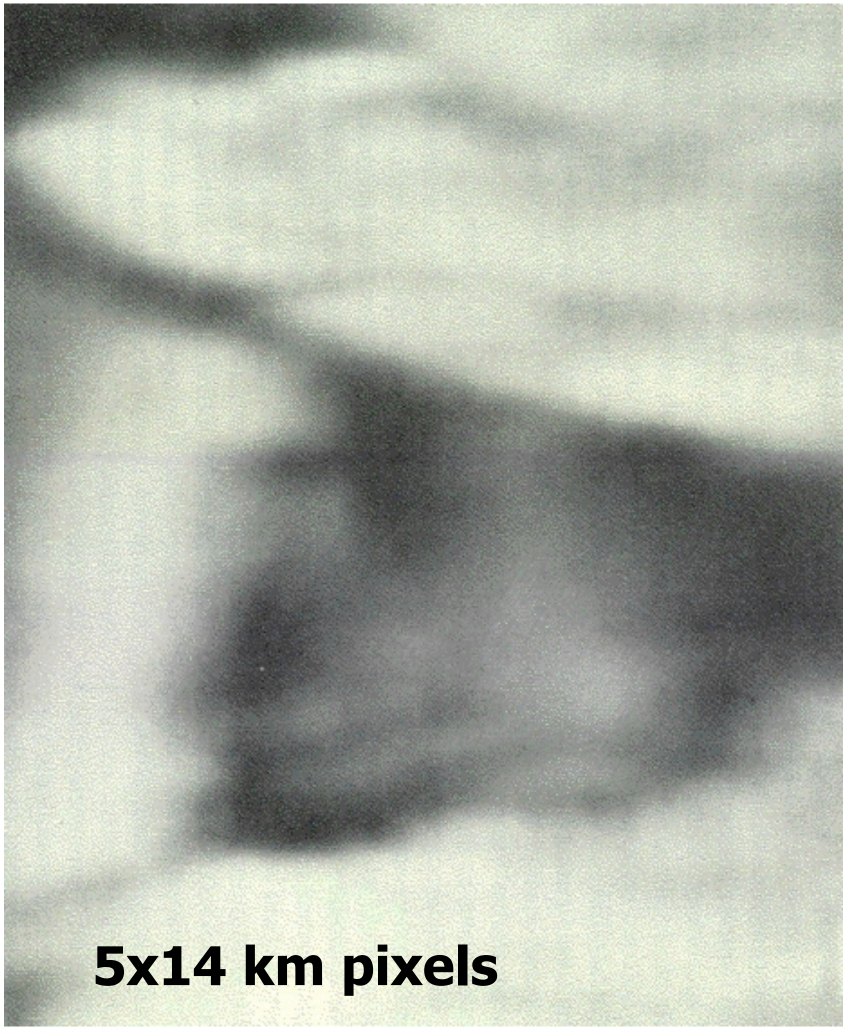


Synthetic Aperture Radar

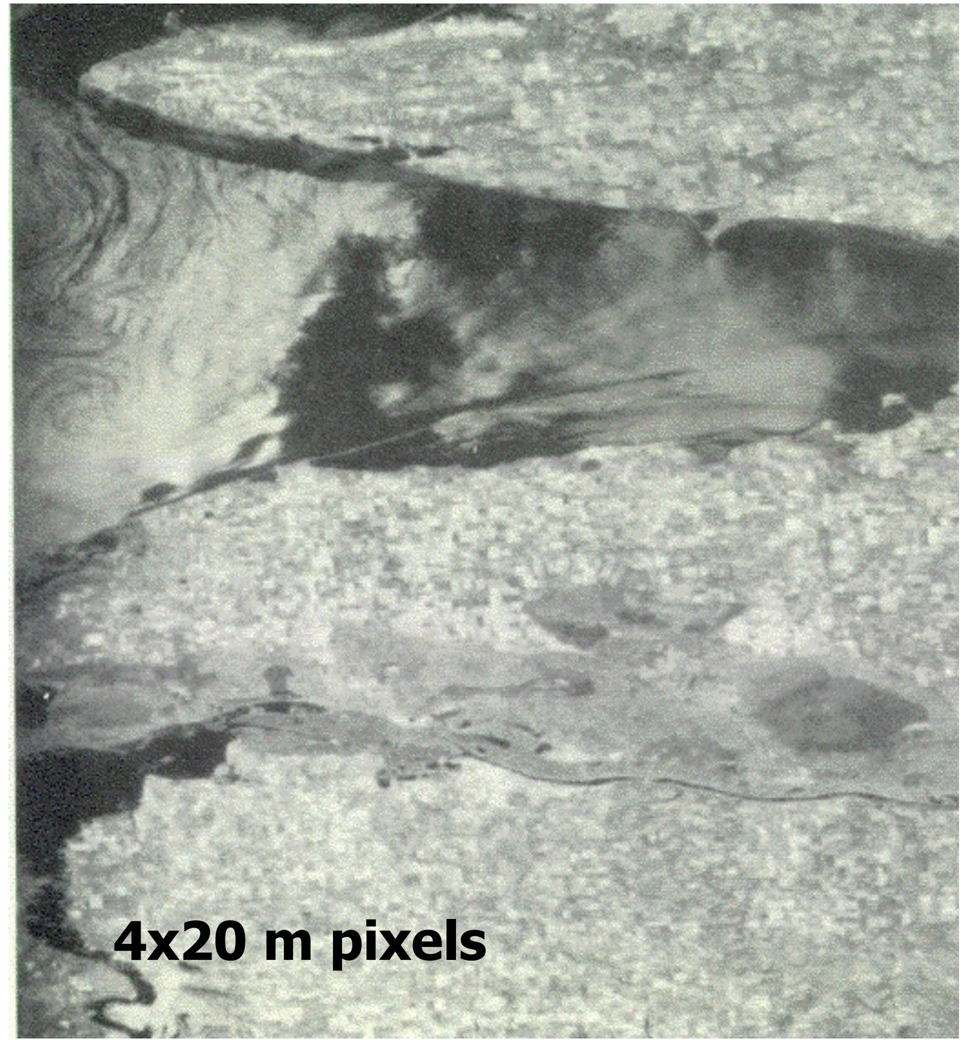


Massonnet and Feigl, 1998

# Radar Interferometry

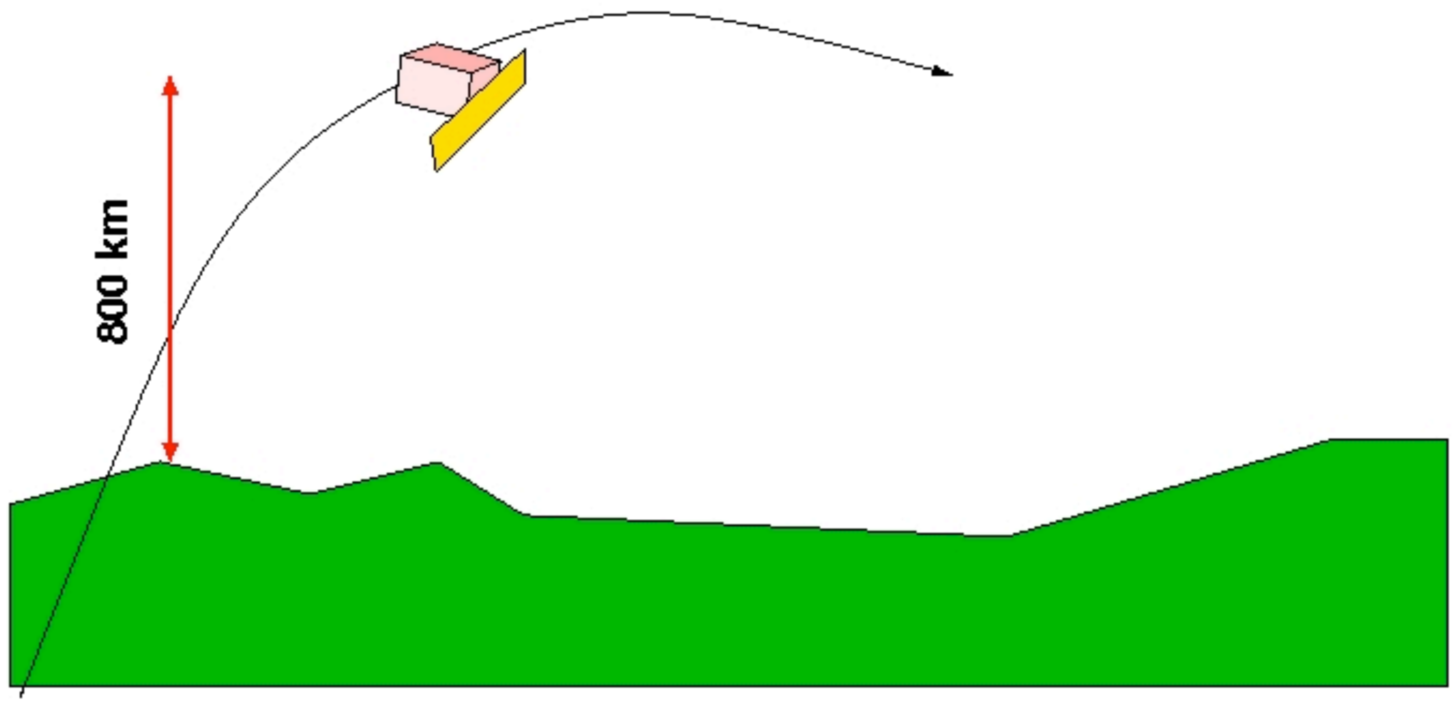

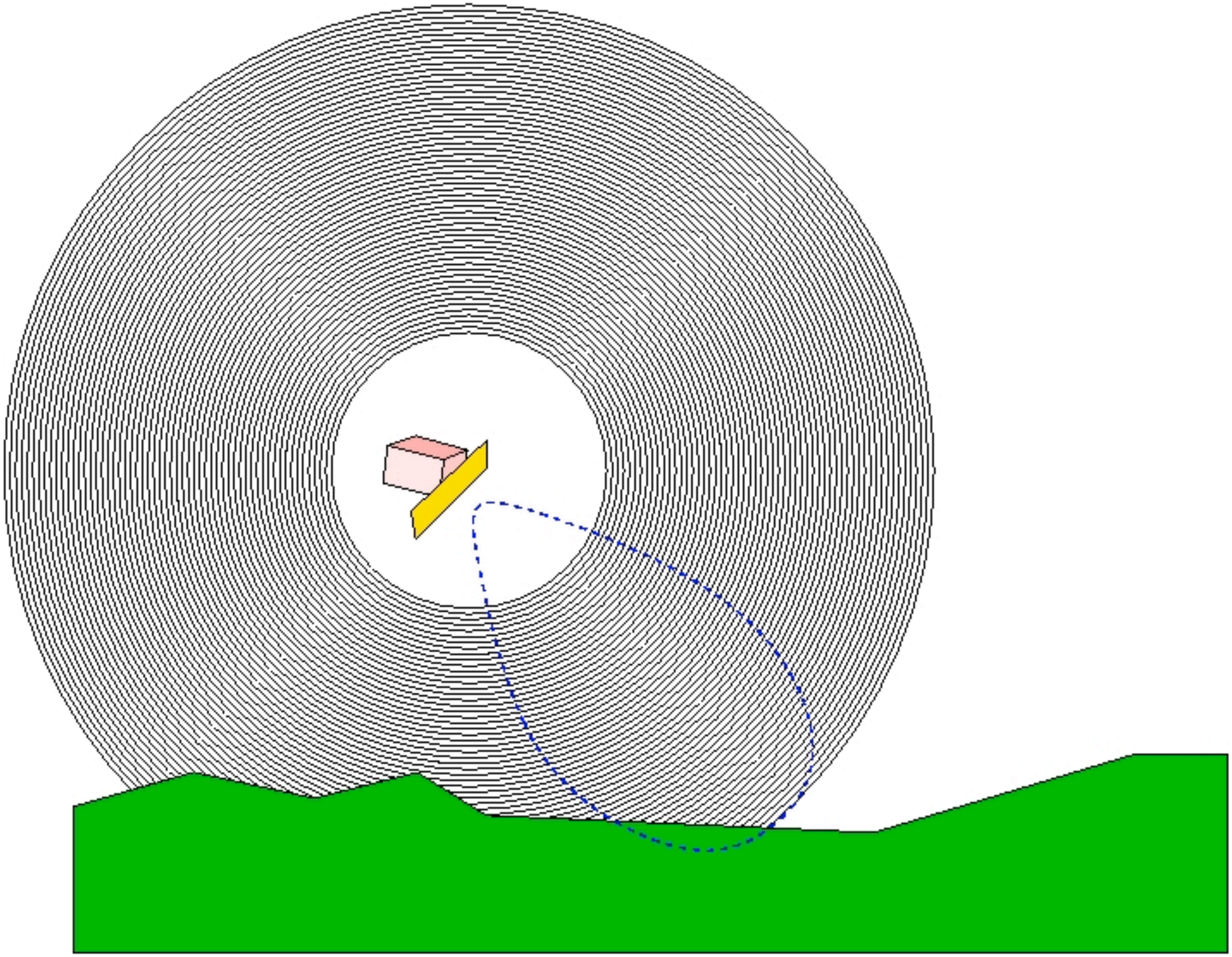

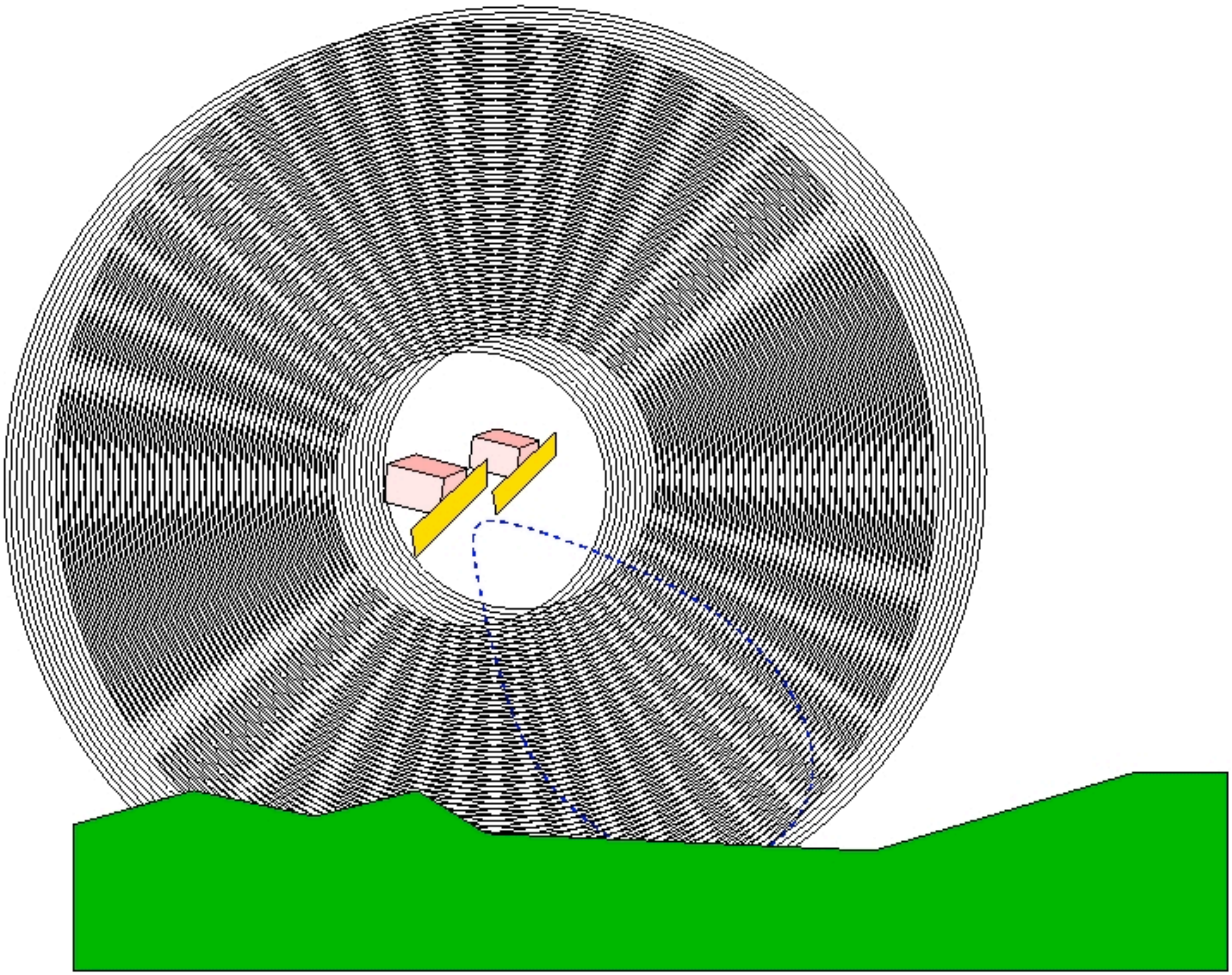

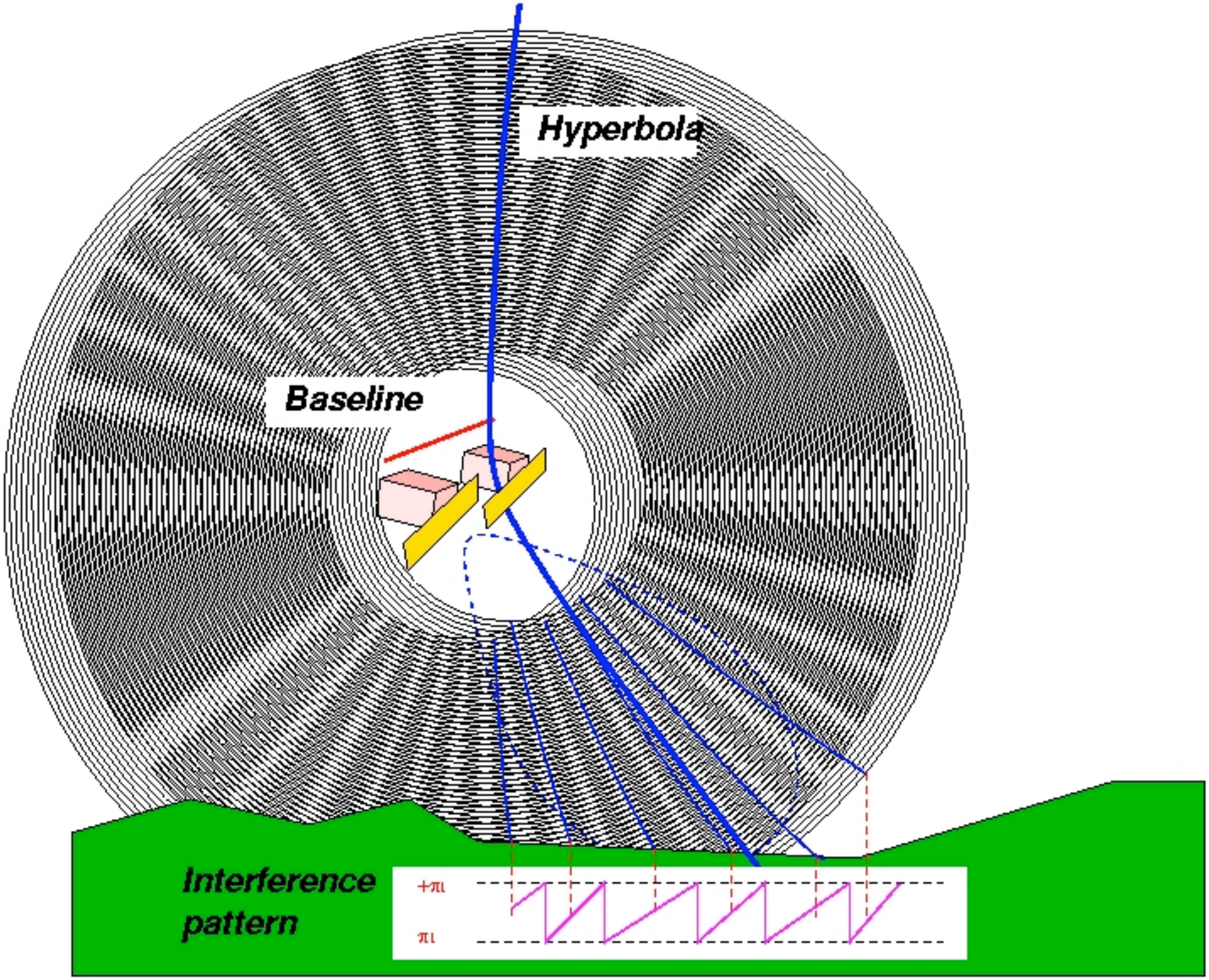
Hyperbola
Baseline
Interference pattern
+π
π

# Example in 2D: interferogram

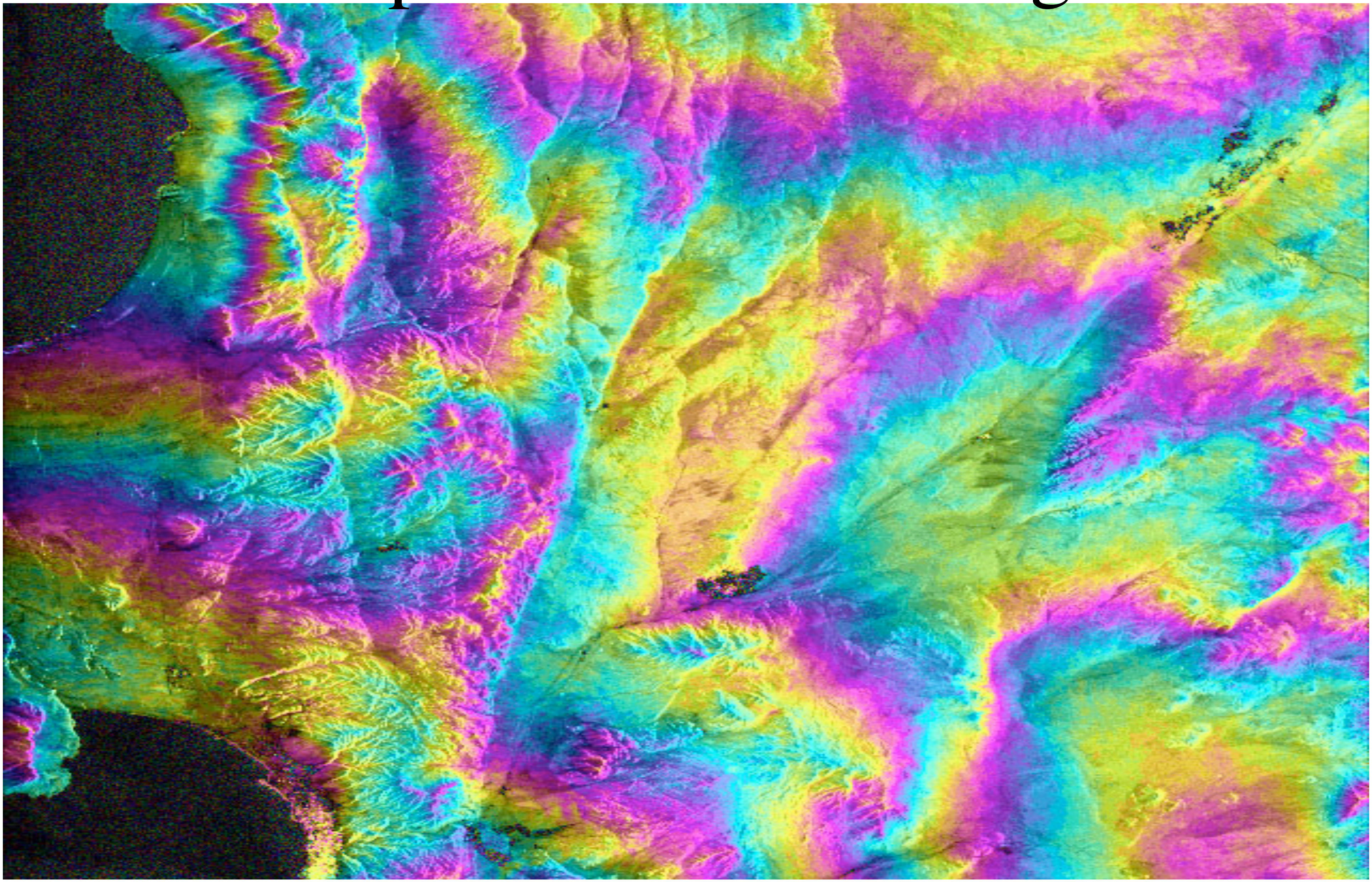

# SAR Interferometry (InSAR)

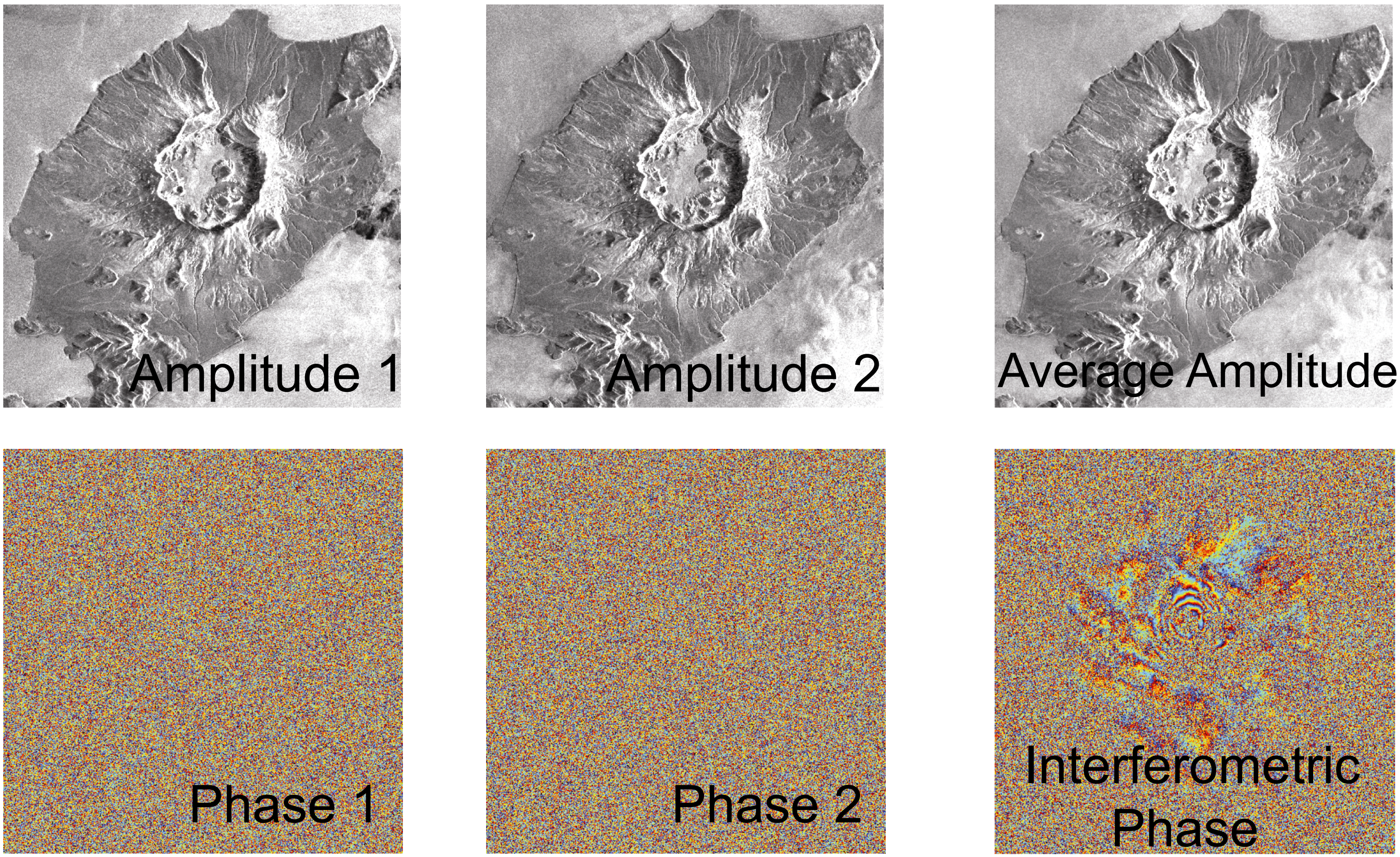

# Basics: Interferogram Formation I

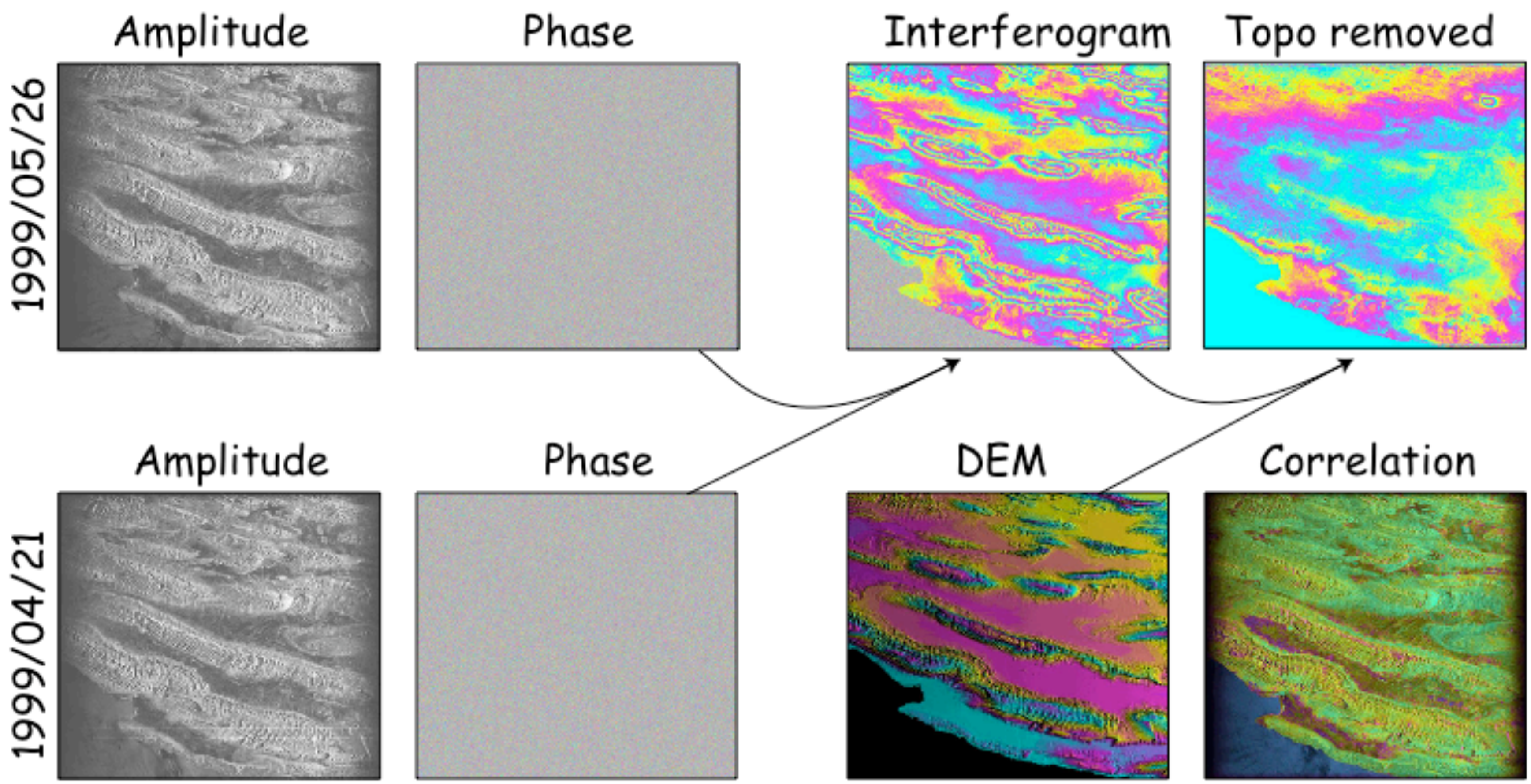

# Effect of SAR Frequency

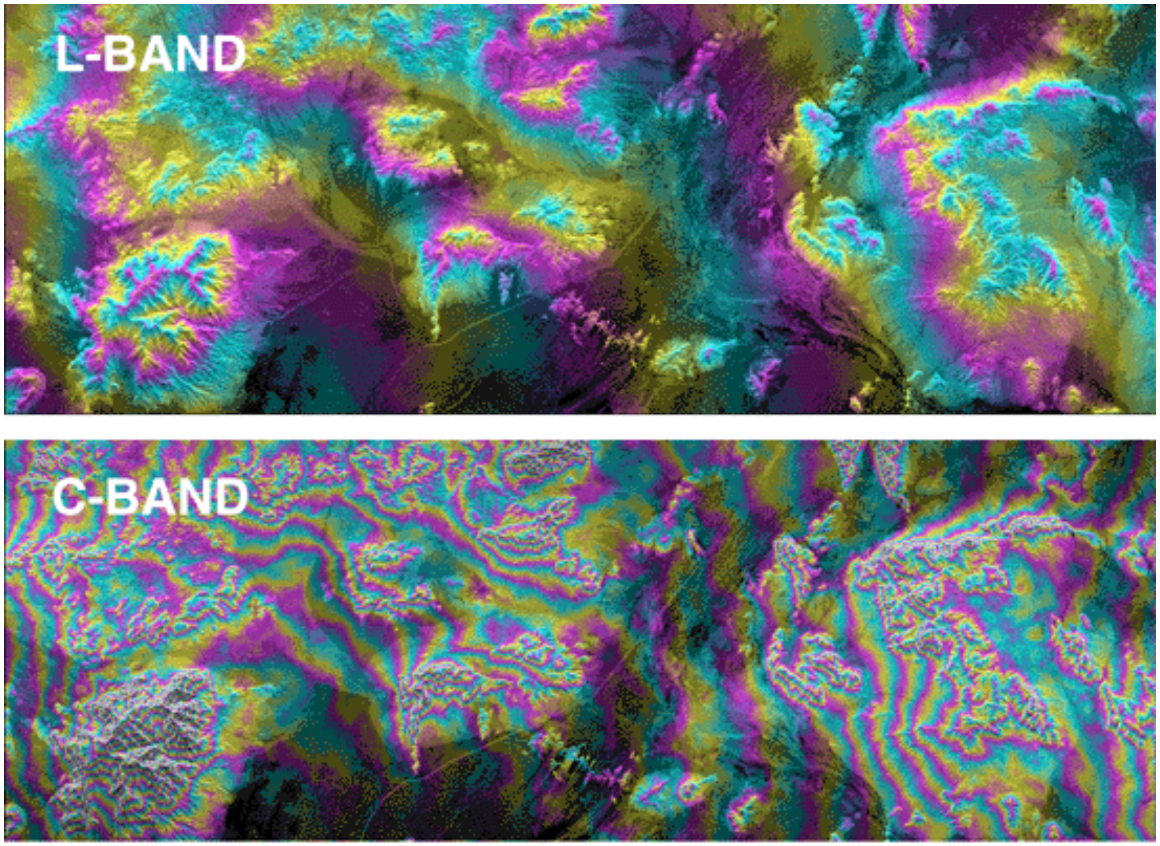


SIR-C L, C BAND INTERFEROGRAMS
FT. IRWIN, CALIFORNIA

L band: longer $\lambda$, fewer fringes, better coherence

# Why is Coherence Better at L-band?

- Coherence is a measure of how well the phase of adjacent pixels agree with each other
  - Random phase = low or zero coherence
- C-band radars usually have poor coherence in vegetated areas.
  - Leaves on trees tend to have size ~ wavelength
    - Therefore are effective scatterers
    - Leaves move (wind, growth) and change (fall off)
- L-band scattering is dominated by features 20-25 cm in scale
  - More likely to be ground features or unchanging features of vegetation (large branches)
- Some other notes on coherence
  - Plowed fields have bad coherence
  - Permanent structures (buildings, roads) usually have good coherence.
  - Surprisingly, certain kinds of swamps seem to have good coherence with returns that depend on the water level.

# Range

Expressed as phase (radians)

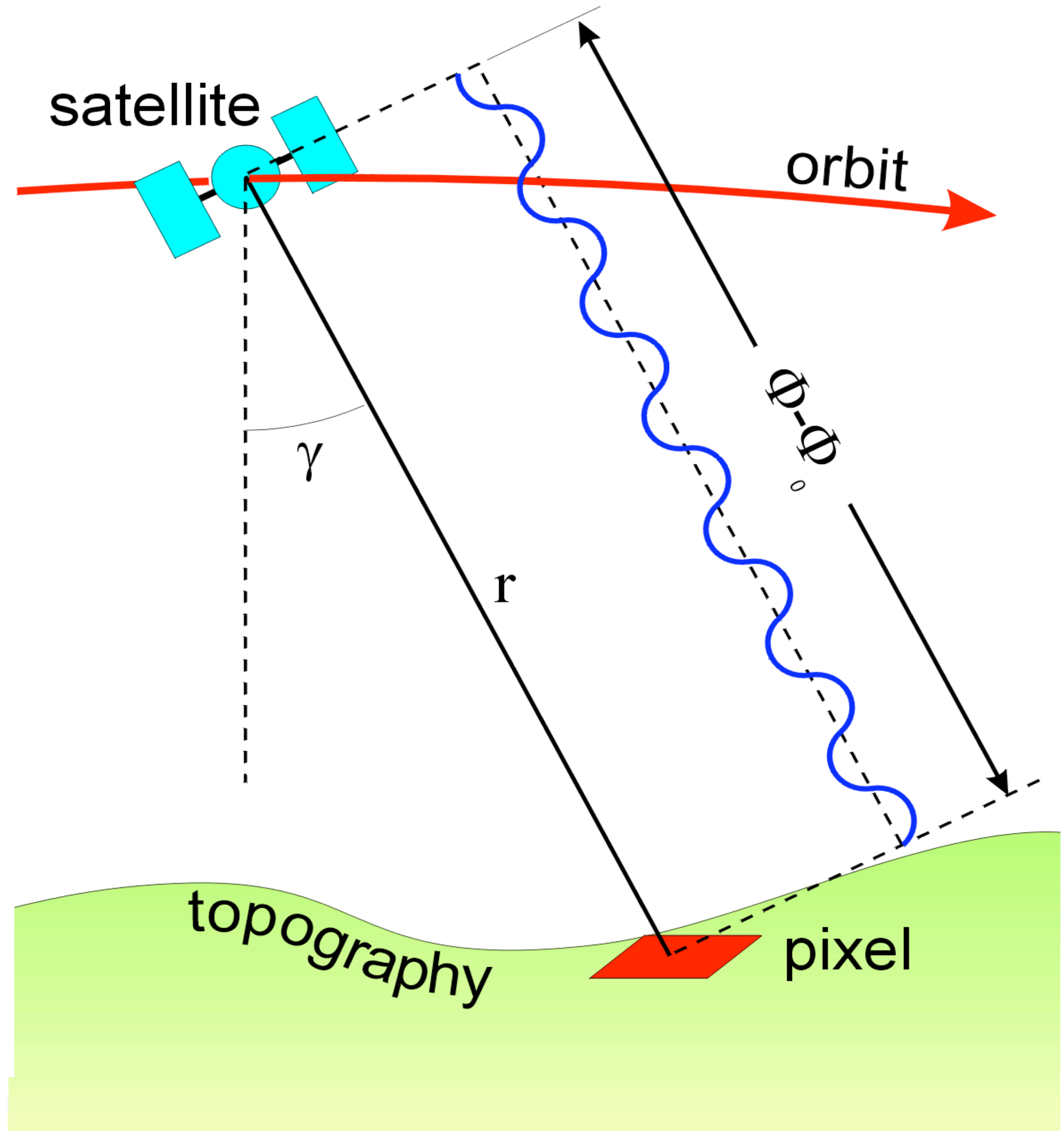

# Range

Expressed as integer cycles + fractional phase

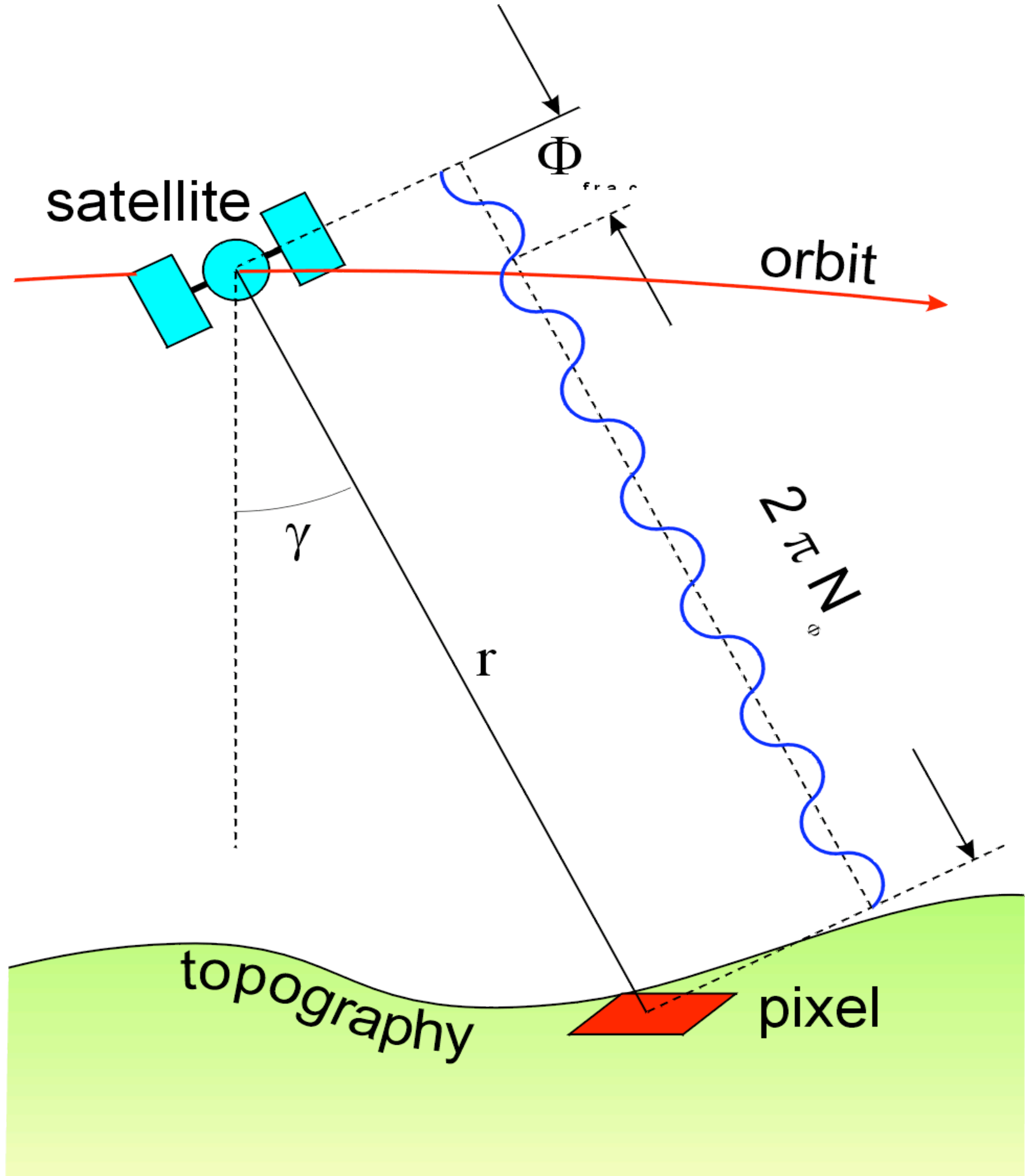

# Phase-range relationship

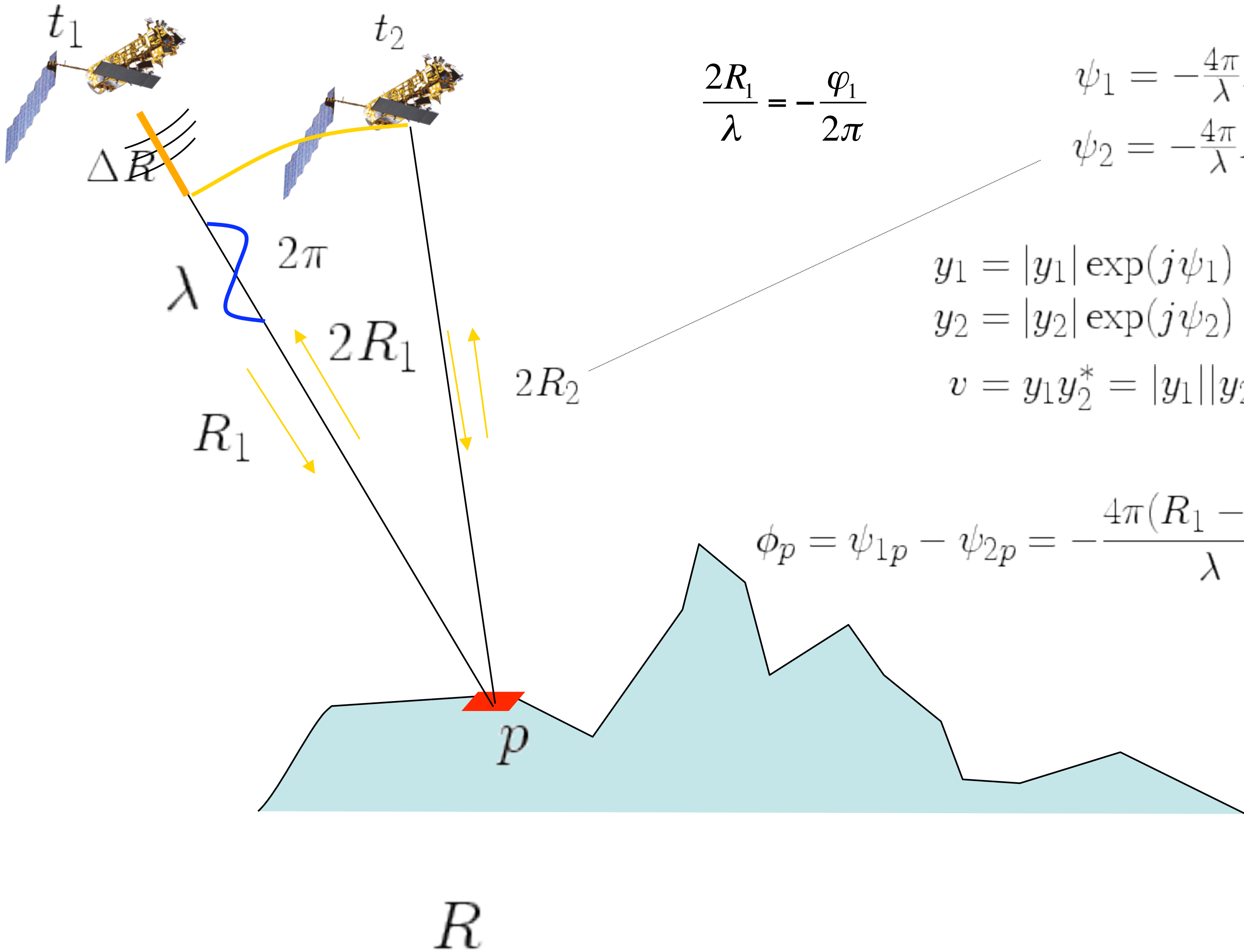


$$\frac{2R_1}{\lambda} = -\frac{\varphi_1}{2\pi}$$

$$\psi_1 = -\frac{4\pi}{\lambda} R_1$$

$$\psi_2 = -\frac{4\pi}{\lambda} R_2$$

$$y_1 = |y_1| \exp(j\psi_1)$$

$$y_2 = |y_2| \exp(j\psi_2)$$

$$v = y_1 y_2^* = |y_1||y_2| \exp(j(\psi_1 - \psi_2))$$

$$\phi_p = \psi_{1p} - \psi_{2p} = -\frac{4\pi(R_1 - R_2)}{\lambda} = -\frac{4\pi \Delta R}{\lambda}$$

# Phase-height relationship

(Far-field approximation)

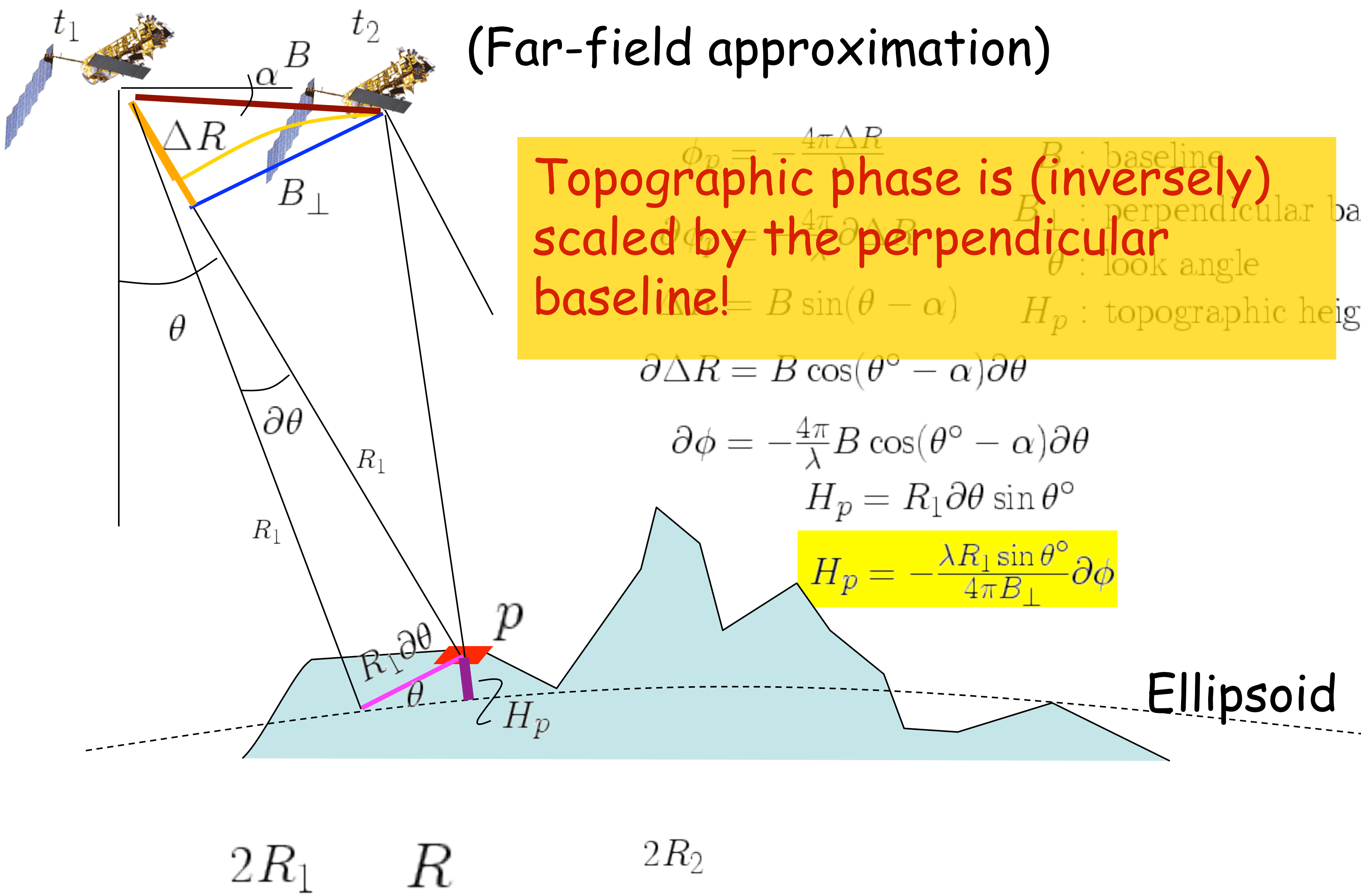


Topographic phase is (inversely) scaled by the perpendicular baseline!

$$\phi_p = -\frac{4\pi\Delta R}{\lambda}$$

$$\partial\phi_p = -\frac{4\pi\partial\Delta R}{\lambda}$$

$$\Delta R = B\sin(\theta - \alpha)$$

$B$ : baseline

$B_\perp$ : perpendicular baseline

$\theta$ : look angle

$H_p$ : topographic height

$$\partial\Delta R = B\cos(\theta^\circ - \alpha)\partial\theta$$

$$\partial\phi = -\frac{4\pi}{\lambda}B\cos(\theta^\circ - \alpha)\partial\theta$$

$$H_p = R_1\partial\theta\sin\theta^\circ$$

$$H_p = -\frac{\lambda R_1\sin\theta^\circ}{4\pi B_\perp}\partial\phi$$

# Height ambiguity

$$H_p = -\frac{\lambda R_1 \sin\theta^\circ}{4\pi B_\perp}\partial\phi$$

Height difference related to 1 phase cycle:

$$H_{2\pi} = \frac{-\lambda R_1 \sin\theta^\circ}{4\pi B_\perp}2\pi = \frac{-\lambda R_1 \sin\theta^\circ}{2B_\perp}$$

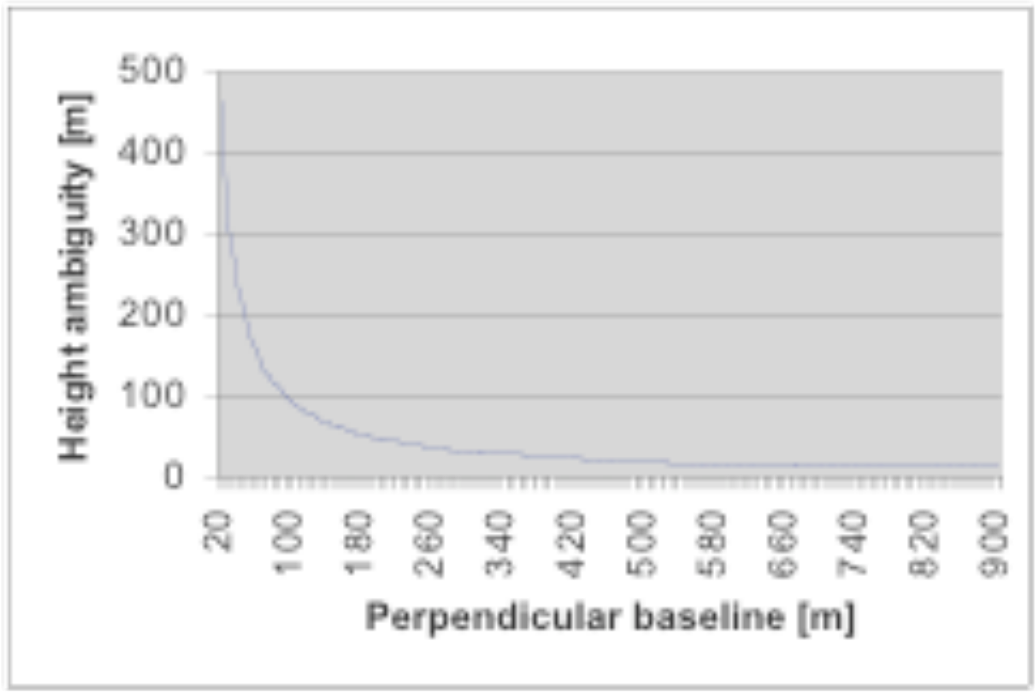

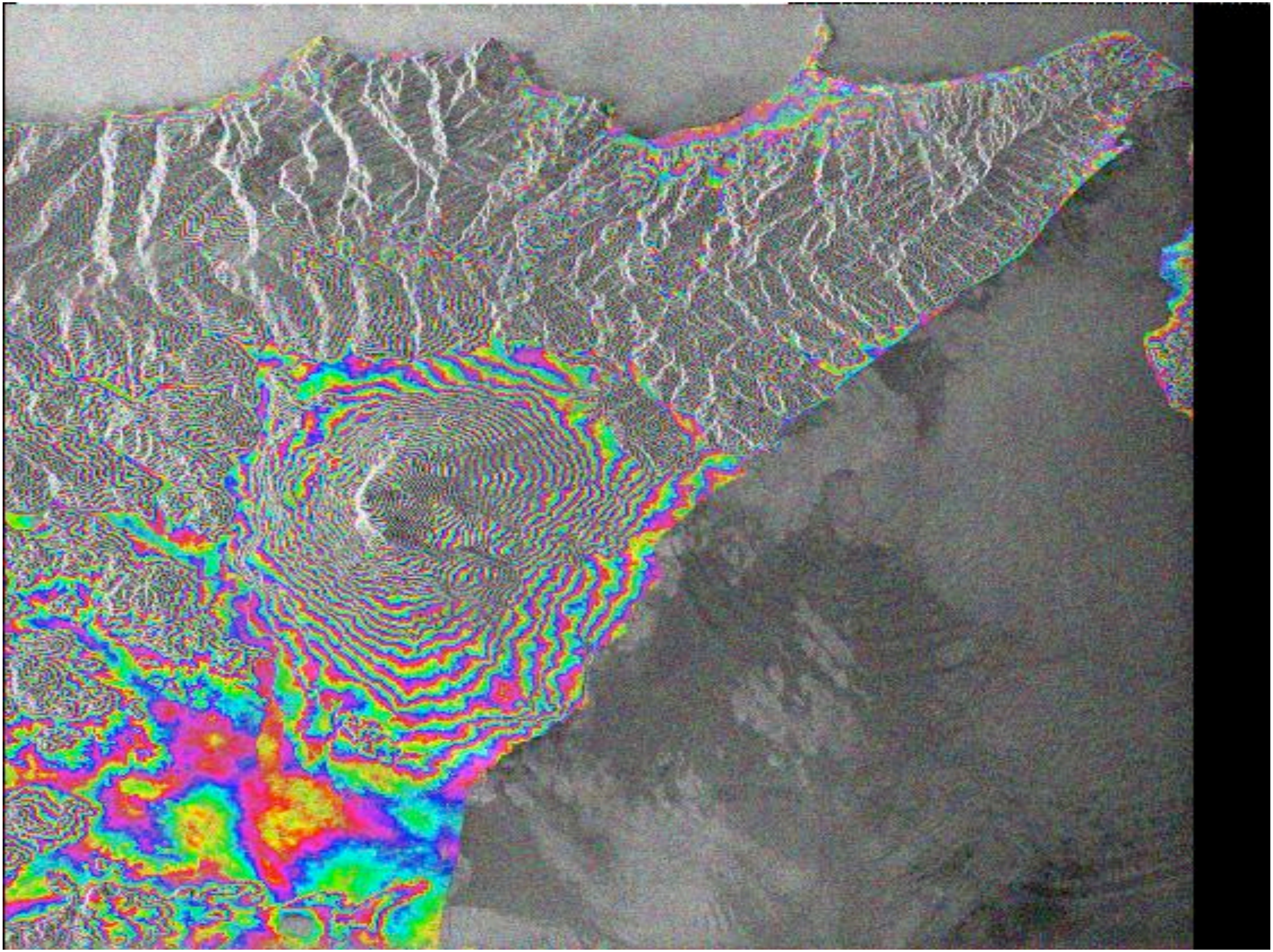

# Baseline dependency, height ambiguity

**Bperp 173 m, Bt= 1day**

**$H_{2pi}$=45m**

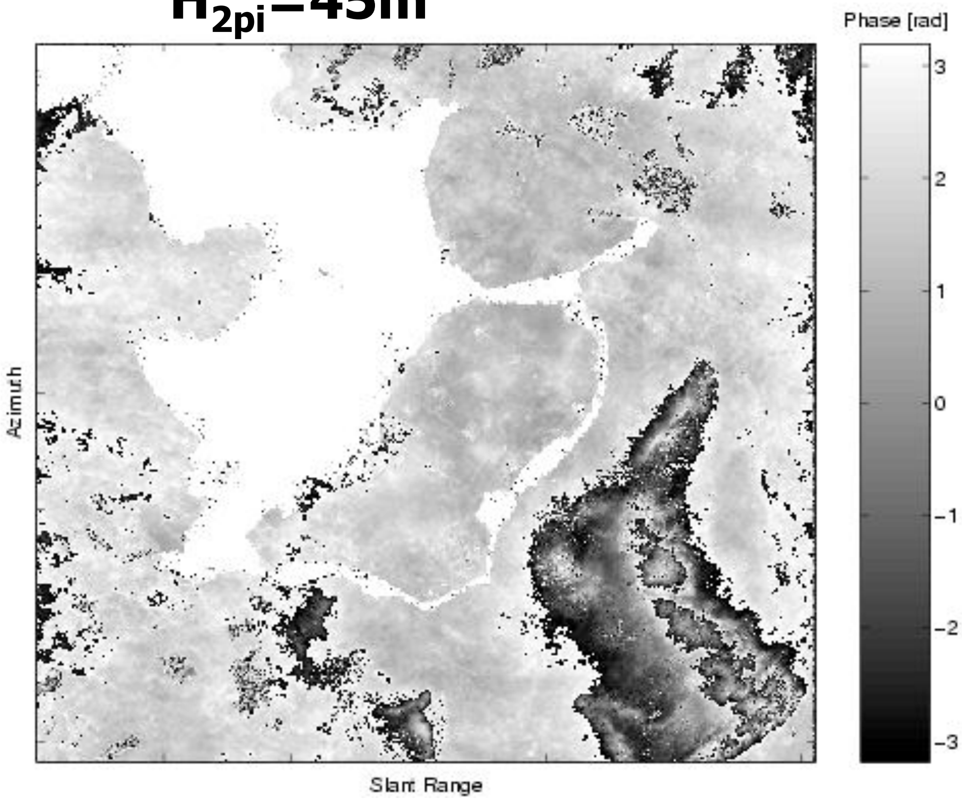


**Bperp 531 m, Bt= 1 day**

**$H_{2pi}$=16m**

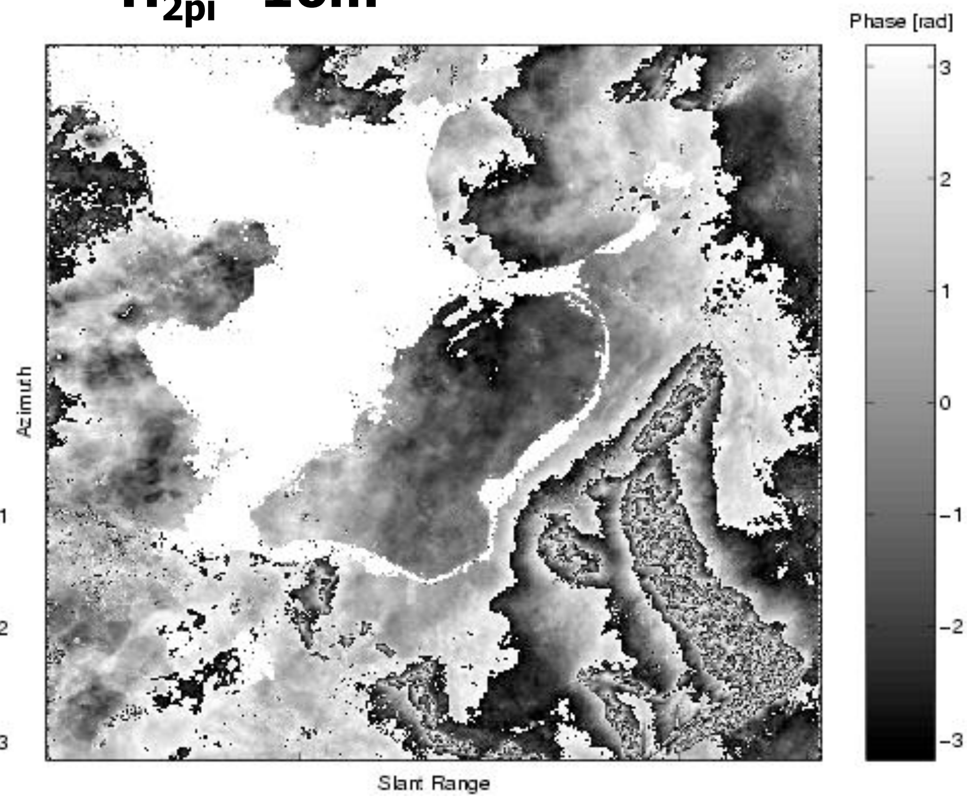

# Phase-deformation relationship

$$\psi_1 = -\frac{4\pi}{\lambda}R_1$$

$$\psi_2 = -\frac{4\pi}{\lambda}R_2$$

$$R_2 = R_1 + D_p$$

**1 cycle LOS deformation is equal to <u>half</u> the physical wavelength**

$$\phi_p = \psi_{1p} - \psi_{2p} = -\frac{4\pi(R_1 - R_2)}{\lambda} =$$

$$\phi_p = -\frac{4\pi}{\lambda}D_p$$

$D_p$ : line-of-sight deformation

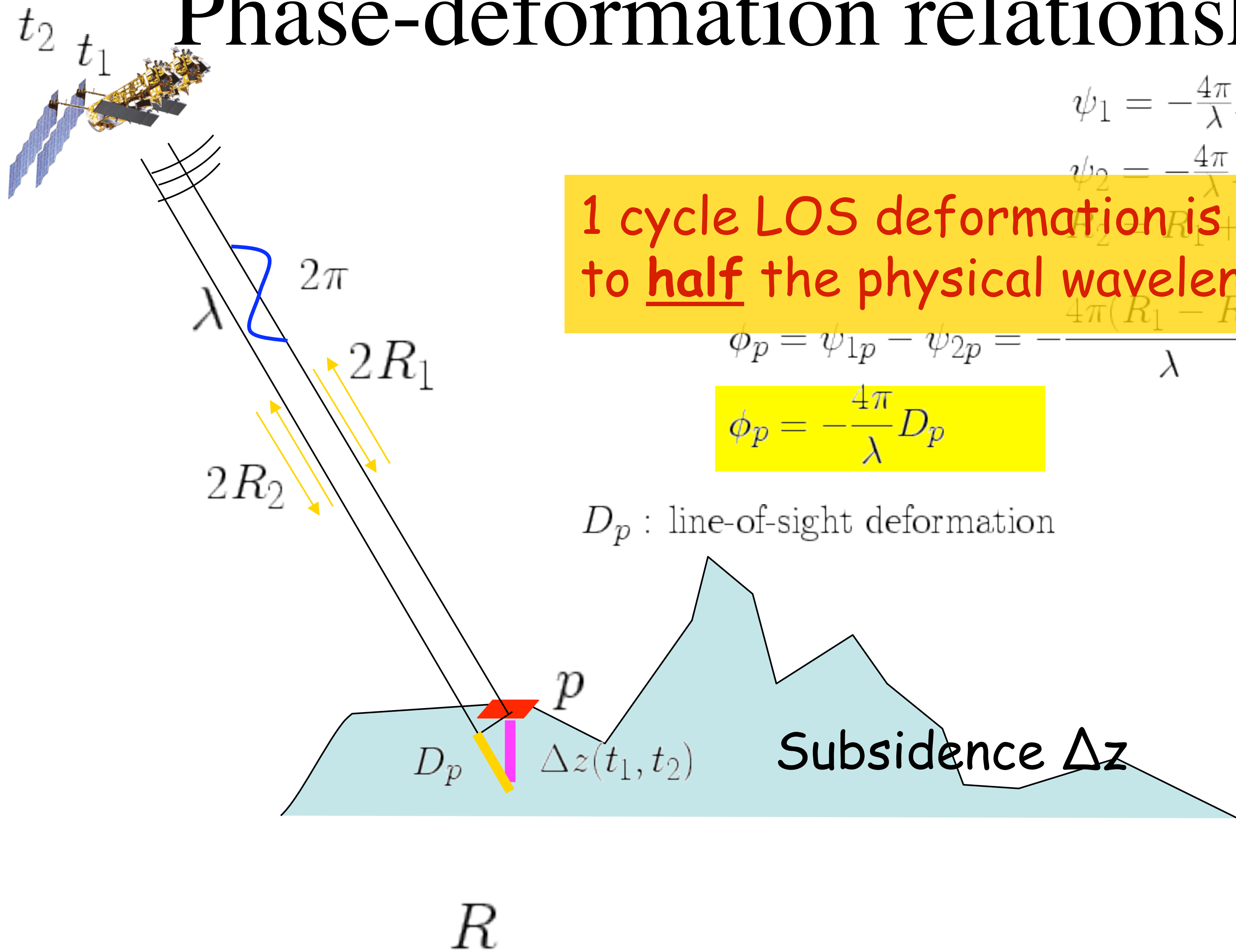

# Interferometric phase - deformation

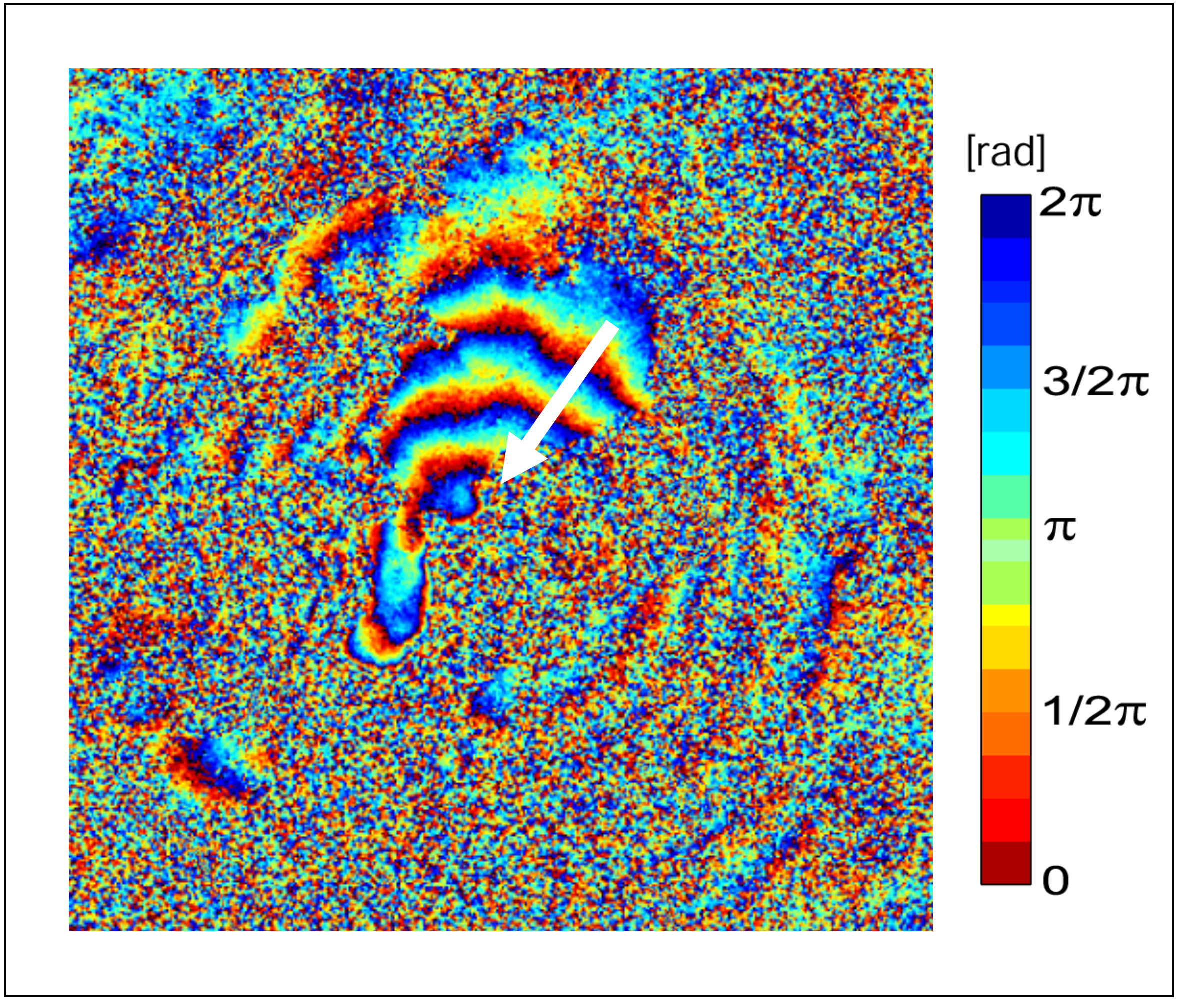


Interferometric phase decreases towards center

⇩

Distance satellite-ground has become shorter towards center

⇩

Relative uplift of the center (9 cm)

# Topography and deformation

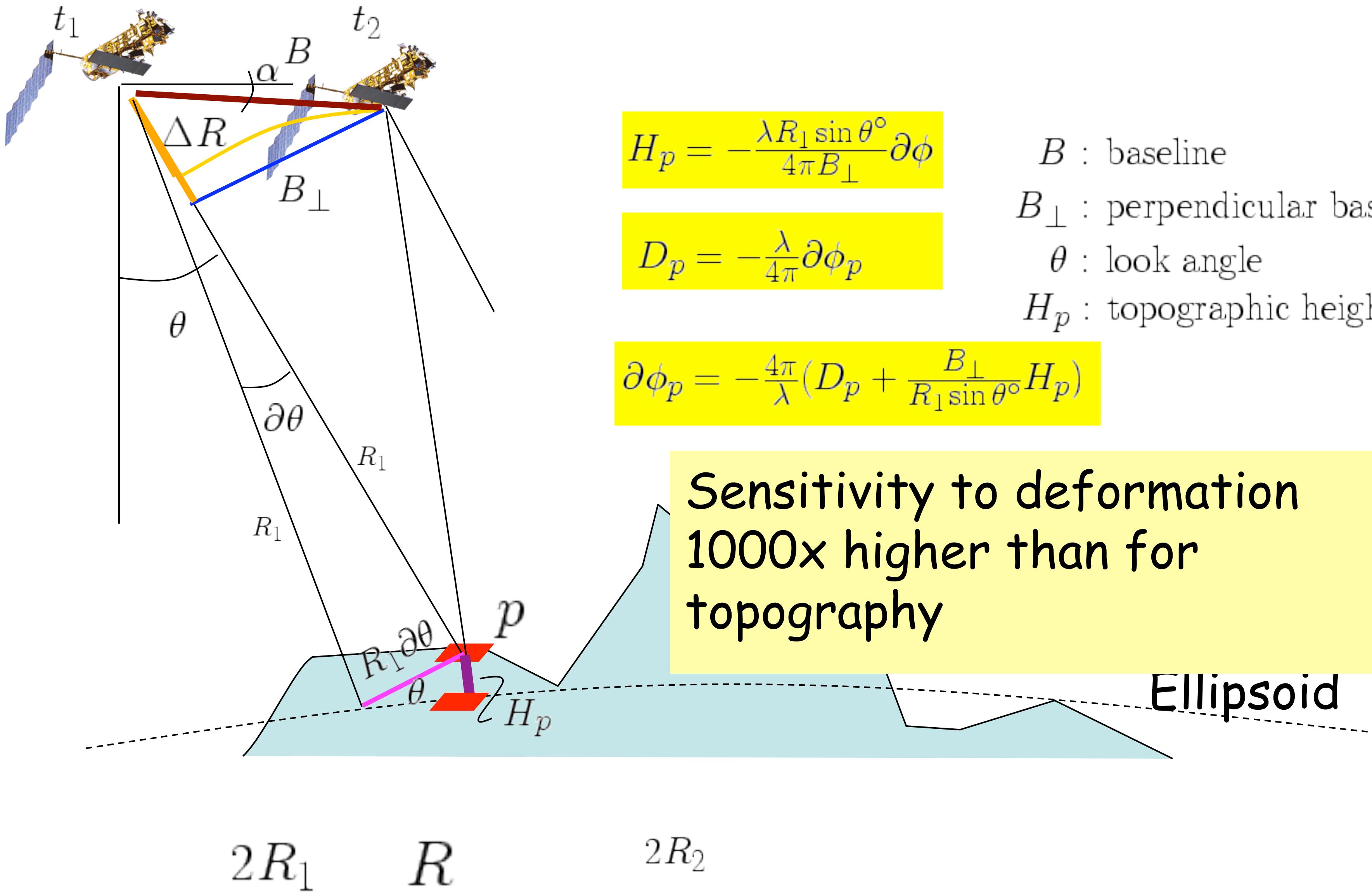


$$H_p = -\frac{\lambda R_1 \sin\theta^\circ}{4\pi B_\perp}\partial\phi$$

$$D_p = -\frac{\lambda}{4\pi}\partial\phi_p$$

$$\partial\phi_p = -\frac{4\pi}{\lambda}\left(D_p + \frac{B_\perp}{R_1 \sin\theta^\circ}H_p\right)$$

$B$ : baseline

$B_\perp$ : perpendicular baseline

$\theta$ : look angle

$H_p$ : topographic height

Sensitivity to deformation 1000x higher than for topography

One interferogram (igram) only provides one component (LOS) of the displacement field - pay attention to LOS vector.

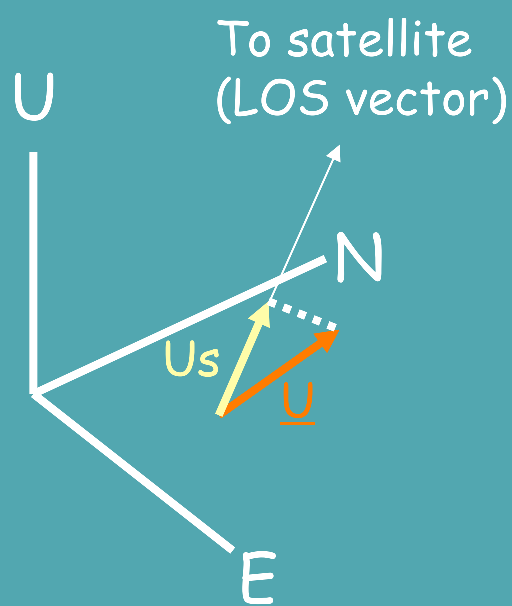


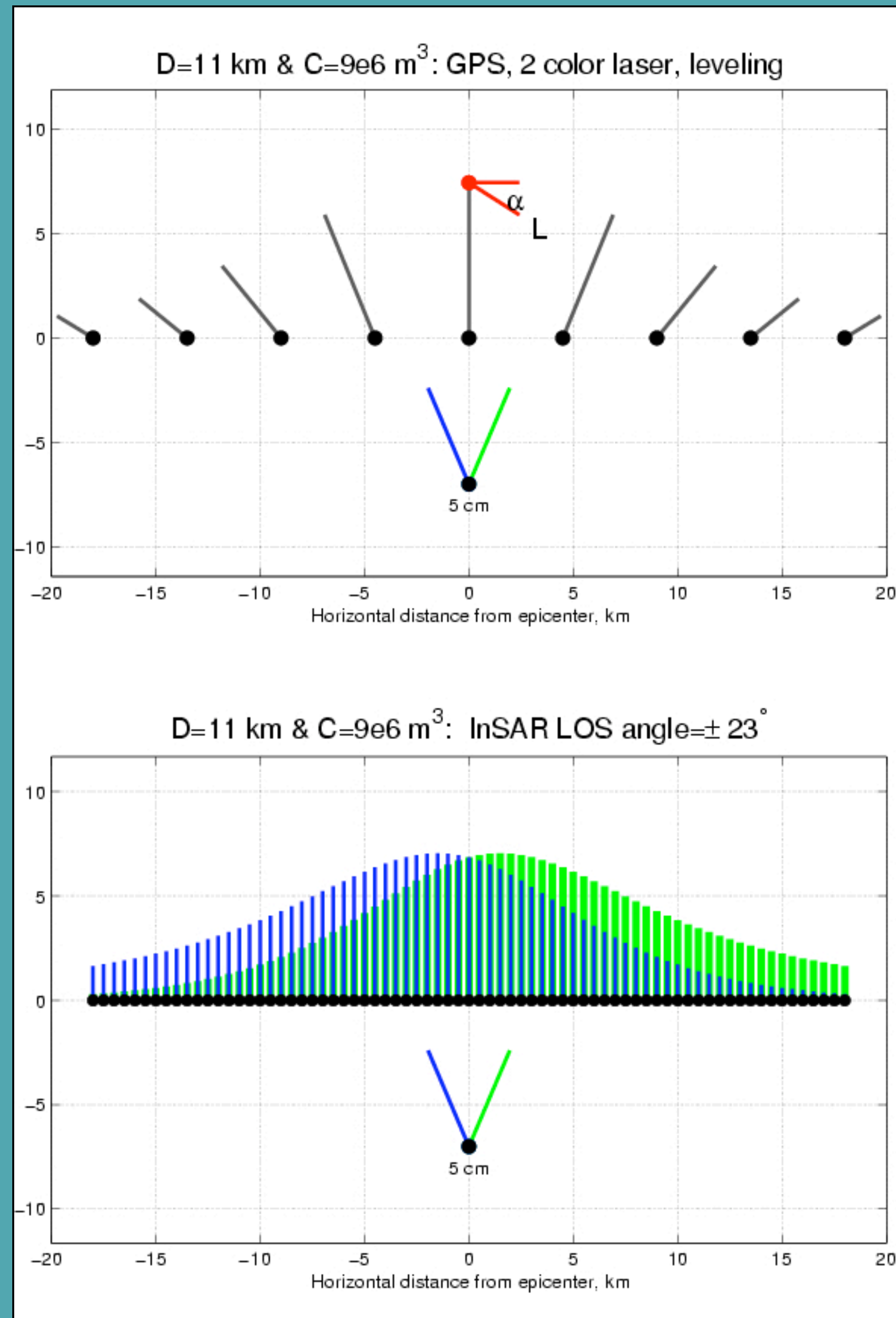

# Atmospheric disturbance

- Spatially varying disturbance signal
- Can be ~5 cm over 20 km
- Spatially correlated but temporally uncorrelated ($\Delta t > 1$ day)
- Introduces covariances in stochastic model

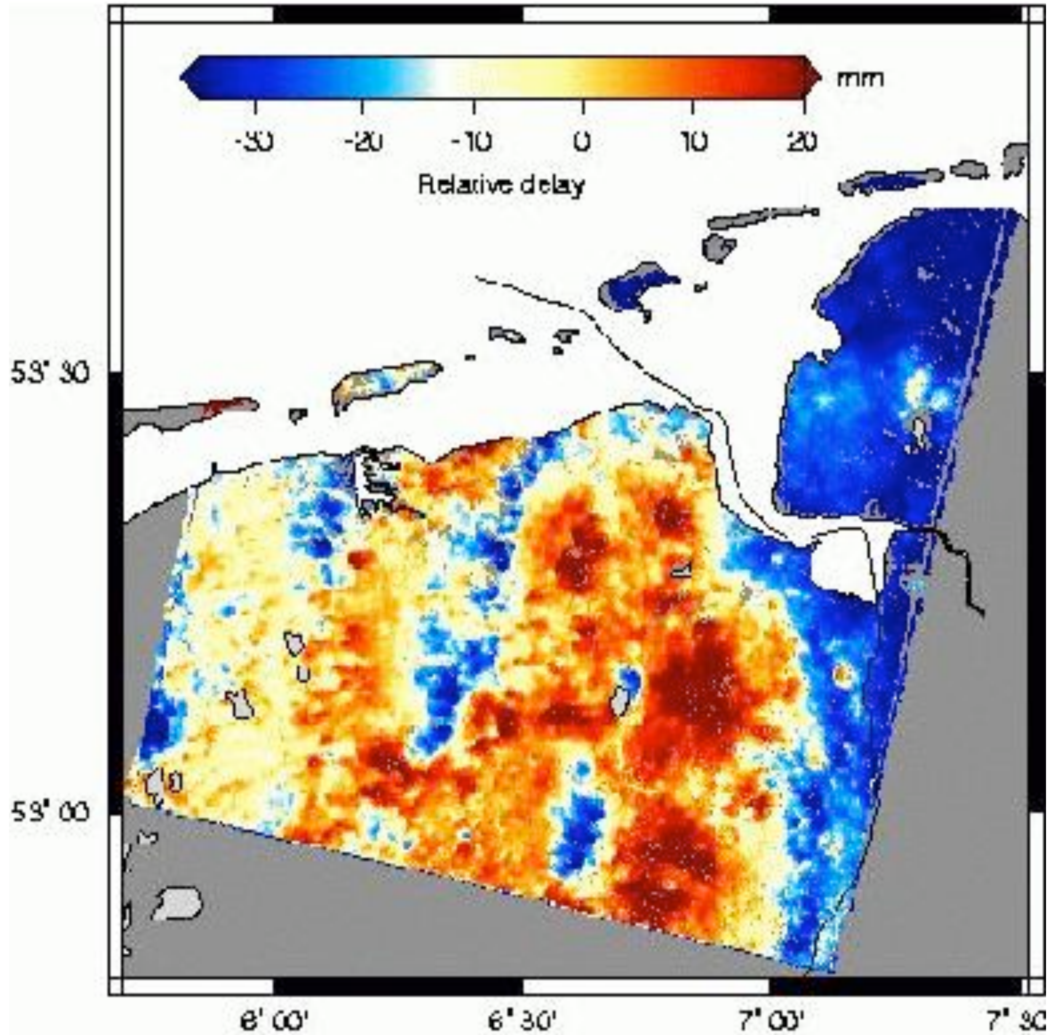

# Example Interferometric Radar Meteorology

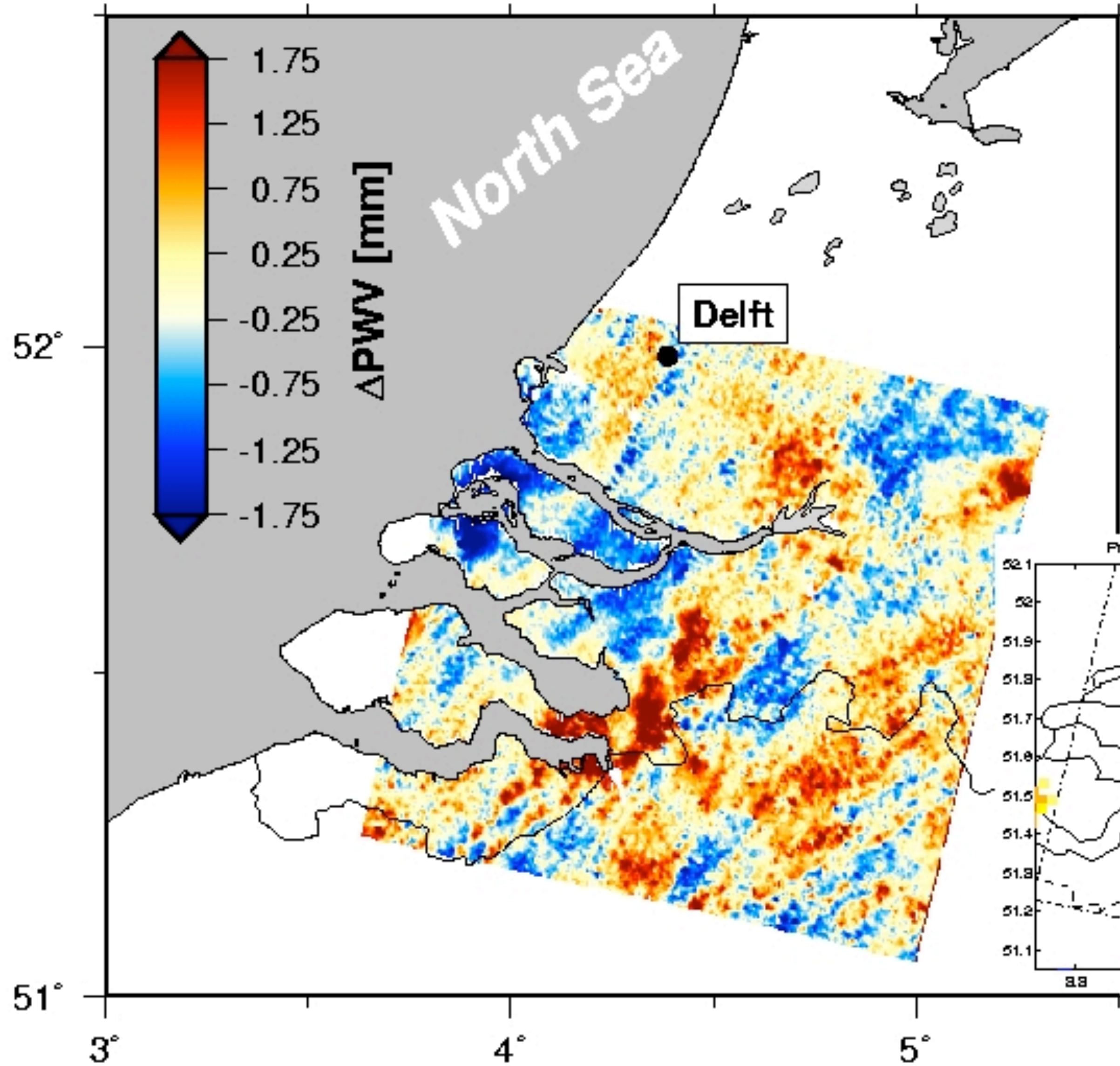


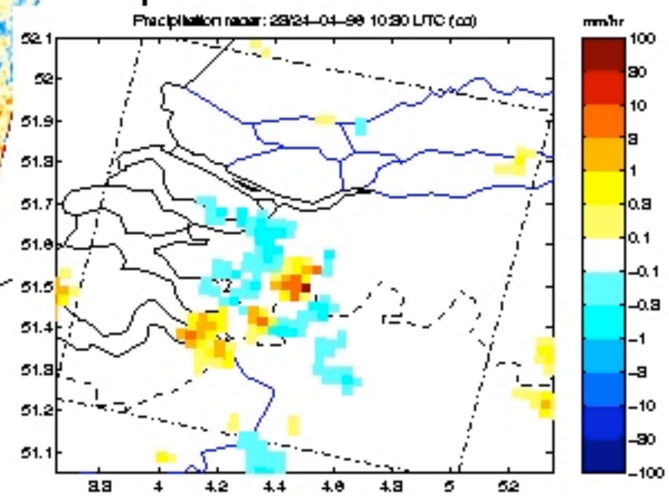

# Geometric decorrelation

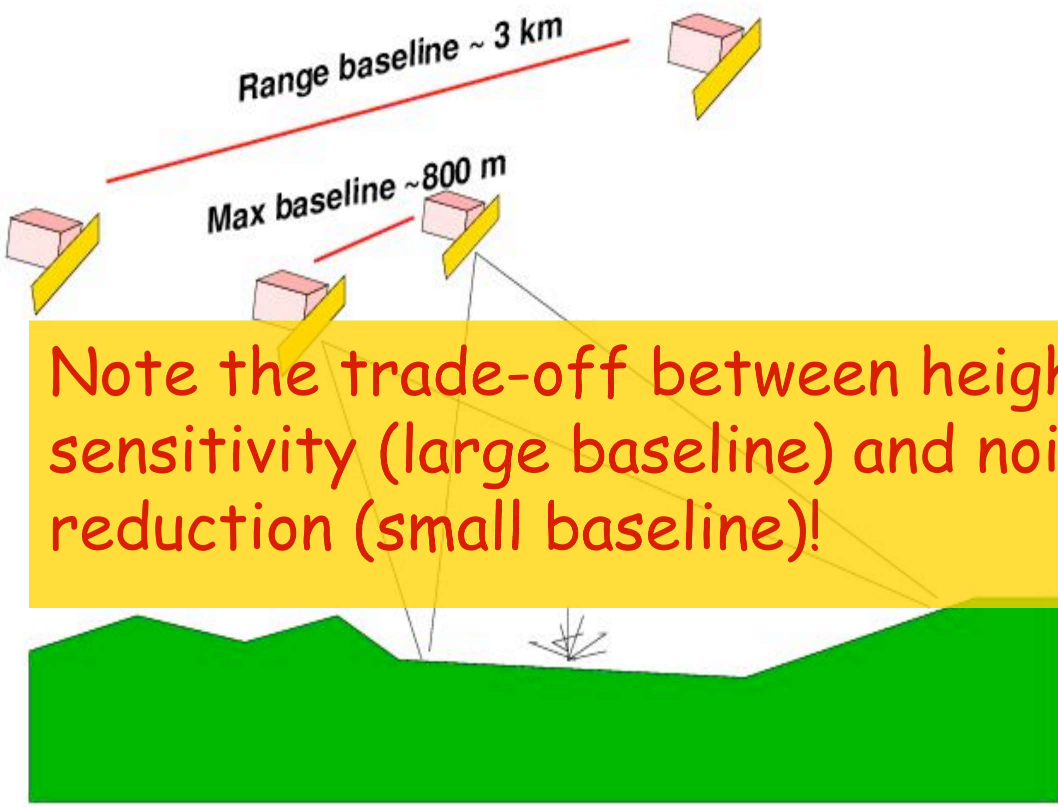


Note the trade-off between height sensitivity (large baseline) and noise reduction (small baseline)!

- Baselines vary
- Relative scattering mechanisms change
- Images become uncomparable
- Function of baseline, Doppler centroid, and terrain slope

# Temporal decorrelation

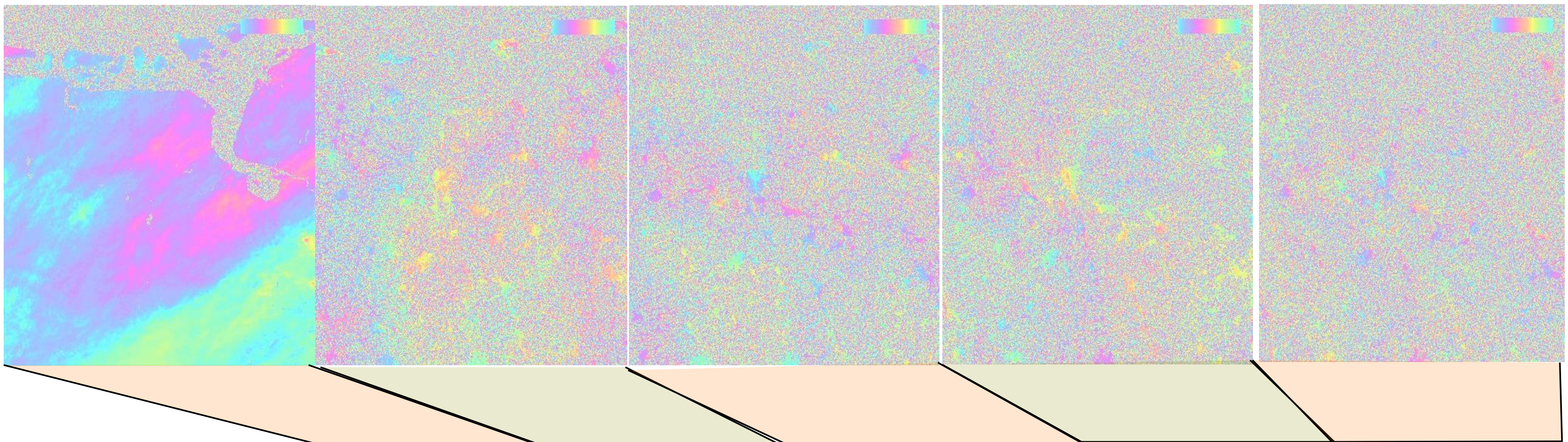

| | | | | | |
|---|---|---|---|---|---|
| Temporal baseline | 1 day | 1 year | 2 years | 3 years | 6 years |
| Perpendicular baseline (m) | 29 | 112 | 93 | 185 | 166 |

# Envisat interferograms (single master)

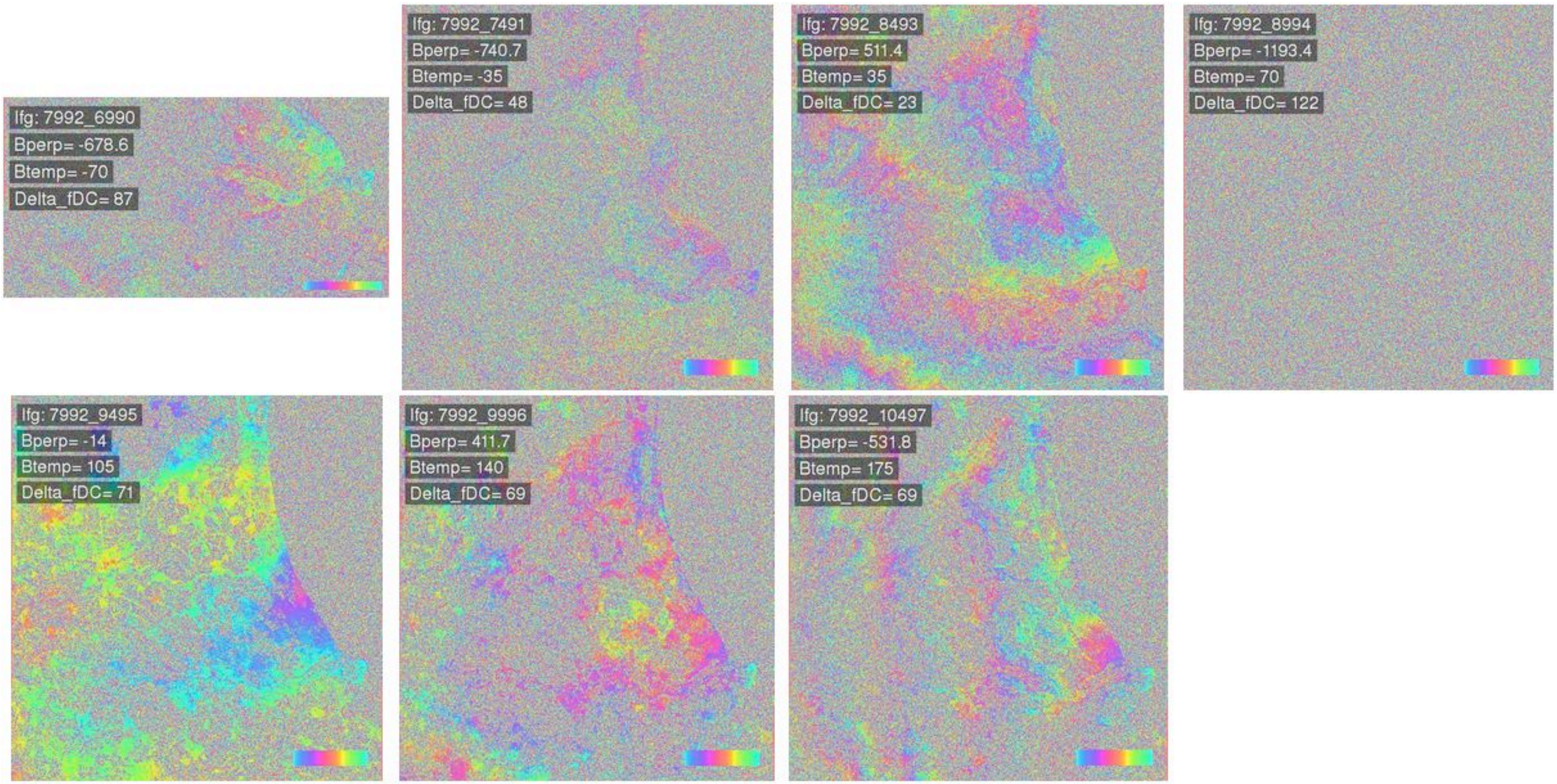

# Volcanoes

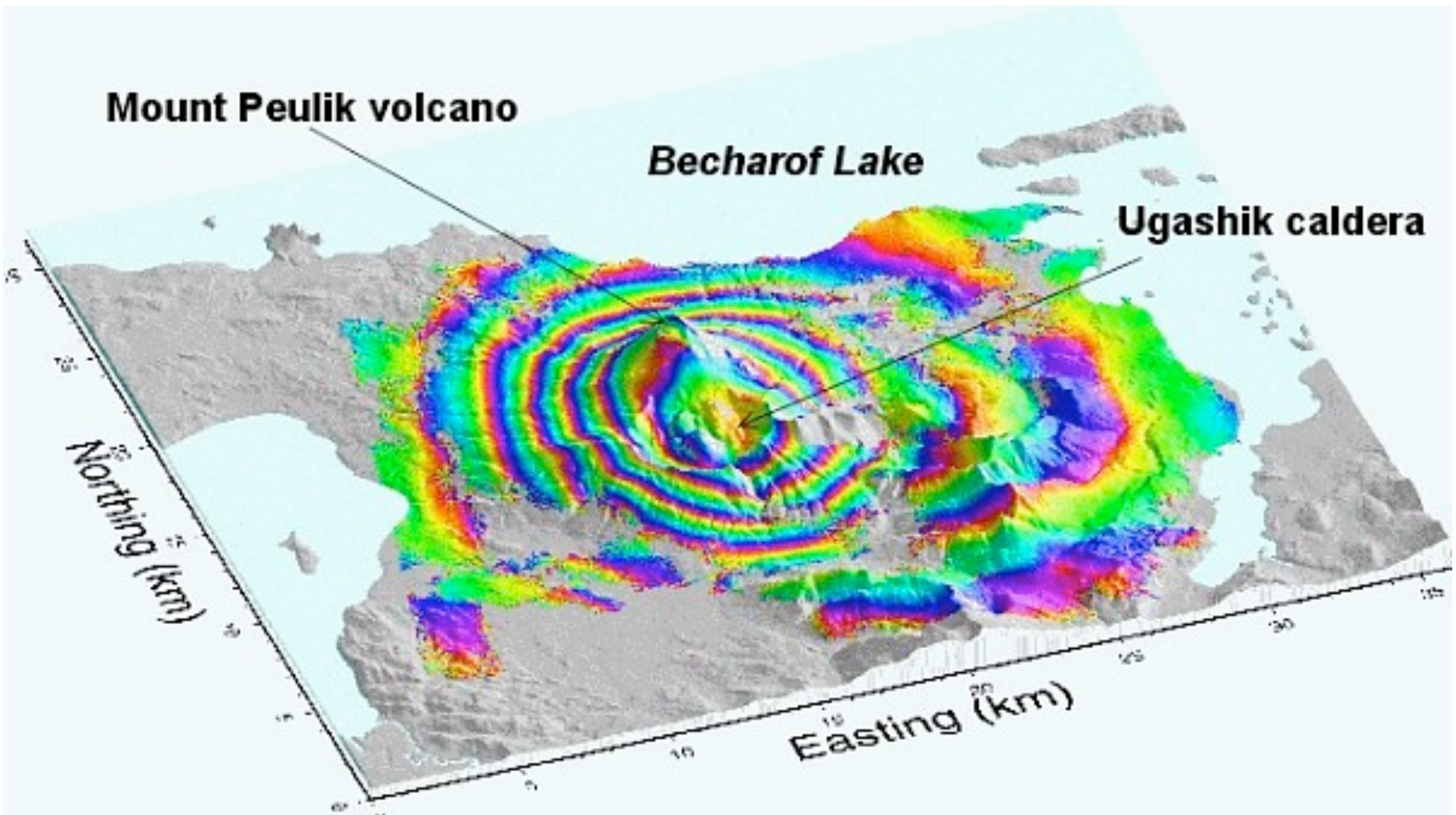
Mount Peulik volcano
Becharof Lake
Ugashik caldera
Northing (km)
Easting (km)

# Mapping Out Large Swaths

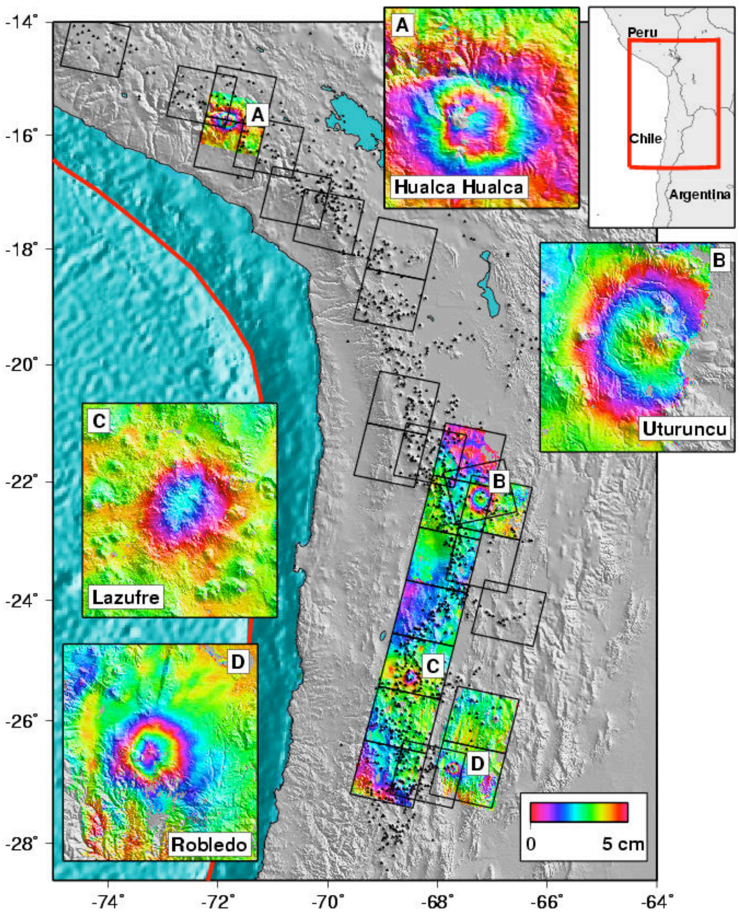


- From Pritchard and Simons (2002)
- Found inflation at 4 volcanic centers in Andes
- None were really expected

# Volcanic source models

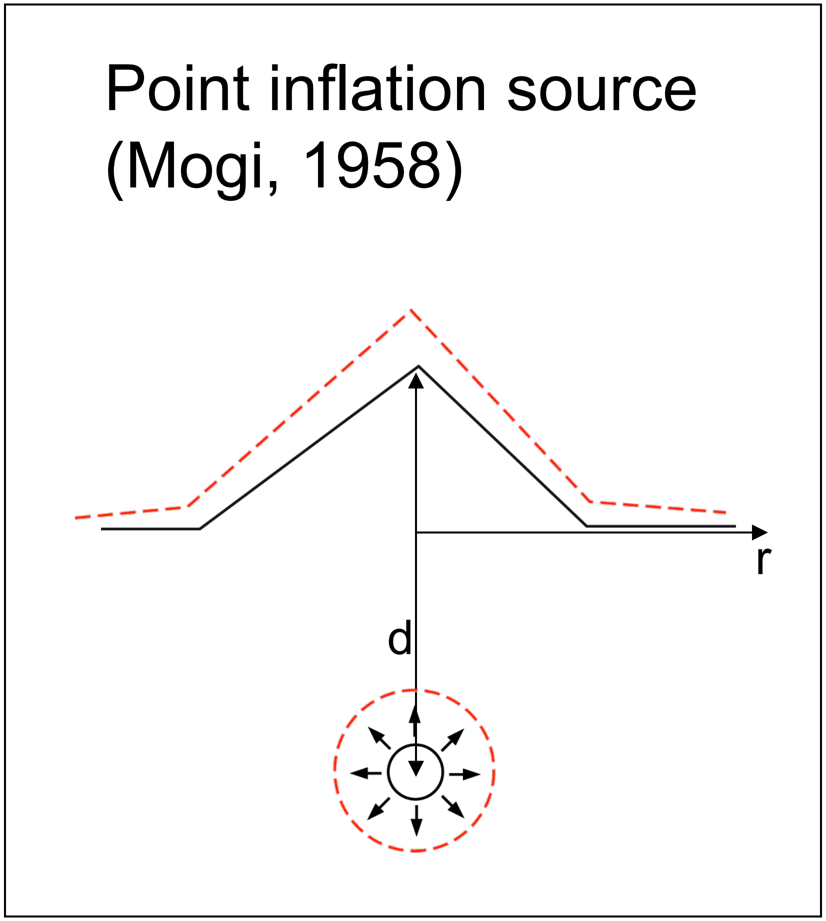


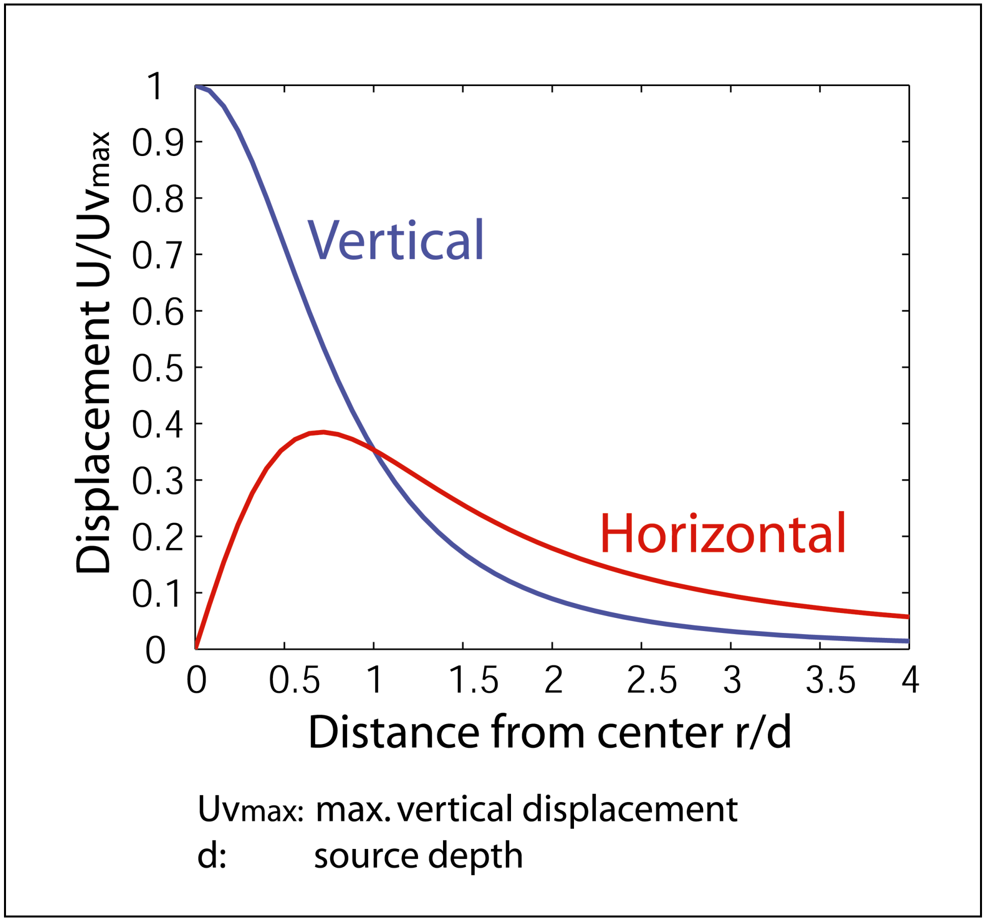

# Okmok Volcano, Alaska-Aleutian arc

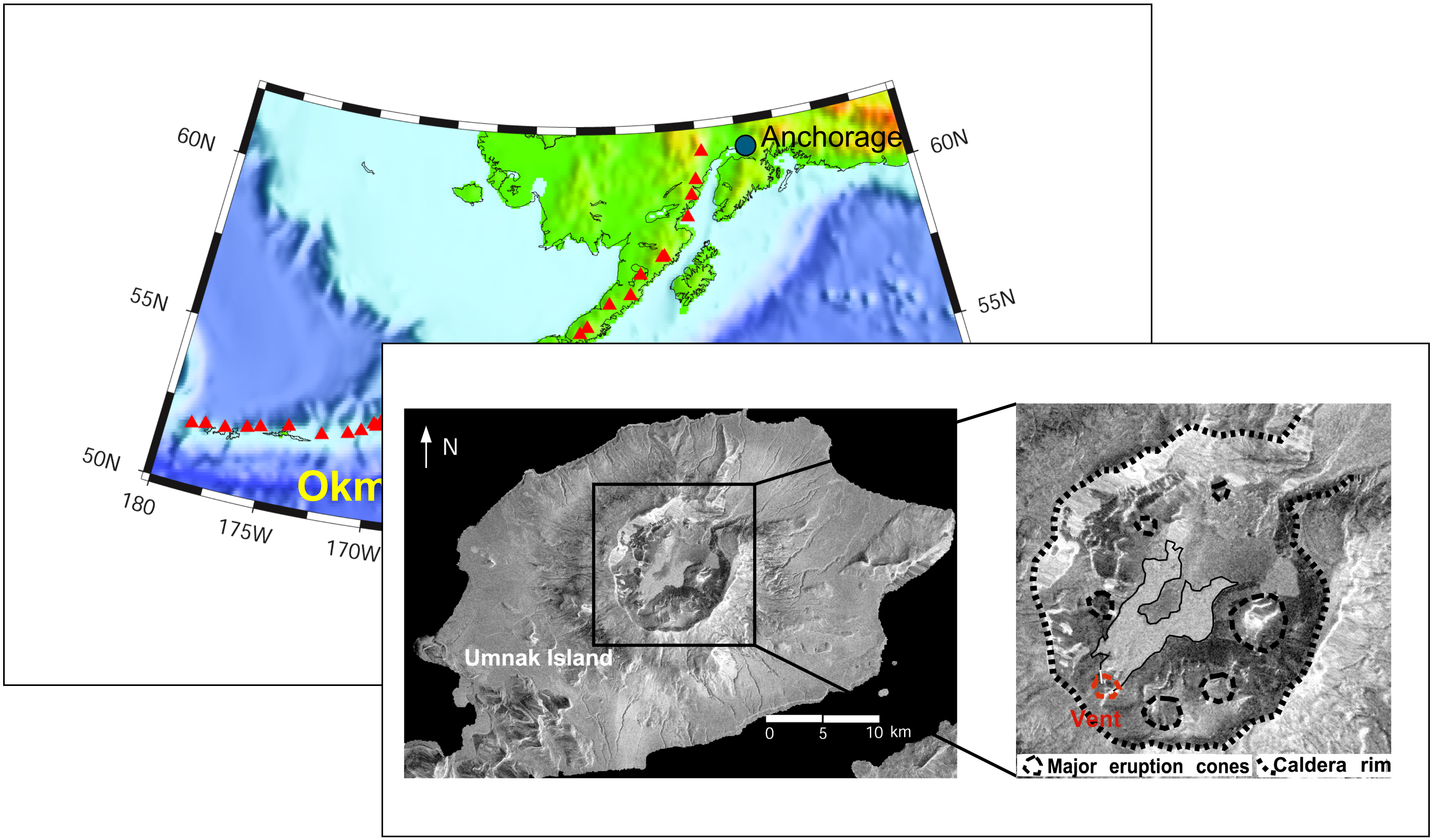

# Deformation

1992 - 1993

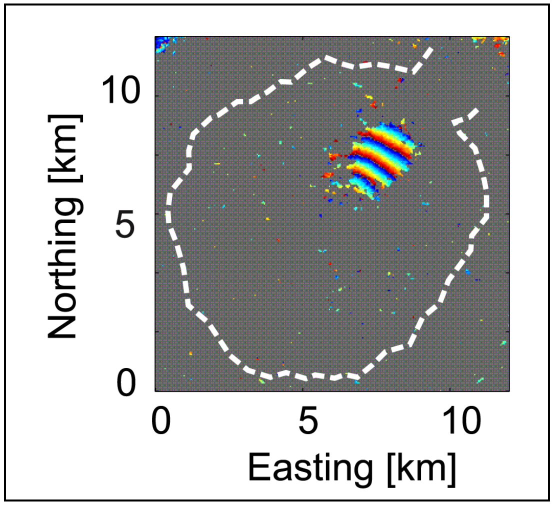


1995 - 1997

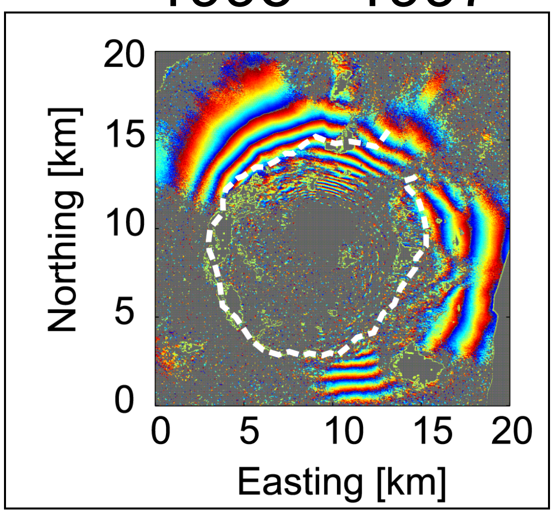


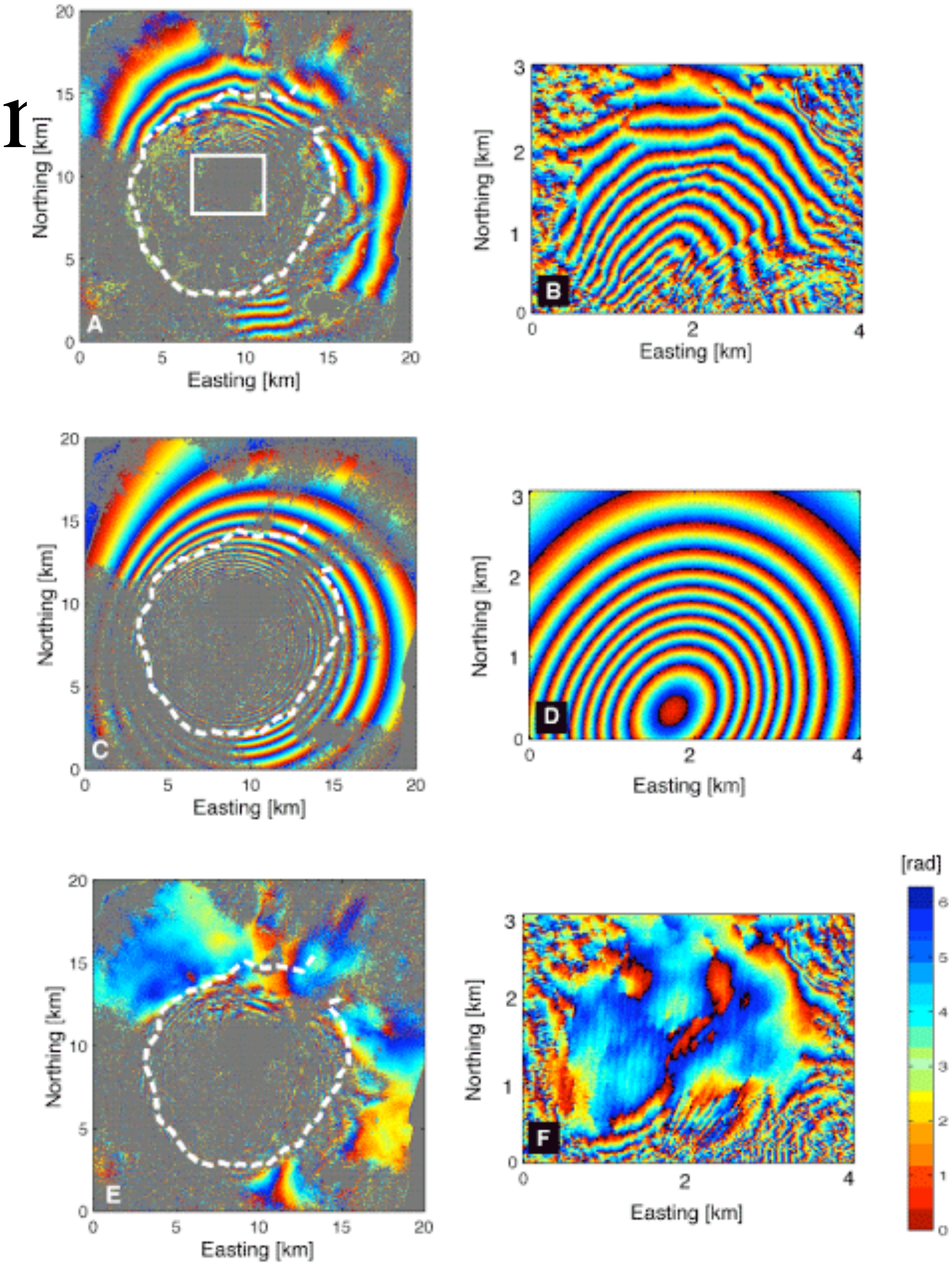

# Source locations and depths

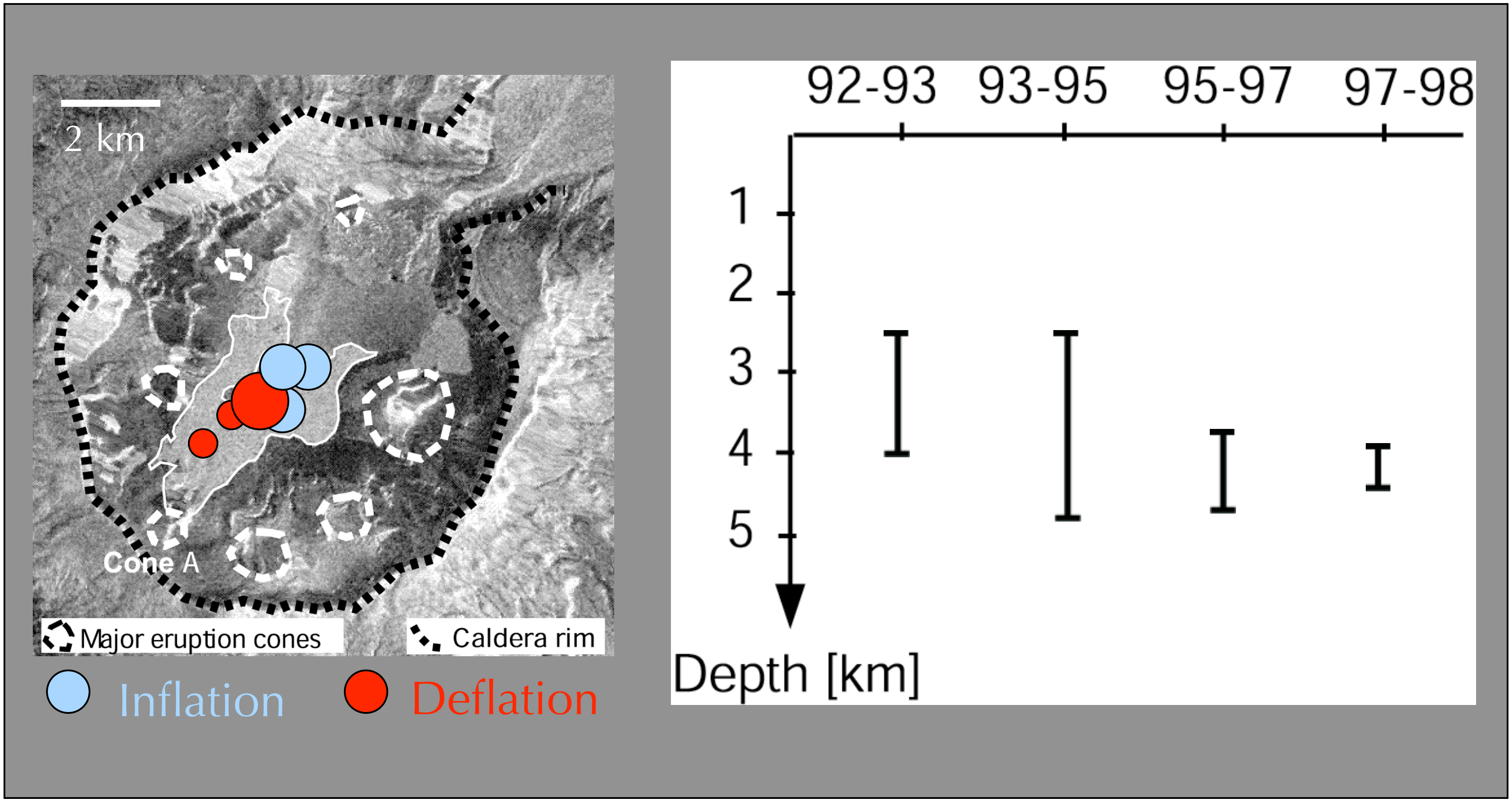

# Time dependence of deformation

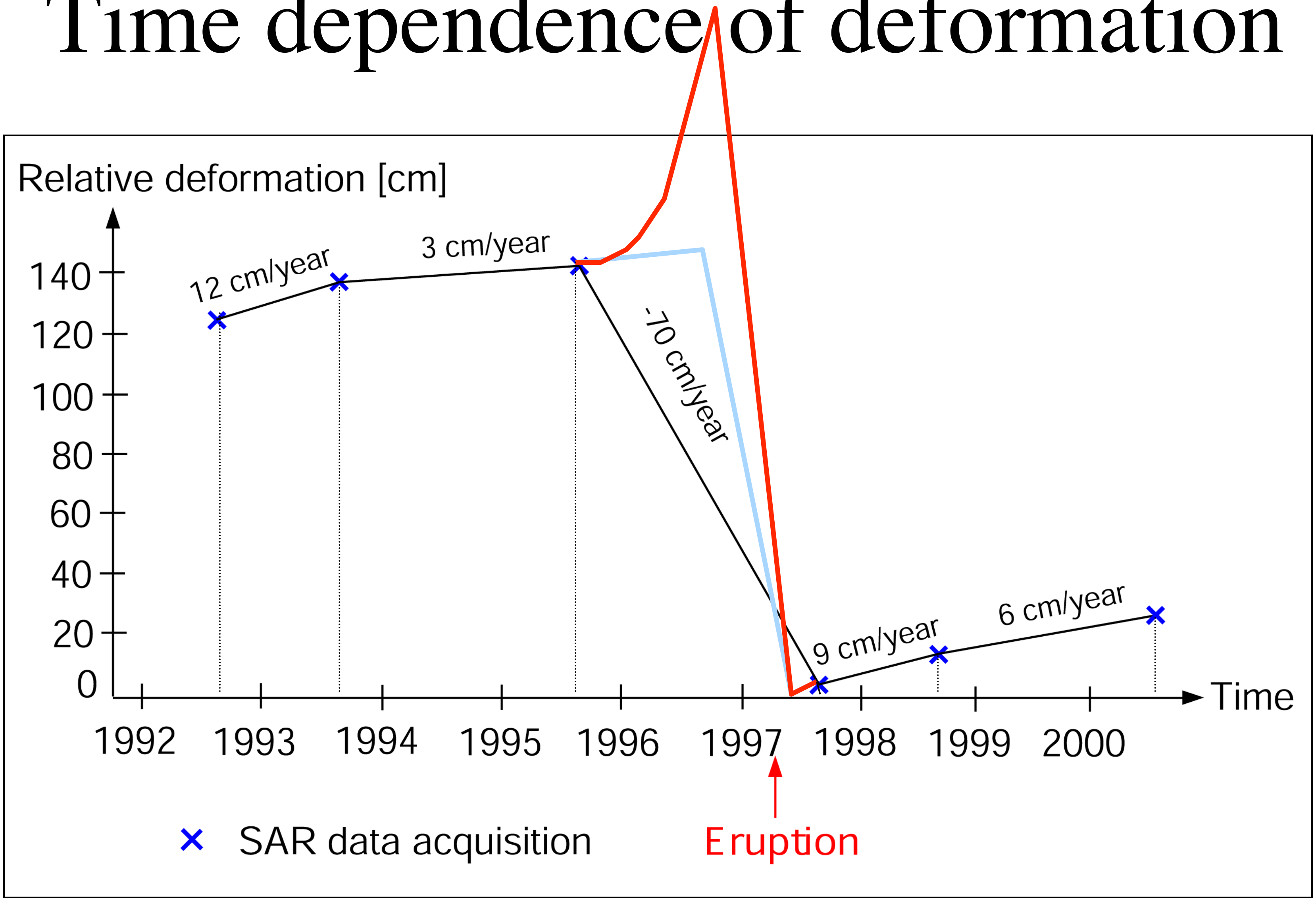

# Magma Volume and Eruption Frequency

- Eruption volume in 1997: $70 \times 10^6\ m^3$

- Average magma accumulation rate during inflation periods: $3\text{-}6 \times 10^6\ m^3/yr$

Estimated recurrence time : 15 years

- Eruptive history:

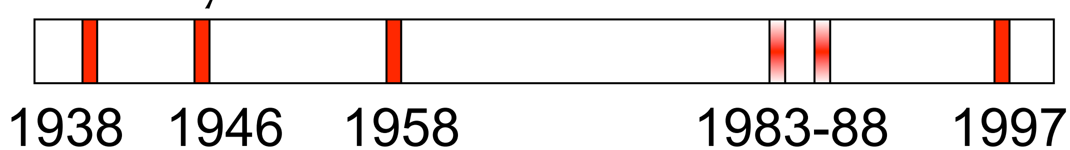


Observed magma accumulation rate is typical for the long term, suggesting continuous supply from a deeper source

Mann et al. (2002)

1992 Mw 7.3 Landers
1999 Mw 7.1 Hector Mine

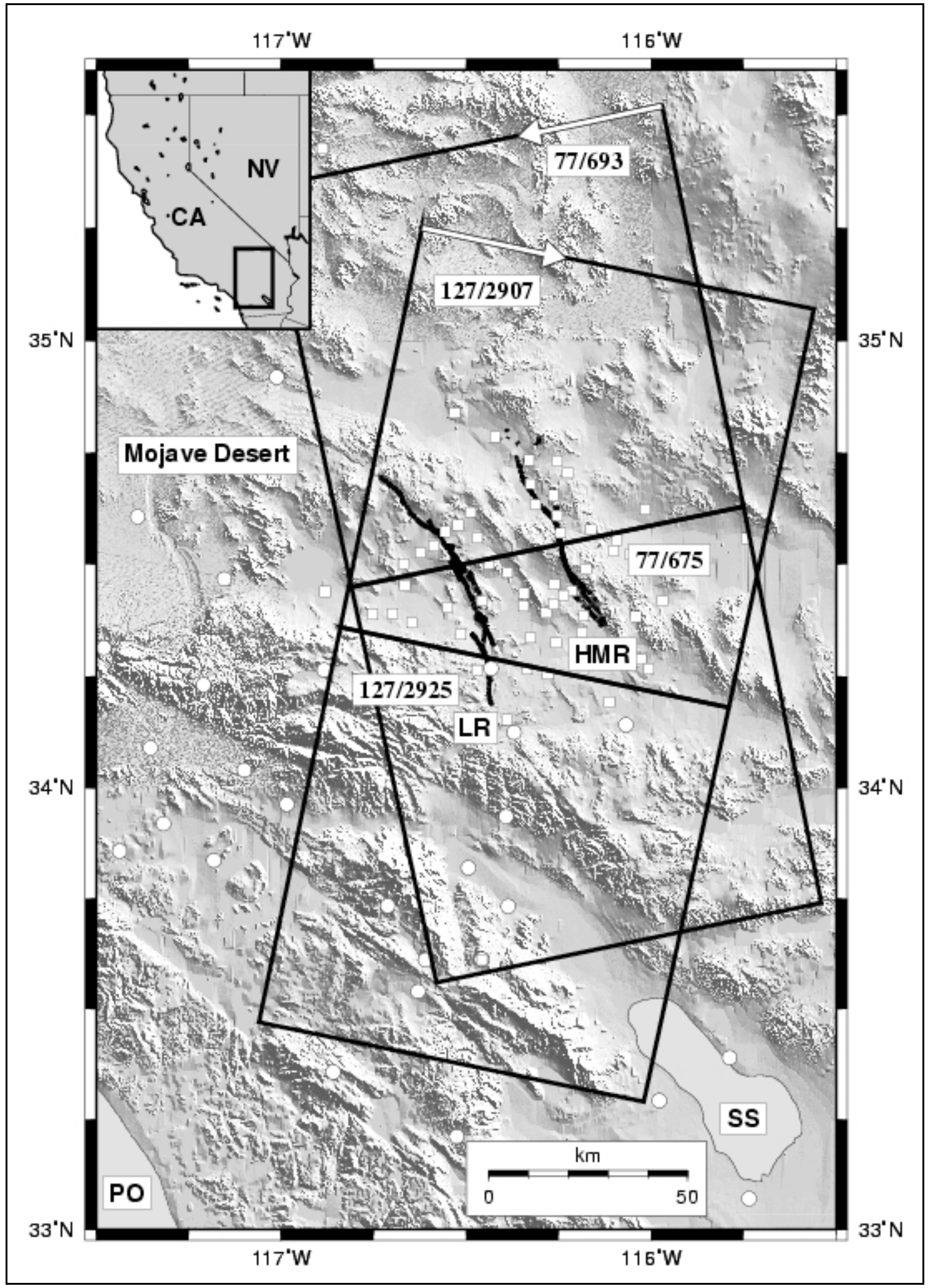

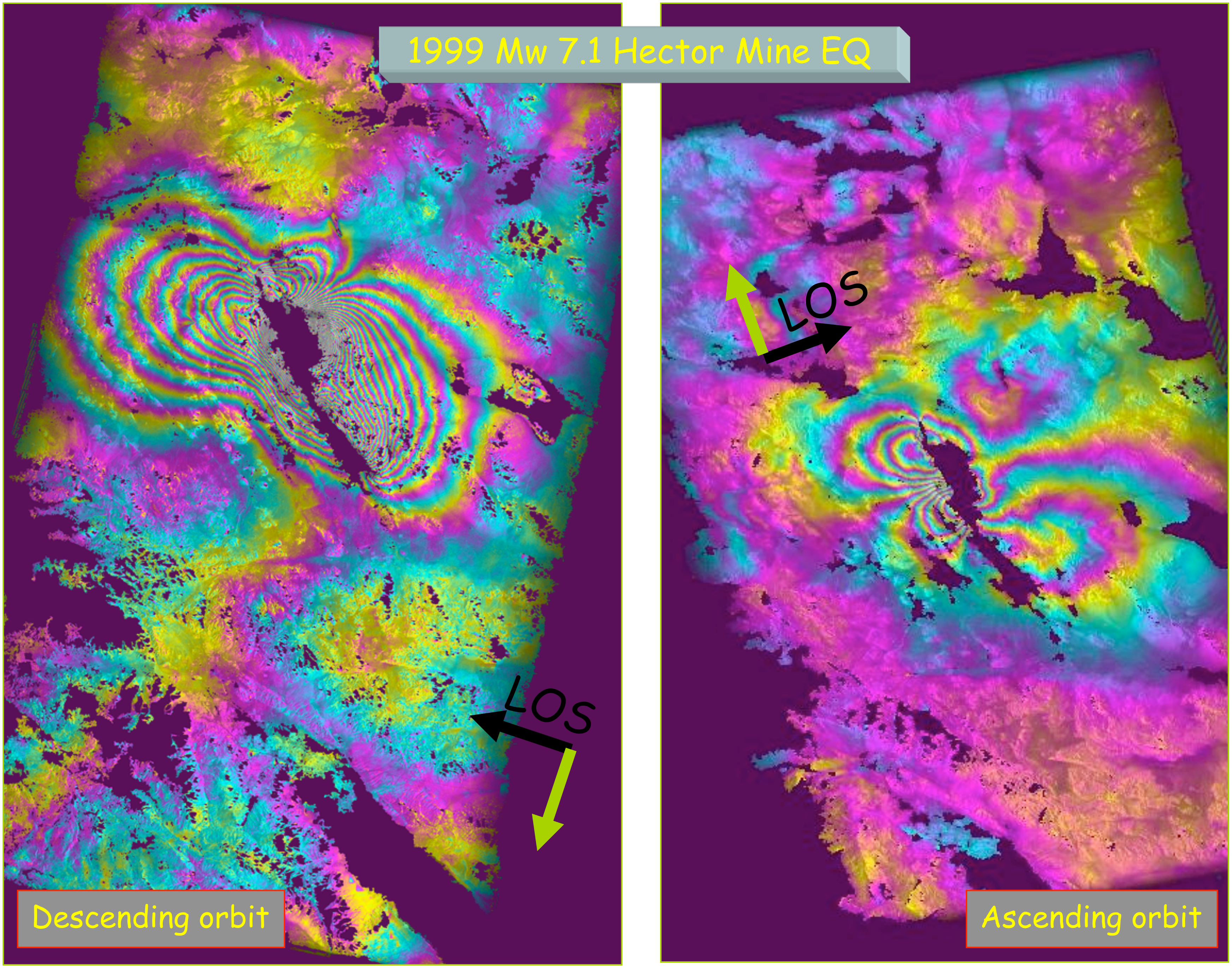
1999 Mw 7.1 Hector Mine EQ
LOS
Descending orbit
LOS
Ascending orbit

# 1999, Mw 7.1 Hector Mine, CA Earthquake

Tracking features in imagery:
How much did a boulder/cactus move?

- Find shift (offset) that maximizes cross-correlation of small ensembles of pixels in two (before/after) images
- With radar data, along track component of offsets is perpendicular to LOS phase
- Does not need to be phase unwrapped
- Sensitivity much less than InSAR
- Can use optical data too (satellite and airphotos)
- Other applications (glaciers, …)

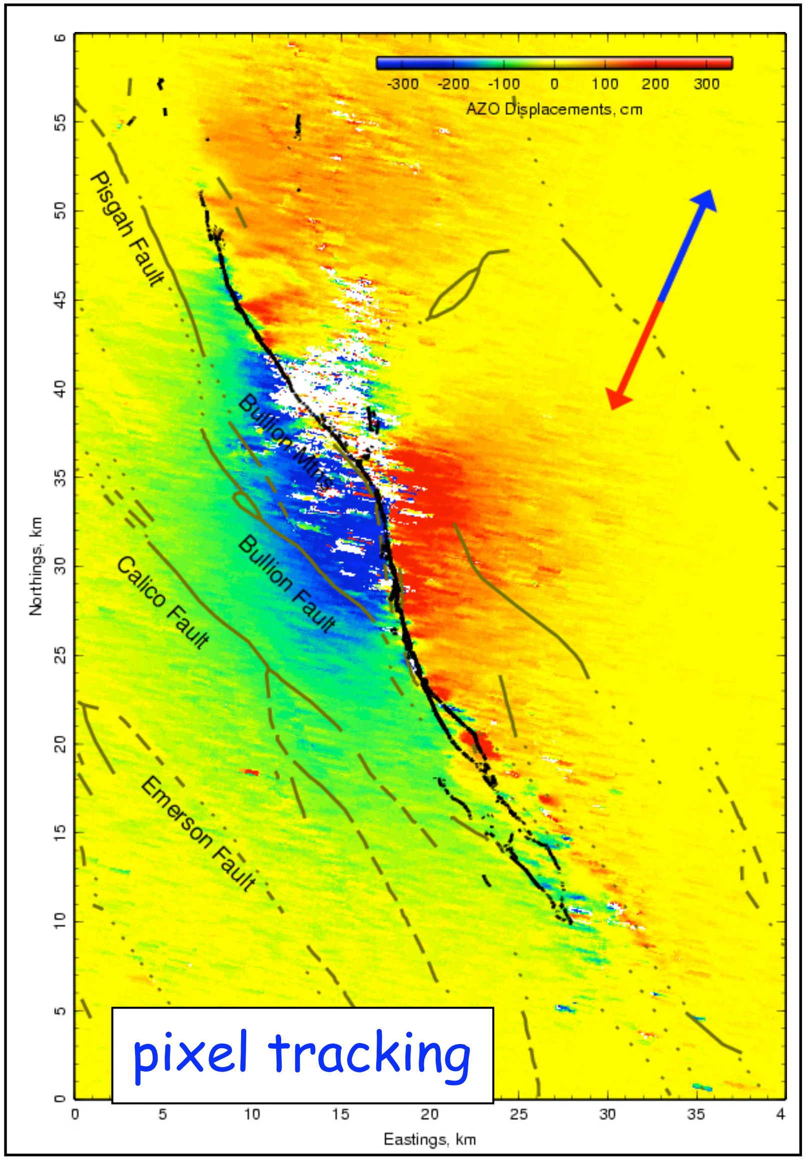

# 1999 Mw 7.1 Hector Mine EQ

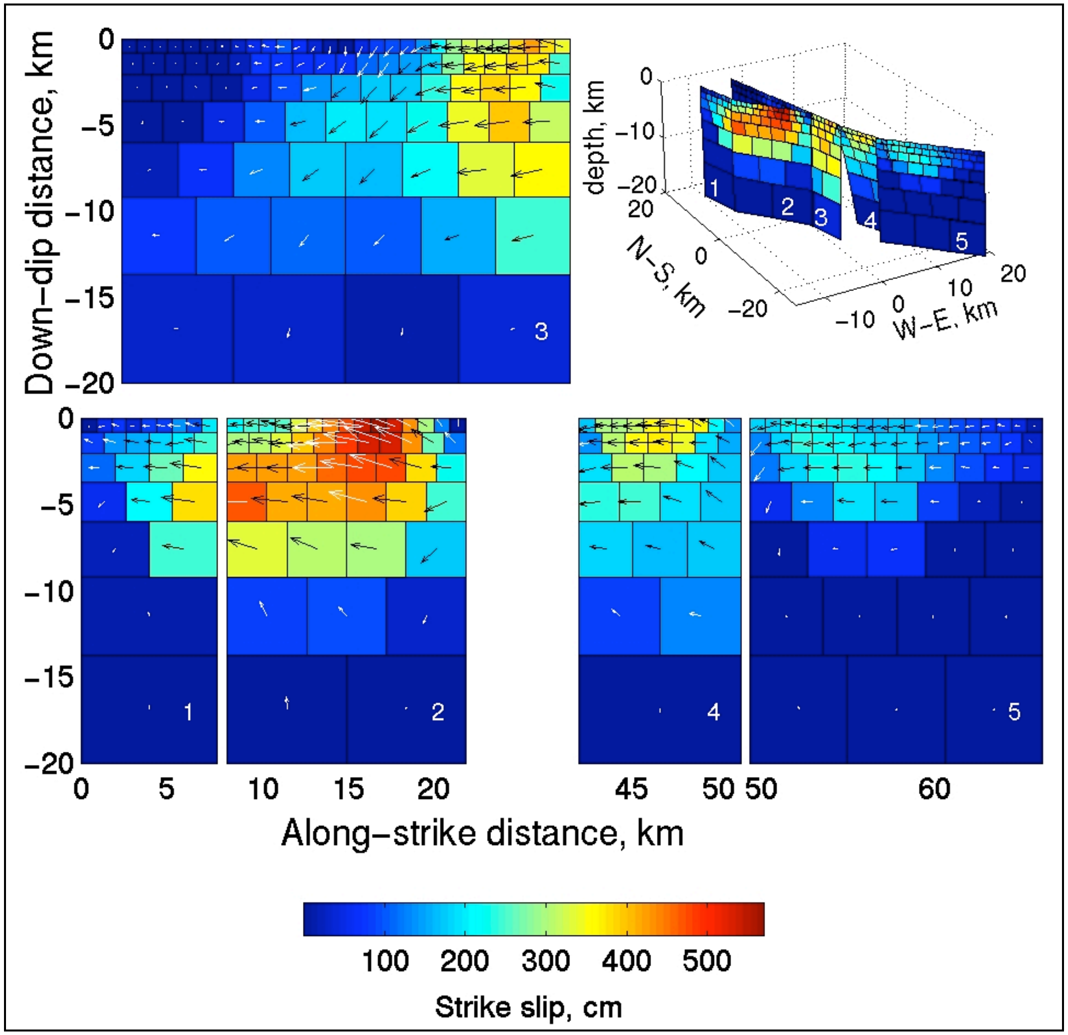


Inferred subsurface coseismic fault slip

3D displacement field

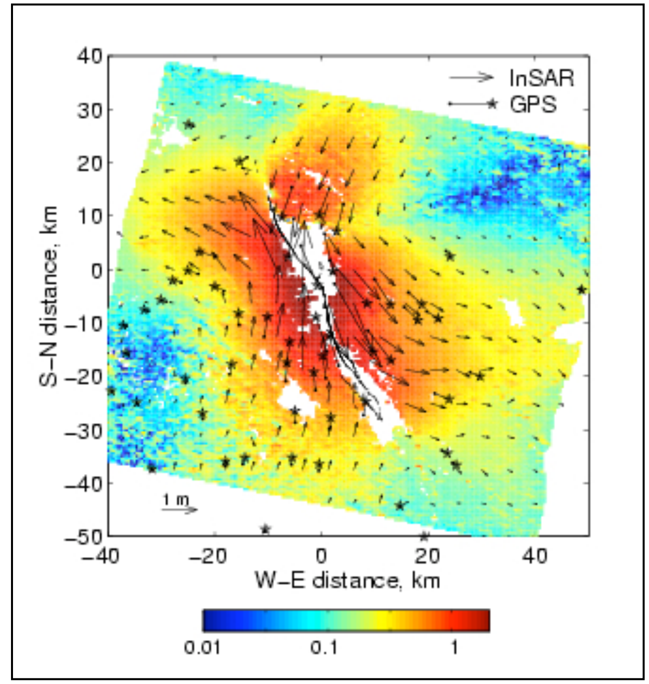


- Significant vertical fault slip
- Fault slip concentrated at shallow depth (7 to 10 km)
- Use as input into post-seismic models

# Flow of Rutford Ice Stream

6 days of displacement, each fringe ~28 mm LOS

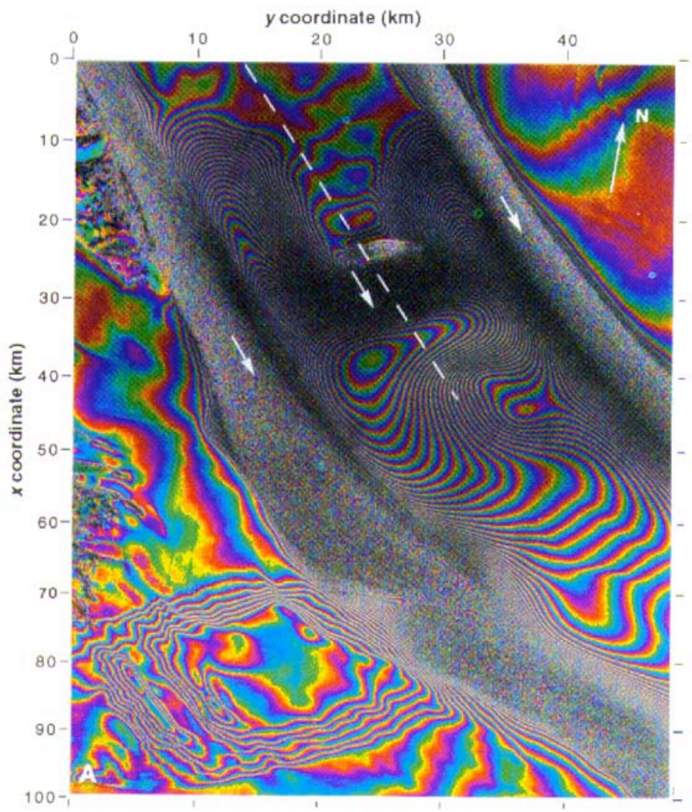


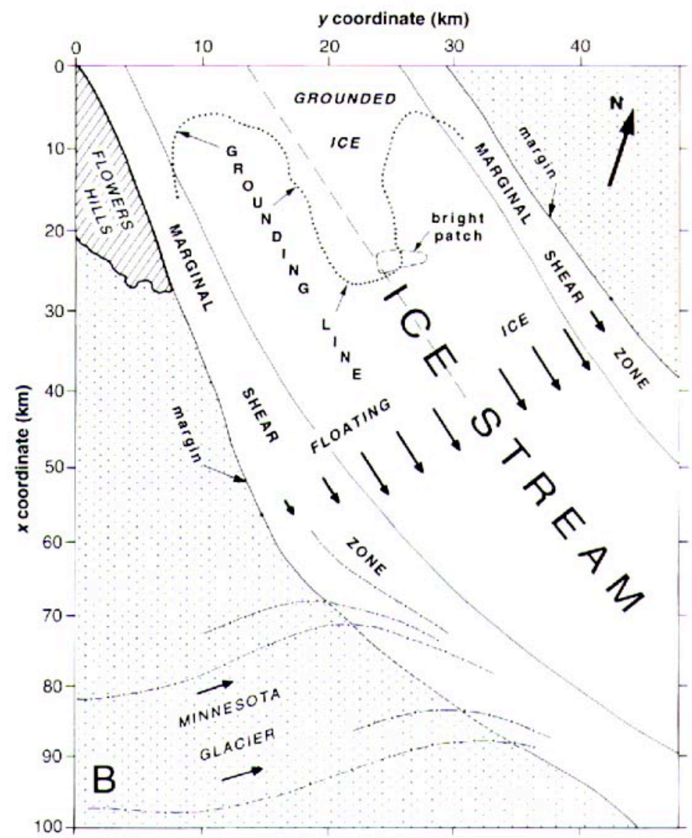


D. Goldstein, JPL

# Patagonia Ice Velocities

## from Shuttle Imaging Radar (SIR-C)

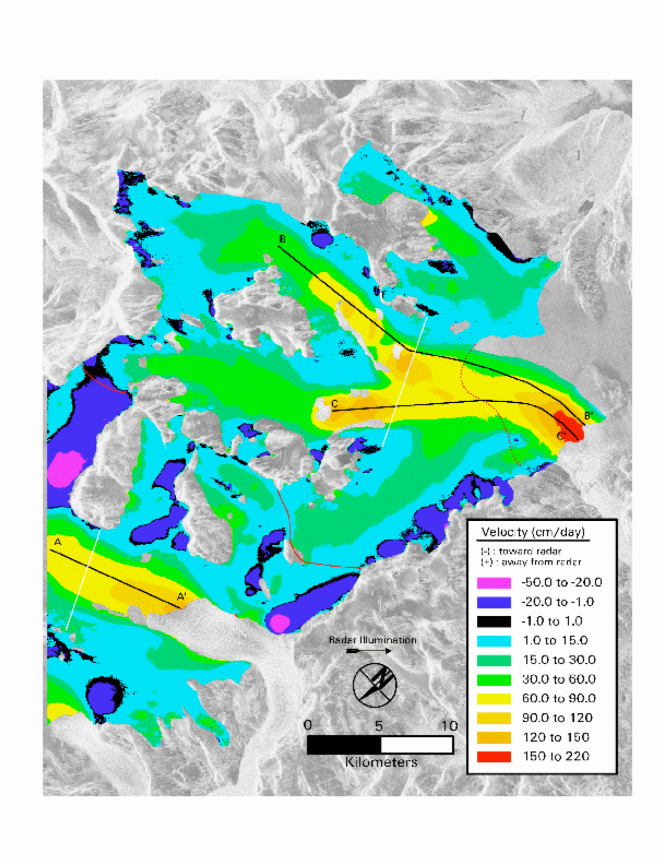


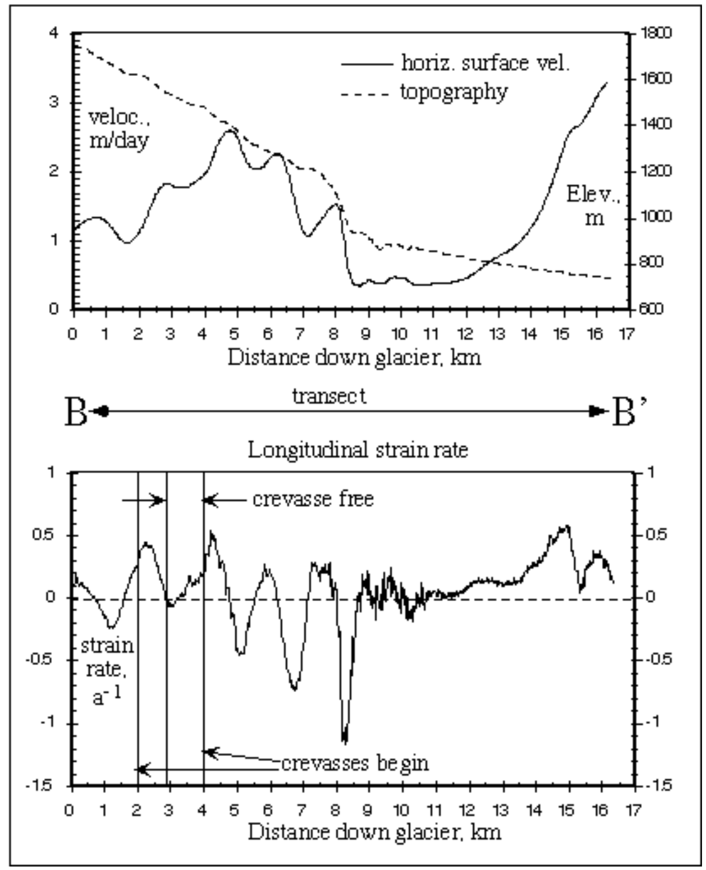


Isacks et al. (1997)

http://www.geo.cornell.edu/geology/SIRC_Pat/patagonia.html

# InSAR Glacier Velocity

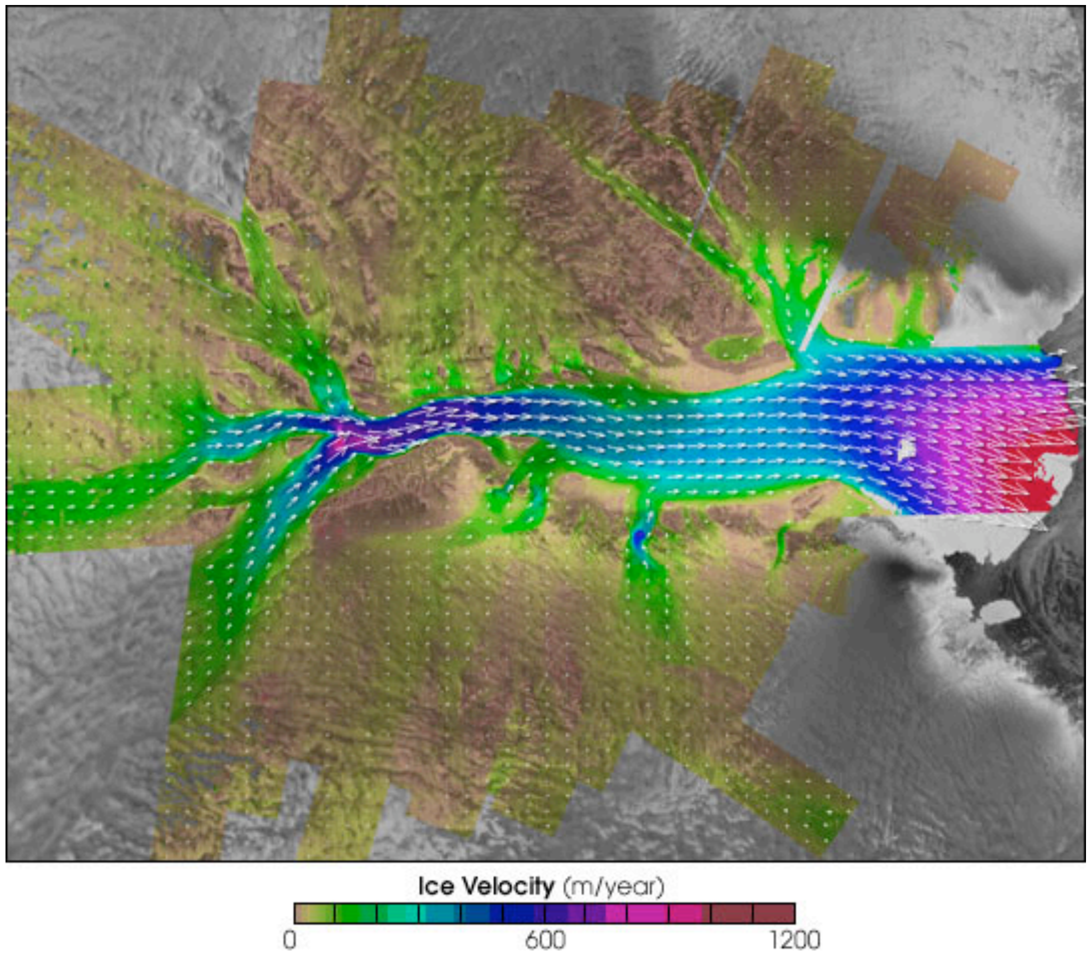

# DInSAR

## Land Subsidence

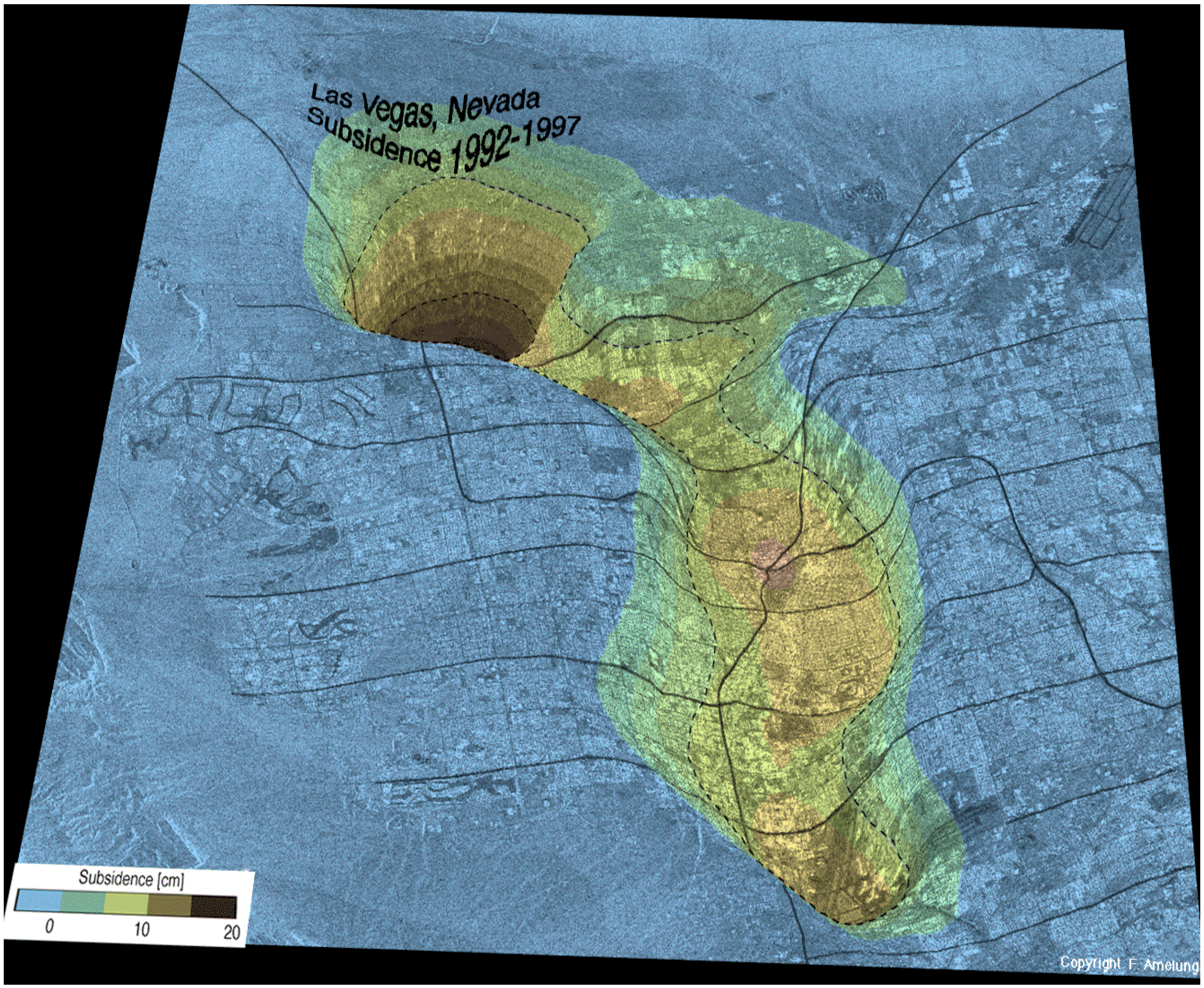

# PS principle

- Pixels with strong and consistent reflections in time.
- Multi-pass InSAR – time series necessary.
- Estimate atmospheric signal:
  - Spatially, not temporally correlated.

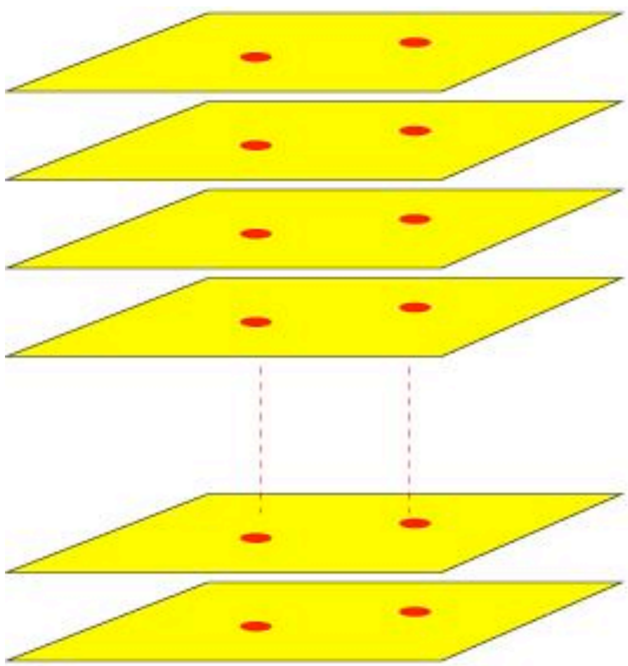

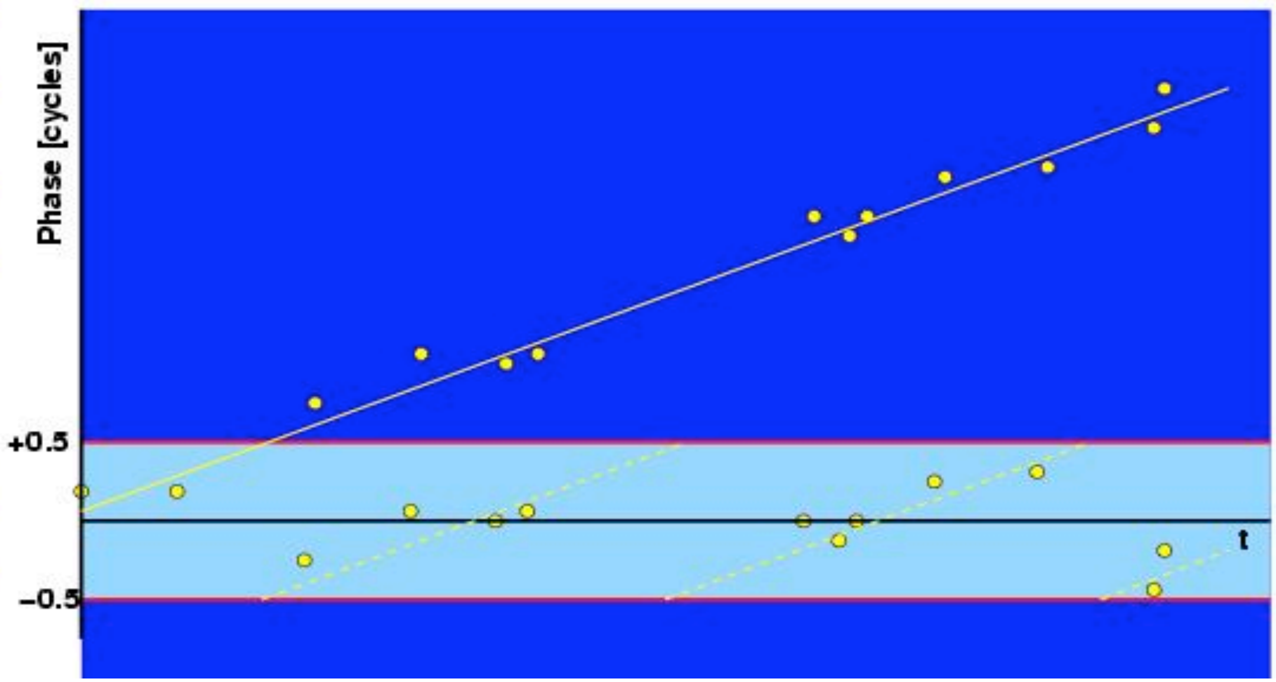

# Persistent Scatterers processing

Preprocessing: Selection test areas

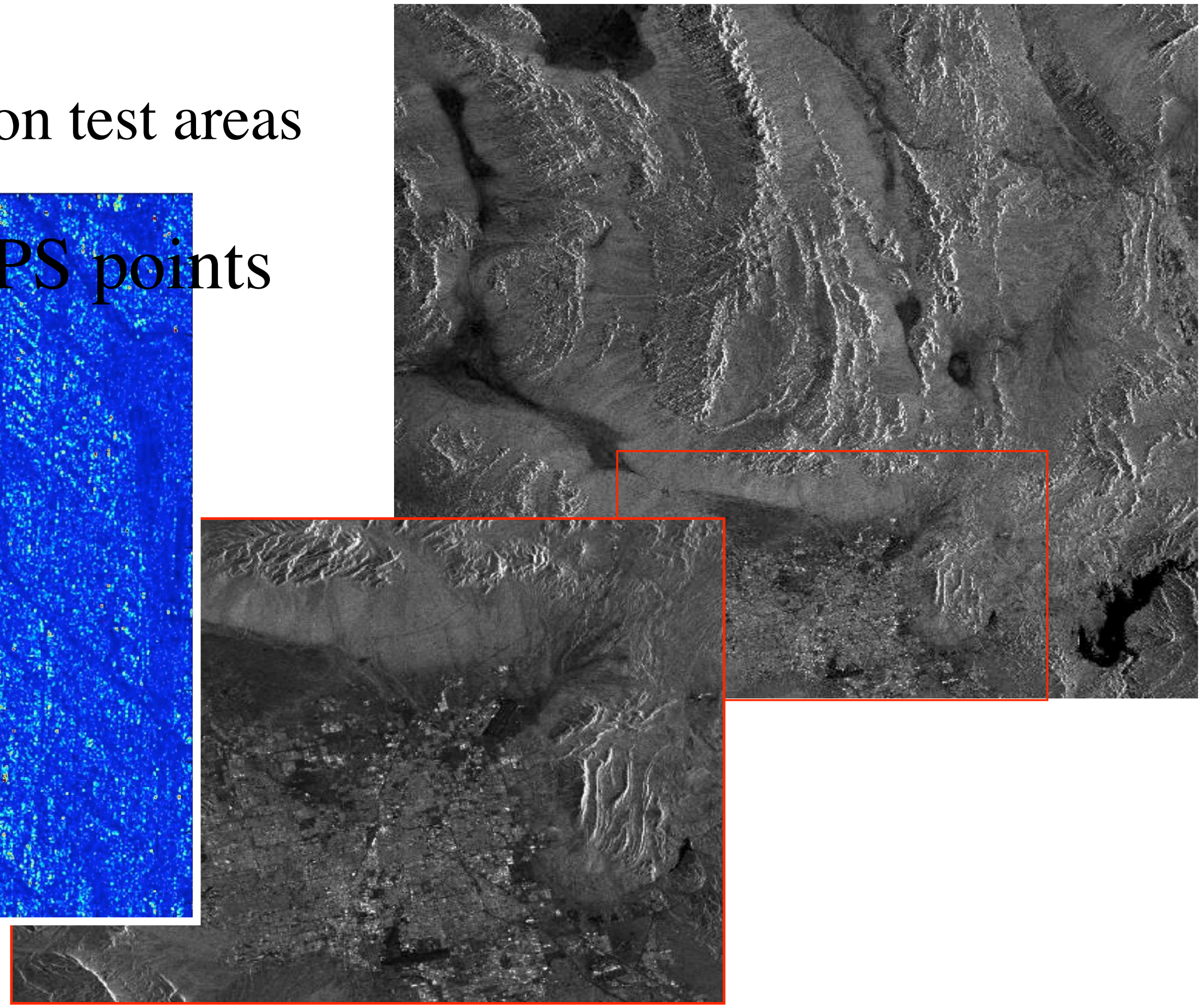

Selection potential PS points

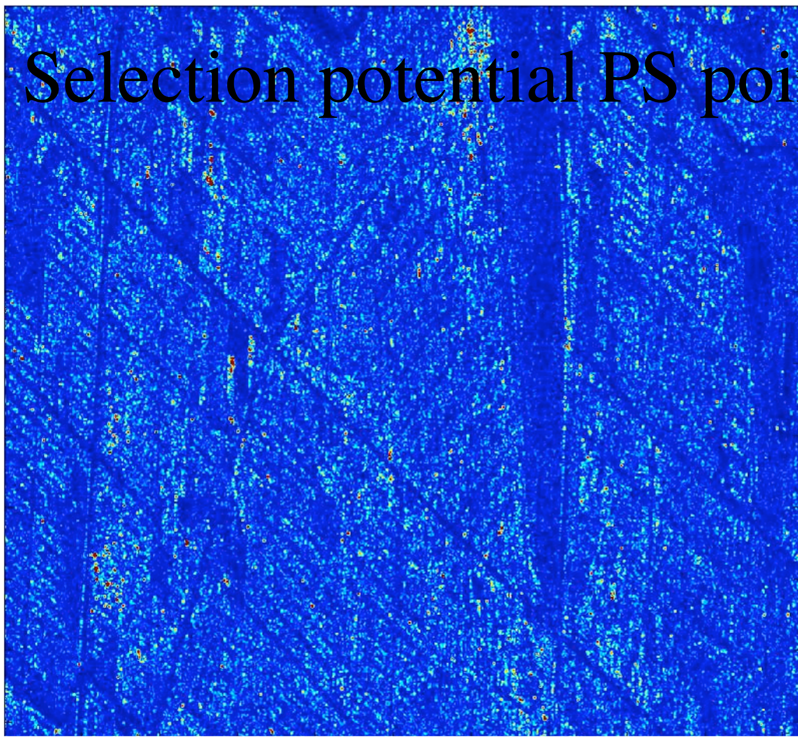

# Persistent Scatterers processing chain

- Persistent Scatterer Candidates selection, based on amplitude dispersion (Ferretti et al., 2001)
- Construction network by Delaunay triangulation

•Integer LSQ estimation of ambiguities and parameters
•Testing of residuals
•Spatial unwrapping (path integration)
•Separation of atmosphere and residual deformation by filtering and Kriging
•Removal Atmospheric Phase Screen
•Selection of Persistent Scatterers

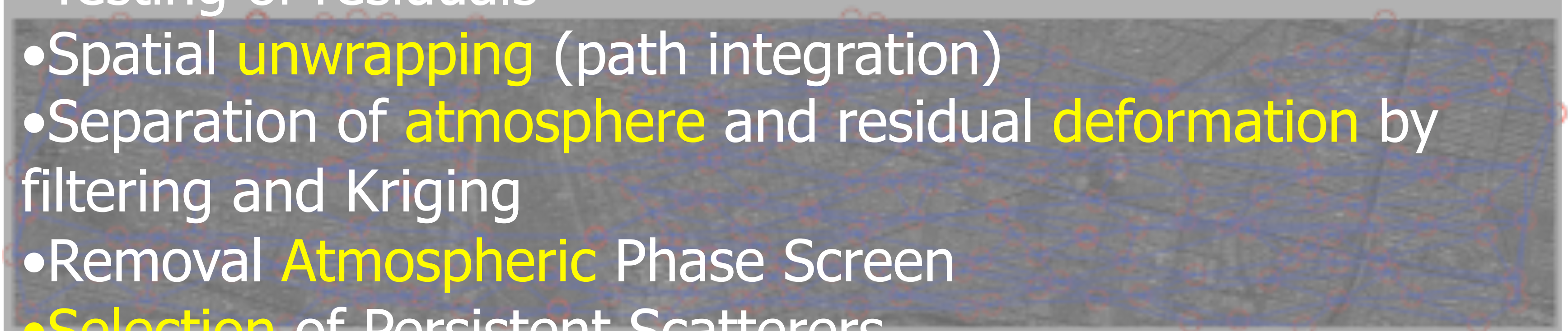

# PS Result for L.A. (U. Milano)